Aqueous Two-Phase System Patterning for Crosstalk-free, Multiplexed Detection of Plasma Biomarkers

by

Arlyne Bellamin Simon

A dissertation submitted in partial fulfillment
of the requirements for the degree of
Doctor of Philosophy
(Macromolecular Science and Engineering)
in The University of Michigan
2013

Doctoral Committee:

Professor Shuichi Takayama, Chair
Assistant Professor Mohamed E. H. El-Sayed
Professor Katsuo Kurabayashi
Associate Professor Sophie Paczesny, Indiana University
Associate Professor Andrew J. Putnam

Dedication

To Mummy, Daddy, and Auntie Ruth:

Beverly S. Stedman, Lionel A. J. Simon, and Ruth Simon,

who always remind me “I can do all things through Christ who strengthens me.”

This dissertation is also dedicated to my great-grandmother, my ‘Mama’,

Agnes Bertrand,

who I carry always in my heart.

Acknowledgements

As I complete my dissertation research, I find myself reflecting on those people who have helped me along the way. The list is extensive because a village of multi-cultural intellectuals, loving friends, prayerful family members, supportive colleagues, and an awesome God, has made sure that I never gave up on my dream.

I would like to say a heartfelt "Thank You," to my family, especially my parents. I am fortunate to have been raised by many loving Mothers: Beverly Stedman, Ruth Simon, Glenda Moulton-Simon, Sharon Simon-Pascal, Athenia Beligny, and Agnes Bertrand. And, I am blessed to have one extremely devoted father – Lionel Simon, who has worked so hard and sacrificed so much to get me here, and who always expressed an avid interest in my education. Many thanks to my parents for always celebrating all my accomplishments, always believing in my abilities, and for not letting me quit, when I was so often tempted. They were right, as always, that "Because God is with me, I will," and I eagerly anticipate the forth-coming "I told you so" remarks that they will indubitably shower me with. I would also like to gratefully acknowledge my brothers (Ali Simon and Allan Laurent) and cousins (Chantal Winston and Mersha Simon) who always checked up on me.

I am beyond grateful to my research advisor, Professor Shuichi Takayama, who believed in my potential from the start. I remember getting an email from him in Fall 2008. He just wanted to see how I was settling in at University of Michigan and gauge my interest in working on a new polymer solution microarray technology, which today is the basis of my

dissertation research. Through his exemplary mentoring, Professor Takayama has led me to innovate new technologies that one day could revolutionize the biotechnology industry. When experiments failed, tempting me to give up, I could always count on Professor Takayama's optimistic spirit and words of encouragement to keep going. The simplicity with which he explained key, but complex, biomedical engineering concepts was remarkable. And, I found myself striving to be as good a teacher as he to my undergraduate mentees or colleagues. I will forever remember the many days Prof. Takayama and I sat together in his office brainstorming new research ideas. The way he transformed an idea into a tangible, creative, research outcome was simply magical. And, just the fact that he respected my opinions enough to let me be part of this creative process gave a major boost to my self-confidence. In all my years of schooling, Prof. Takayama was the best teacher and mentor that I have ever had. It is my hope that I can emulate, at least in part, his extraordinary patience and work ethic in my career.

Next, I would like to thank my committee members, Dr. Sophie Paczesny, Prof. Katsuo Kurabayashi, Prof. Andrew Putnam, and Prof. Mohammed El-Sayed, for their support and guidance. I am especially grateful to Dr. Paczesny and Prof. Kurabayashi; although I was never formally a member of their labs, they have always made me feel like I was one of their students. Dr. Paczesny's passion for her research was awe-inspiring, and I am grateful for her efforts in ensuring that my research projects were successfully completed. Like Prof. Takayama, Prof. Kurabayashi exudes patience and creativity, so discussions with him were always enjoyable.

I would also like to thank Ms. Nonna Hamilton, the Macro program's senior administrative assistant. She has been instrumental in the success of my graduate career. In

fact, she is one of the main reasons I chose to attend graduate school at the University of Michigan. She exudes a calming energy and possesses motherly qualities, which I knew I would need being so far from my family. I call her my Fairy Godmother, and I am profoundly grateful that she kept her promise and did not retire before I graduated.

John Frampton, a post-doctoral researcher in Prof. Takayama's lab, has served as my research mentor for nearly 3 years. I am very grateful for his excellent mentoring and genuine friendship. John has taught me a lot about experimental design, time-management, and grant writing. I am going to miss the opportunities to just swivel my chair around and say, "Hey John, I have a question. Got a minute?" He always had a minute, sometimes an hour. He made sure that my questions were thoroughly answered. He made sure that my experimental design was sound. He made sure that we worked on research projects that we were absolutely passionate about so that we could enjoy doing them. For his efforts, I am very gratefully appreciative.

I am also very grateful to all members of the Takayama Lab: John Frampton, Brendan Leung, Chris Moraes, Toshiki Matsuoka, Sung Jin Kim, Minsub Han, Sasha Cai Lesher-Perez, Joseph Labuz, Byoung Choul Kim, Joshua White, David Lai, Stephen Cavnar, Taisuke Kojima, Madhuresh Sumit, and Chao Zhang. We were truly the 'Happiest Students on Earth.' It has been an honor and a privilege to work with passionate, creative, intelligent, witty, motivated scientists and engineers. Together, we have enjoyed numerous brainstorming sessions, discussed pertinent results in science publications, worked side-by-side on research projects, celebrated birthdays/weddings/baby showers, and participated in many Lab Fun Bunch Times. I feel extremely blessed to have formed such wonderful friendships with esteemed colleagues.

Next, I would like to kindly acknowledge my friends at UM, especially Ingrid Sanchez, Mayte Brown, Andreja Jovic, Son-Ca Nguyen, Tapiwa Mushove, Aayush Shah, and Yash Adhia who always kept me smiling.

Words cannot express my deep gratitude to my lifelong best friends: Tracy Durand, 'Shayna' Laudat, Maura Almeida, Lucinda Cindy Stevens, and Nefertari Galiba-Ndiour. I am wonderfully blessed to have such caring, loving, and understanding girlfriends. Distance did not prevent their *daily* words of inspiration, prayers of blessings, and thoughtful care packages. I could not have gotten his far without their unfailing friendship.

Lastly, I would like to acknowledge the Ronald E. McNair Program, for seeding the passion in me to pursue a Ph.D. I would also like to acknowledge the Rackham Merit Fellowship, the Tissue Engineering and Regeneration Training Grant, the Coulter Translational Research Grant, as well as the National Science Foundation Innovation-Corps Program for funding my graduate studies.

Table of Contents

List of Figures

List of Tables

List of Abbreviations

ATPS ..... aqueous two-phase systems

PEG ..... poly(ethylene) glycol

DEX ..... dextran

ELISA ..... enzyme-linked immunosorbent assay

AlphaLISA ..... amplified luminescent proximity homogeneous assay

Ab ..... antibody

AccB ..... acceptor bead

Abstract

Highly sensitive and robust protein assay platforms are urgently needed to improve diagnosis and inform therapeutic decisions in many disease areas. However, current bioassays for multiplexed protein biomarker detection are plagued by nonspecific antibody cross-reactions, which often lead to false positive detection and misdiagnoses. The work presented in this dissertation fills this key technological gap in protein assay development, and describes two innovative multiplexed bioassays that completely eliminate antibody cross-reactions.

First, we introduce a multiplexed bead-based assay that not only prevents antibody cross-reactions, but also does not require any wash steps. We circumvented the antibody crosstalk problem by stably co-localizing antibody-conjugated beads in droplets of immiscible aqueous polymer solutions. We demonstrated this assay's clinical utility by measuring the levels of proinflammatory biomarkers (chemokine ligand 9, chemokine ligand 10, interleukin-6, and interleuikin-8) in plasma samples from from 88 bone marrow transplant (BMT) patients. Our assay accurately discriminated BMT patients afflicted with and without chronic graft-versus-host disease (GVHD) patients within 2 hours.

Second, we describe a multiplexed ELISA that eradicates antibody cross-reactions by confining and spatially patterning detection antibodies within droplets of phase-separating polymers. We used this crosstalk-free assay to measure a panel of four acute GVHD biomarkers (tumor necrosis factor-alpha, hepatocyte growth factor, elafin, and ST2) in plasma samples from 81 BMT patients. Not only does this assay eliminate antibody crosstalk, but it

also reduces antibody costs by 100-fold because assays only require 0.5 μl detection antibody volume instead of 50 μl required by conventional ELISA.

Notably, both crosstalk-free multiplexed platforms can be read using commercially available plate readers, indicating that these assay platforms can be valuable tools for diagnosis complex diseases like GVHD.

Chapter One

Introduction

1.1 Importance of Multiplexed Protein Biomarker Analysis

Protein biomarkers are becoming increasingly essential in clinical research, disease diagnosis, and drug development. In clinical research, biomarkers advance our understanding of complex disease pathophysiology (Roberts *et al.* 2006). In oncology, noninvasive biomarker screens are used for early cancer detection and diagnosis (Lilja *et al.* 2008, Kulasingam and Diamandis 2013). In the pharmaceutical industry, biomarkers are used to evaluate drug safety and efficacy, driving 'go / no go' decisions in drug development (Khleif *et al.* 2010). In fact, significant improvements in the ability to predict which drug candidates are likely to fail in clinical trials saves US $100 million in drug development costs per drug (DiMasi *et al.* 2003). Recognizing these benefits of protein biomarkers, emphasis has been placed on biomarker discovery in many disease areas (Wang *et al.* 2012, Armenta *et al.* 2009).

Until recently, it was believed that single biomarkers were sensitive and specific enough to reliably detect early-stage disease. For example, an elevated level of prostate specific antigen (PSA) is generally indicative of prostate cancer, and is used as a basis to perform prostate surgeries. But, only 25% of men who have prostate biopsies due to elevated PSA actually have prostate cancer. This means that most prostate surgeries and radiation therapy are due to overtreatment, and unnecessarily exposes men to medical complications such as impotence, urinary incontinence, and rectal bleeding (Goodwin *et al.* 2013)! Because normal protein levels

are highly variable among individuals, it is difficult to distinguish between normal and diseased individuals based on levels of a single biomarker (Paczesny *et al.* 2009, Kim *et al.* 2010). Instead, the simultaneous measure of multiple protein biomarkers in single biological samples i.e. multiplexed protein detection better evaluate disease complexity and is therefore more clinically useful. Unfortunately, several technical challenges limit the widespread use of multiplexed protein assays in research, clinical, and pharmaceutical settings. Here, we provide an overview of multiplexed protein assays, focusing on these technical limitations.

1.2 Limitations of Current Multiplexed Protein Immunoassays

The sandwich enzyme-linked immunosorbent assay (ELISA) has been the gold standard for immunoassays since its discovery in 1971 (Engvall and Perlmann 1971). Since then ELISAs have been applied to multiplexed protein analysis, using planar-based or bead-based technologies (MacBeath 2003, Kingsmore 2006).

In conventional planar assays, capture antibodies are spatially immobilized onto a solid substrate (microwell plates or glass slides) in discrete locations. Typically a mixture of detection antibodies is added over the entire array as a cocktail and target biomarkers are sandwiched between the capture and labeled detection antibodies, eliciting a colorimetric, fluorescent, or chemiluminescent signal (**Fig. 1.1A**). Of these detection methods, only fluorescence-based assays can spectrally resolve signals from individual biomarkers because detection antibodies can be conjugated to different fluorophores. In contrast, both chemiluminescent and colorimetric immunoassays require spatial separation of signals to achieve multiplexed detection. The main drawback of these planar assay formats is the cocktail of detection antibodies, which dramatically reduces assay sensitivity and specificity because of higher background levels and

nonspecific binding of detection antibodies, referred to as antibody crosstalk. Therefore, the concentration of each detection antibody must be optimized, and costly and labor-intensive systematic evaluations of all nonspecific interactions between each antibody and all other antibodies and biomarkers must be performed one by one (Gonzalez 2008; Perlee 2004). Due to cross-reactivity, some antibodies are removed from a panel, reducing the amount of information that can be gathered from the multiplexed biomarker study.

Bead-based assays consist of microbeads (5.6 μm) coated with capture antibody (**Fig. 1.1B**). Protein biomarkers bind to the freely circulating multi-color beads within microwells. Like in planar assays, a cocktail of labeled detection antibodies is introduced into the microwell, and after washing off unbound antibody, the beads are hydrodynamically focused in a core stream of a two-color flow cytometry-like instrument. Beads are excited at two different wavelengths (532 nm and 635 nm), exciting both the red/orange fluorochromes inside the beads as well as the labeled detection antibodies, thereby identifying and quantifying the detected protein biomarker.

The key advantage of these multiplex bead-based assays is the ability to spectrally resolve the signal generated by multiple biomarkers. The drawback is that bead-based assays suffer not only from detection antibody crosstalk but also from capture antibody crosstalk because the capture antibody-coated microbeads are also suspended in solution, allowing capture antibodies to interact. The dominant player in this field is Luminex. In theory, up to 100 different microbeads can be distinguished by the Luminex multi-analyte profiling (xMAP) technology. In reality, however, 50-plex is the maximum reported for these bead-based multiplexed immunoassays because background signals increase and test robustness is significantly reduced by poor assay specificity due to both antibody crosstalk and optical crosstalk (Siebert *et al.*

2012). In addition, variability is dependent on the biomarker measured. For example, interleukin-2 and interleukin-6 had good correlations (R^2>0.95) between two Luminex methods but tumor necrosis factor, interleukin-5, and interferon-gamma had poor correlations (Berhoud *et al.* 2011). In addition to poor specificity, both planar- and bead-based assays formats have long assay times with numerous wash steps and high sample consumption. These disadvantages stress the importance for the need for novel multiplexed technologies that eliminate crosstalk and wash steps in a simple, inexpensive, scalable, and flexible format.

One commercially available singleplex assay, amplified luminescent proximity homogeneous assay (AlphaLISA), overcomes most of the limitations of conventional ELISA. Benefits of AlphaLISAs include no wash steps, small sample volumes, and wide dynamic ranges (> 4 logs). The dynamic range is the range over which there is a linear relationship between the biomarker concentration and the assay signal. AlphaLISAs' broad dynamic range means the assay can detect biomarkers from sub-pg/ml to 10 ng/ml whereas conventional ELISAs have narrow dynamic ranges (~2 logs). Thus, frequently samples in ELISAs that have target biomarker concentrations above the dynamic range must be diluted for the assay. Dilution reduces the concentration of the measured biomarkers, making it absolutely critical for assays to have pg/ml and fg/ml detection limits.

In AlphaLISAs, protein biomarkers are sandwiched between biotinylated detection antibodies and antibody-conjugated acceptor beads (**Fig. 1.2**). Then, streptavidin-donor beads bind to biotinylated detection antibodies. Laser excitation at 680 nm causes the photosensitizing agent (phthalocyanine), contained in the donor beads, to excite ambient oxygen to its singlet state. If the donor and acceptor beads are brought within 200 nm by co-recognition of the same antigen, singlet oxygen molecules react with thioxene derivatives on the acceptor bead, resulting

in amplified luminescent emission at 615 nm (Eglen *et al.* 2008). However, the major limitation of AlphaLISAs is the inability to perform multiplexed protein detection in the current format. This inherent disadvantage results because signals generated by the circulating antibody-biomarker complexes cannot be spatially or spectrally resolved. Innovative methods to multiplex highly specific and sensitive, no-wash assays while eliminating antibody cross-reactivity between antibodies, will dramatically advance the field of proteomics.

1.2.1. Assay Specificity

One of the main technical challenges in developing multiplexed protein assays is assay specificity. Assay specificity is affected by antibody affinity (the strength of the interaction between an antibody and its target antigen) and antibody cross-reactivity (nonspecific binding between detection antibodies).

To detect low abundant target proteins, high affinity antibodies are needed. A low affinity antibody for an abundant *non-target* biomarker may bind equally well as a high affinity antibody for a low abundant *target* biomarker. If this occurs, data generated gives false indications of the level of these two biomarkers in the sample. This is particularly problematic because clinically useful proteins in blood span a concentration range of 11 orders of magnitude (Anderson and Anderson 2002). For example, 50 mg/ml albumin indicates severe liver disease or malnutrition whereas > 10 pg/ml interleukin-6 indicates inflammation or infection. Thus, to reliably detect all protein biomarkers in blood samples, assays must have dynamic ranges of at least 11 logs. Moreover, bioassays should particularly be able to detect proteins at sub-pg/ml sensitivities because low abundant cytokines are diluted to femtomolar concentrations when released into the 17-liter interstitial fluid.

Given the diversity in dynamic range of *in vivo* protein concentrations, it is possible that the antibodies used in conventional singleplexed assays are not suitable for multiplexed protein assays. Extensive characterization of affinity, specificity, cross-reactivity, and binding kinetics of generated antibodies are crucial processes to identify optimum antibodies for multiplexed assays. However, these are painstaking processes. Tedious antibody purification methods such as dialysis, chromatography, or ammonium sulfate precipitation must be performed to isolate antibodies (Grodzki and Berenstein 2010). Next, tests must be done to identify optimal antibodies, which have rapid association rates and slow dissociation rates. Recently developed antibody affinity microarrays are still in their infancy; hence, current multiplexed assays still use the same antibodies as conventional singleplex assays (Poetz *et al.* 2005; Schwenk *et al.* 2007). Because of the limitations in antibody choice, many multiplexed assays have high detection limits. For example, label-free protein detection via surface plasmon resonance (SPR) has achieved detection limits of a 0.2 – 2 ng/ml when the SPR signal is not amplified and a few pg/ml when the signal is amplified (Ro *et al.* 2008, Teramura *et al.* 2006). Similarly, mass spectrometry lacks the sensitivity to detect low abundance biomarkers, with limits of detection of approximately 2 μg/ml (Addona *et al.* 2009). Multiplexed ELISAs usually have detection limits between 1 – 100 pg/ml (Kingsmore 2006). Most recently, single-molecule arrays (Simoa) can detect as low as 14 fg/ml prostate-specific antigen (PSA) in patient sera (Rissin *et al.* 2010). In Simoa-type assays, samples are compartmentalized into arrays of very small volume chambers. While many chambers do not contain any analyte, the few chambers that do contain the analyte will have the molecule in such a small volume that the concentration will be higher than in bulk solution. By combining this concentration-by-microcompartmentalization technique with single molecule detection, the method enables orders of magnitude higher sensitivity of detection. The

technology currently multiplexes up to 10-plex but suffers from antibody crosstalk and increased background signals similar to conventional planar arrays due to the use of detection antibody cocktails. The assays also require custom, expensive hardware to perform.

While achieving fg/ml detection limits by the Simoa platform is a significant technological advancement in multiplexed assays, PSA levels in cancer patients are generally in ng/ml concentrations. In addition, as aforementioned, PSA is not good for discriminating between diseased and healthy patients. This brings into view a good point – the importance or value of detection limits. The limit of detection (LoD) is the lowest analyte concentration that is reliably differentiated from the limit of blank (LoB). Specifically, LoB = $mean_{blank}$ + 1.645(SD_{blank}), and LoD = LoB + 1.645($SD_{low\ concentration\ sample}$), where SD is the standard deviation (Armbruster and Pry 2008). The ability to measure fg/ml biomarker concentrations is only important if the target biomarker is low abundant in patient body fluids. In some cases, like graft-versus-host disease, biomarkers such as chemokine ligand 9 (CXCL9) and chemokine ligand 10 (CXCL10) are in ng/ml quantities while interleukin-6 and interleukin-8 are in sub-pg/ml quantities. If the multiplexed assay has a narrow dynamic range or if researchers aim to minimize patient sample consumption, samples may be diluted. Upon dilution, concentrations of the interleukins may be in the fg/ml range while the chemokines may be in the pg/ml range. In this scenario, fg/ml detection of the interleukins is crucial.

Antibody cross-reactivity arises when detection antibodies bind nonspecifically to epitopes of a non-target protein, generating false positive signals (Theilacker *et al.* 2011) (**Fig. 1.3**). This phenomenon is widespread in conventional multiplexed assays because detection antibodies are usually introduced into the assay as a cocktail. Furthermore, as the number of antibody pairs increase in multiplexed assays, the likelihood of nonspecific interactions

increases. To mitigate risks of cross-reactivity, tedious systematic evaluations of nonspecific interactions between each antibody and each measured protein must be performed one by one (Shao *et al.* 2003; Gaster *et al.* 2011; Shweitzer *et al.* 2002; Gonzalez *et al.* 2008). Even with such precautions, assay sensitivity decreases because of high background levels sometimes as much as 2- to 5-fold compared to singleplex assays (Kingsmore 2006). Some methods circumvent the antibody cross-reactivity problem by performing multiple singleplex tests or so-called sequential ELISA, where each singleplex test measures only one target protein at a time. This time-intensive process has been described in detail (Fiema *et al* 2012). In another format (the direct ELISA), arrayed antigens are used to measure labeled antibodies. But the multiplexing ability of this platform is limited because it only reaches detection limits of 100 ng/ml, which is far too high to measure low abundance biomarkers (Haab 2001). Hydrogel arrays require surface modification for gel adherence, hinder diffusion of biomarkers and capture antibodies, and are affected by loss of antibody-coated beads within the gel (Ikami *et al*. 2010). Microfluidic approaches are difficult because of complex fabrication, lots of fluidic connections, poor reproducibility, and the need for user training (Gaster *et al.* 2009, Barbee *et al.* 2010; Li *et al.* 2012; Fan *et al.* 2008). Antibody co-localization arrays are limited by evaporation of nanoliter detection antibody solutions (Pla-Roca *et al.* 2012). Consequently, emerging technologies that use nucleic-acid aptamers are being investigated.

Aptamers are single-stranded RNA or DNA oligonucleotides 15 to 60 base pairs in length that bind with high affinity and high specificity to specific molecular targets. Aptamers are advantageous because they are synthesized *in vitro* with high reproducibility (Hu and Zhang 2013). One innovative, aptamer-based assay uses Slow Off-rate Modified Aptamers (SOMAmers), enabling protein detection with 7 logs of dynamic range (~ 100 fM – 1 mM). This

technology takes advantage of folded protein-binding pockets as well as the unique nucleotide sequence of each aptamer for each target protein (Gold *et al.* 2010). Aptamer assays are, of course, not without their disadvantages. These assays still require multiple wash steps and unlike antibodies, the three-dimensional shape of nucleic-acid aptamers is greatly affected by solution conditions, limiting the binding of aptamers to target proteins (McKeague and DeRosa 2012).

1.2.2. Matrix Interference

Another technical challenge that affects the sensitivity of multiplexed immunoassays is matrix interference from multiple endogenous antibodies, particularly human anti-animal antibodies (HAAAs). Prevalence of these interfering HAAAs in patients may result from an immune response that occurs after exposure to animals (e.g. veterinarians, pet owners), blood transfusion, and even diets rich in cheese (Hawkins *et al.* 1980). These circulating anti-animal antibodies can reach gram per liter concentrations in the blood (Kricka 1999). They interfere with assay results because they form bridges between capture and detection antibodies independently of the target protein biomarker, resulting in false positive signals (**Figure 1.4A)** (Fitzmaurice *et al*. 1998). These HAAAs can also cause false negative signals by preventing target proteins from binding to either the capture or detection antibodies (**Figure 1.4B**). To inhibit HAAA interference in immunoassays, plasma samples can be pretreated or diluted in appropriate blocking buffers or tubes. One effective blocking buffer is the Heterophilic Blocking Reagent (HBR) from Scantibodies Laboratory (Peter *et al*. 2011, DeForge *et al.* 2010, Poulsen and Jensen 2007). Specifically, the HBR blocks all anti-animal species (anti-rabbit, anti-goat, anti-sheep, anti-mouse) as well as anti-subtypes of mouse monoclonals (anti-mouse IgG_1, anti-mouse IgG_2), preventing HAAAs from interfering with the immunoassay.

1.2.3. Assay Precision

Sensitive multiplexed assays should have coefficient of variation (CV) less than 20% (Armbruster and Pry 2010). Intra- and inter-assay precision must be evaluated by assaying several replicates (< 20) of an identical sample. Ideally, intra- and inter-assay precision will be identical, but that is not usually the case because of variation between batches of antibodies, day-to-day variability, and plate-to-plate variability. Consequently, bead-based multiplex assays report intra-assay CVs <15% and inter-assay CVs between 15% and 36% (Liu *et al.* 2005, Prabhakar *et al.* 2004).

1.3 Aqueous Two-Phase Systems

In this dissertation, we capitalize on the immiscibility of aqueous polymers to eradicate some of the technical limitations of multiplexed protein assays. In this section, an overview of aqueous two-phase systems is provided.

1.3.1. Brief overview of aqueous two-phase systems

An aqueous two-phase system (ATPS) is formed when two immiscible aqueous polymers are mixed in solution, resulting in phases with water content between 80 wt% and 99 wt% (Albertsson 1986). The most common ATPS is poly(ethylene glycol) (PEG) and dextran (DEX), where the upper phase is constituted primarily of PEG and the lower phase is primarily DEX. Phase separation is dictated by differences in hydrophobicity as well as repulsive interactions between the two incompatible polymers. For instance, if there is an increase in number of

hydrophobic groups on DEX, dextran will become compatible with PEG, making it less likely for an ATPS to form.

ATPSs are generally used for the gentle separation of biomolecules (proteins, nucleic acids), particles, and cells in aqueous environments. Partitioning of biomolecules in an ATPS is dependent on several factors, namely the pH, salts, size, molecular weight, and ionic composition of the biomolecule as well as the molecular weight of the immiscible polymers. Fortunately, there are some general trends observed when partitioning biomolecules within an ATPS: (1) reducing polymer molecular weight results in greater affinity for biomolecules to that phase, (2) larger particles partition to the interface and DEX, and (3) operating at polymer concentrations beyond the critical point (i.e. equivolume phases) increases the partitioning of biomolecules at the interface.

1.3.2. Applications of aqueous two-phase systems

Traditionally, ATPSs were used for cell, protein, and particle isolation and purification on the macroscale, as an alternative to centrifugation and liquid-liquid systems. Since then, our lab has pioneered the use of ATPS for microscale patterning, particularly for gene silencing and gene over-expression, cell co-cultures, and localized sonoporation (Tavana *et al.* 2009, Yaguchi *et al.* 2010, Fang *et al.* 2012, Frampton *et al.* 2013). We have also extended the use in microfluidics-based approaches for aqueous droplet generation (Lai *et al.* 2011). Similarly, other labs have used ATPSs for synthesizing artificial cells, separating white blood cells from blood samples, and showing reversible phase transitions (Long *et al.* 2007, Tsukamoto *et al.* 2009, Boreyko *et al.* 2013).

1.4 Dissertation Overview

This work will be divided into two main parts. Part 1 describes the main objectives of this interdisciplinary thesis research – use of aqueous two-phase systems to develop a no-wash, multiplexed, bead-based assay. Part 2 describes the use of ATPSs for other biological applications, namely preventing antibody cross-reactions in heterogeneous assays, enabling localized sonoporation *in vitro*, and spatially patterning extracellular matrices. Specifically, Chapter 2 demonstrates the utility of ATPSs to spatially pattern matched pairs of antibody-conjugated beads in discrete microliter dextran droplets. Co-localization of antibody pairs not only enabled multiplexing of a no-wash bead assay but also inherently prevented antibody cross-reactions between different detection antibodies. Detecting and quantifying levels of four chemokines and cytokines in cytokine-stimulated human alveolar epithelial cells as well as plasma from bone marrow transplant patients validated this innovative multiplexed assay. Chapter 3 extends the development of this cross-reactivity-free homogeneous assay by making this multiplexed assay user-friendlier. Efforts here were towards reducing user pipetting steps by lyophilizing corresponding antibody-bead pairs in dextran droplets in custom 96-well microplates. Chapter 4 provides details on the utility of ATPSs to prevent antibody cross-reactions in heterogeneous multiplexed ELISAs. Next, Chapter 5 provides insights for future work, with emphasis on the need for higher plexing levels for biomarker discovery and signal transduction applications.

In Part 2, Chapter 6 describes how ATPSs can be used to confine ultrasound contrast agent microbubbles, enabling localized sonoporation of mammalian cells. Finally, Chapter 7 details use of ATPSs for the high throughput patterning of contractile collagen microgels.

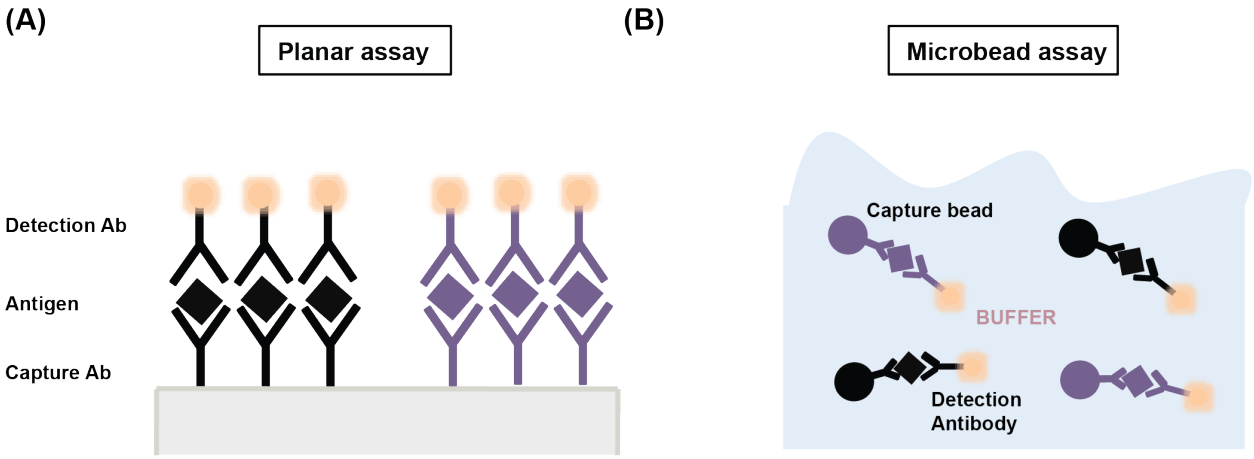

Figure 1.1: Schematic representation of conventional multiplexed assays.

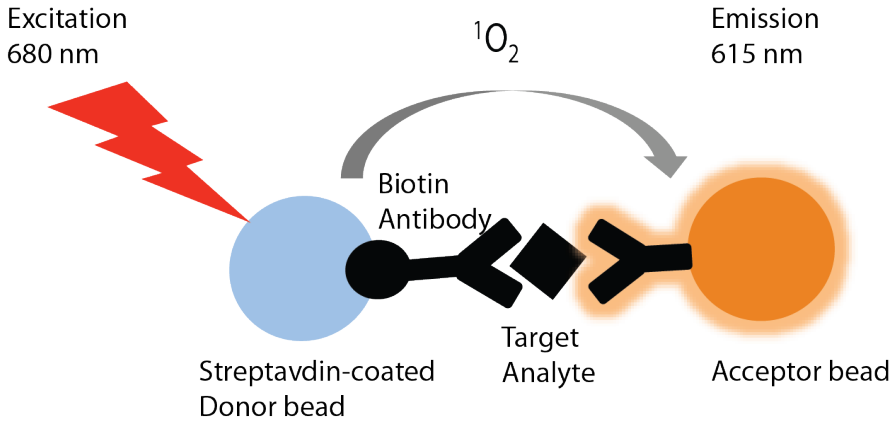

Figure 1.2: Schematic showing mechanism of AlphaLISAs.

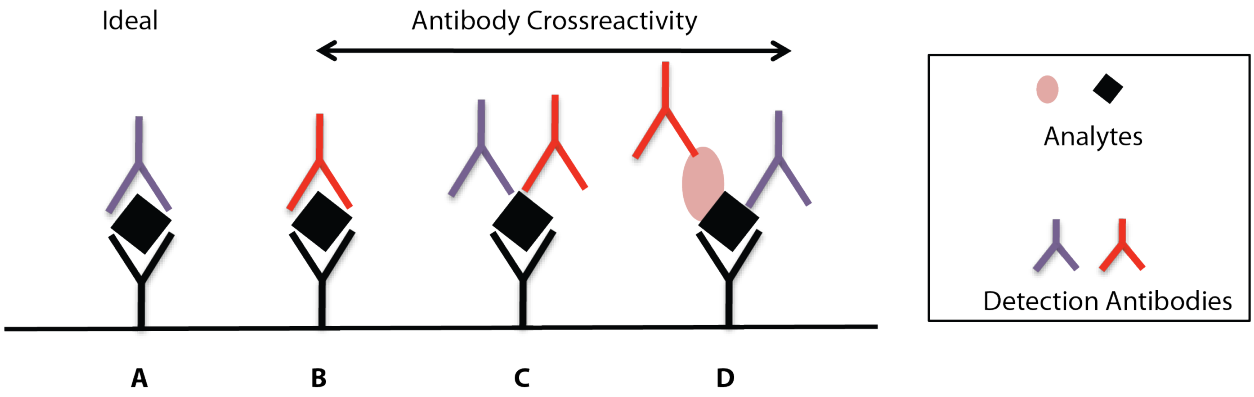

Figure 1.3: Schematic showing different types of antibody cross-reactivity. (**A**) Ideal sandwich assay where matched antibody pairs sandwich target analyte. (**B-D**) False positive signals are generated when detection antibodies bind to non-target analytes.

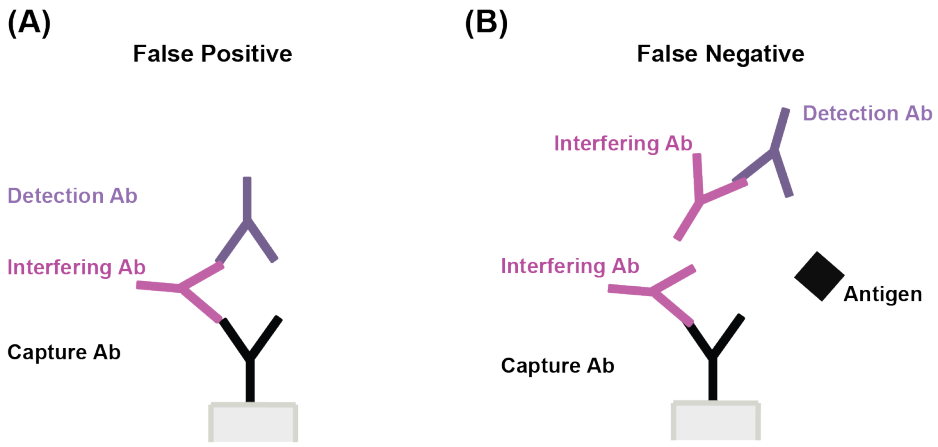

Figure 1.4: Schematic showing how human anti-animal antibodies interfere with immunoassays. (**A**) False positive signals result when interfering antibodies form a bridge between capture and detection antibodies. (**B**) False negative signals result when interfering antibodies bind to capture OR detection antibodies, preventing the target antigen from binding correctly.

1.5 References

Anderson, N. L. and N. G. Anderson. The Human Plasma Proteome: history, character, and diagnostic prospects. *Mol. Cell. Proteomics* **1**, 845-867 (2002).

Anderson, L. and C. Hunter. Quantitative mass spectrometric multiple reaction monitoring assays for major plasma proteins. *Mol. Cell. Proteomics* **5**, 573 (2006).

Armenta, J. et al. Differential Protein Expression Analysis Using Stable Isotope Labeling and PQD linear ion trap MS technology. *J Am Soc Mass Spectrom* **20**, 1287-1302 (2009).

Barbee, K. et al. Multiplexed protein detection using antibody-conjugated microbead arrays in a microfabricated electrophoretic device. *Lab Chip* **10**, 3084-3093 (2010).

Berthoud T. K. et al. Comparison of commercial kits to measure cytokine responses to Plasmodium falciparum by multiplex microsphere suspension array technology. *Malaria Journal* **10**, 115-123 (2011).

Boreyko, J. et al. Aqueous two-phase microdroplets with reversible phase transitions. *Lab Chip* **13**, 1295-1301 (2013).

DiMasi, J. et al. The price of innovation: new estimates of drug development costs. *J Health Econ* **22**, 151-185 (2003).

Eglen, R. et al. The use of AlphaScreen technology in HTS: current status. *Curr Chem Genomics* **1**, 2-10 (2008).

Engvall, E. & Perlmann, P. Enzyme-linked immunosorbent assay (ELISA). Quantitative assay of immunoglobulin G. *Immunochemistry* **8**, 871-874 (1971).

Fan, R. et al. Integrated barcode chips for rapid, multiplexed analysis of proteins in microliter quantities of blood. *Nat Biotechnol* **26**, 1373-1378 (2008).

Fang, Y. et al. Rapid generation of multiplexed cell cocultures using acoustic droplet ejection followed by aqueous two-phase exclusion patterning. *Tissue Eng Part C Methods* **9**, 647-657 (2012).

Fiema, B. et al. High throughput sequential ELISA for validation of biomarkers of acute graft-versus-host disease. *J Vis Exp* (2013).

Fitzmaurice, T. et al. False Increase of Cardiac Troponin I with Heterophilic Antibodies. *Clin Chem* **44**, 2212-2214 (1998).

Frampton, J. et al. Aqueous Two-Phase System Patterning of Microbubbles: Localized Induction of Apoptosis in Sonoporated Cells. *Adv Func Mater* (2013).

Gaster, R. et al. Autoassembly protein arrays for analyzing antibody cross-reactivity. *Nano Lett* **11**, 2579-2583 (2011).

Gaster, R. et al. Matrix-insensitive protein assays push the limits of biosensors in medicine. *Nat Med* **15**, 1327-1332 (2009).

Gold, L. et al. Aptamer-Based Multiplexed Proteomic Technology for Biomarker Discovery *PLoS One* **5**, e15004 (2010).

Gonzalez, R.M. et al. Development and validation of sandwich ELISA microarrays with minimal assay interference. *J Proteome Res* **7**, 2406-2414 (2008).

Hawkins, B. et al. Population study of heterophile antibodies. *Vox Sang* **39**, 339-342 (1980).

Ikami, M. et al. Immuno-pillar chip: a new platform for rapid and easy-to-use immunoassay. *Lab Chip* **10**, 3335-3340 (2010).

Keshishian, H. et al. Quantitative, multiplexed assays for low abundance proteins in plasma by targeted mass spectrometry and stable isotope dilution. *Mol. Cell. Proteomics* **6**, 2212 (2007).

Khleif, S. et al. AACR-FDA-NCI Cancer Biomarkers Collaborative consensus report: advancing the use of biomarkers in cancer drug development. *Clin Cancer Res* **16**, 3299-3318 (2010).

Kim, B. et al. The multiplex bead array approach to identifying serum biomarkers associated with breast cancer. *Breast Cancer Res* **11**,R22 (2009).

Kingsmore, S.F. Multiplexed protein measurement: technologies and applications of protein and antibody arrays. *Nat Rev Drug Discov* **5**, 310-320 (2006).

Kricka, L. Human Anti-Animal Antibody Interferences in Immunological Assays. *Clin Chem* **45**, 942-956 (1999).

Kulasingam, V. and E. Diamandis. Proteomics analysis of conditioned media from three breast cancer cell lines: a mine for biomarkers and therapeutic targets. *Mol Cell Proteomics* **6**, 1997-2011 (2007).

Kuzyk, M. A. et al. Multiple reaction monitoring-based, multi- plexed, absolute quantitation of 45 proteins in human plasma. *Mol. Cell. Proteomics* **8**, 1860 (2009).

Lai, D. et al. Rounded multi-level microchannels with orifices made in one exposure enable aqueous two-phase system droplet microfluidics. *Lab Chip* **20**, 3551-3554 (2011).

Li, H. et al. Microarray-to-microarray transfer of reagents by snapping of two chips for cross-reactivity-free multiplex immunoassays. *Anal Chem* **84**, 4776-4783 (2012).

Lilja, H. et al. Prostate-specific antigen and prostate cancer: prediction, detection and monitoring. *Nat Rev Cancer* **8**, 268-278 (2008).

Liu, M. et al. Multiplexed Analysis of Biomarkers Related to Obesity and the Metabolic Syndrome in Human Plasma, Using the Luminex-100 System. *Clin Chem* **51**, 1102-1109 (2005).

Long, M. et al. Budding and asymmetric protein microcompartmentation in giant vesicles containing two aqueous phases. *J Am Chem Soc* **130**, 756-762 (2008).

MacBeath, G. Protein microarrays and proteomics. *Nat Genet Suppl* **32**, 526-532 (2002).

McKeague, M. and M. DeRosa. Challenges and Opportunities for Small Molecule Aptamer Development. *J Nucleic Acids* **2012**, 768913 (2012).

Osuchowski, M.F. & Remick, D.G. The repetitive use of samples to measure multiple cytokines: the sequential ELISA. *Methods* **38**, 304-311 (2006).

Paszsny S. *et al*. A biomarker panel for acute graft-versus-host disease. *Blood* **113**, 273-274 (2009).

Peter, A. *et al*. Increased Cyclosporine Concentrations in the Absence of Cyclosporine Administration. *Clin Chem* **57**, 670-674 (2011).

Pla-Roca, M. et al. Antibody colocalization microarray: a scalable technology for multiplex protein analysis in complex samples. *Mol Cell Proteomics* **11**, M111.011460 (2012).

Poulsen, F. and K. Jensen. A luminescent oxygen channeling immunoassay for the determination of insulin in human plasma. *J Biomol Screen* **12**, 240-247 (2007).

Prabhakar, U. et al. Validation and comparative analysis of a multiplexed assay for the simultaneous quantitative measurement of Th1/Th2 cytokines in human serum and human peripheral blood mononuclear cell culture supernatants. *J Immunol Methods* **291**, 27-38 (2004).

Ro H-S. et al. Surface plasmon resonance imaging of protein arrays for analysis of triple protein interactions of HPV, E6, E6AP, and p53. *Proteomics* **6**, 2108-2111 (2006).

Roberts, M. et al. Cardiovascular biomarkers in CKD: pathophysiology and implications for clinical management of cardiac disease. *Am J Kidney Dis* **48**, 341-360 (2006).

Schweitzer, B. et al. Multiplexed protein profiling on microarrays by rolling-circle amplification. *Nat Biotechnol* 20, 359-365 (2002).

Shao, W. et al. Optimization of Rolling-Circle Amplified Protein Microarrays for Multiplexed Protein Profiling. *J Biomed Biotechnol* 2003, 299-307 (2003).

Tavana, H. et al. Nanolitre liquid patterning in aqueous environments for spatially defined reagent delivery to mammalian cells. *Nat Mater* **8**, 736-741 (2009).

Teramura Y. et al. Surface plasmon resonance-based highly sensitive immunosensing for brain natriuretic peptide using nanobeads for signal amplification. *Anal Biochem* **357**, 208-215 (2006).

Theilacker, N., Roller, E.E., Barbee, K.D., Franzreb, M. & Huang, X. Multiplexed protein analysis using encoded antibody-conjugated microbeads. *J R Soc Interface* 8, 1104-1113.

Tsukamoto, M. et al. Cell separation by an aqueous two-phase system in a microfluidic device. *Analyst* **10**, 1994-1998 (2009).

Wang, X. et al. Urine metabolomics analysis for biomarker discovery and detection of jaundice syndrome in patients with liver disease. *Mol Cell Proteomics* **8**, 370-380 (2012).

Yaguchi, T. et al. Micropatterning bacterial suspensions using aqueous two phase systems. *Analyst* **11**, 2848-2852 (2010).

Chapter Two

Antibody Co-localization in Aqueous Two-Phase Systems Enables Multiplexed Detection of Disease Biomarkers in Plasma

This chapter describes a multiplexed homogenous immunoassay that co-localizes antibody-conjugated beads in droplets of immiscible aqueous polymer solutions. This microscale reagent patterning strategy forms the basis of a no-wash, multiplexed protein assay that can measure proinflammatory chemokines and cytokines from cell culture supernatants and human plasma. The assay can be completed in 2 hours with high sensitivity and specificity. Data from this multiplexed homogeneous assay correlated strongly with data from conventional singleplex amplified luminescent proximity homogeneous assays (AlphaLISAs). Moreover, confinement of capture and detection antibody reagent pairs to individual immiscible polymer droplets prevented antibody cross-reactions, thereby facilitating robust high-throughput biomarker screening in clinical research laboratories.

2.1 Introduction

Protein analysis is clinically important for patient stratification and early disease detection as well as for research in signal transduction (Paczesny *et al.* 2009; Kingsmore *et al.* 2008; Chan *et al.* 2004). The ideal protein assay should be quantitative with high sensitivity and specificity, rapid, inexpensive in terms of reagents and sample consumption, and compatible with standard lab equipment. The enzyme-linked immunosorbent assay (ELISA) is the most common clinically used quantitative protein assay. Because no one biomarker can provide all relevant information there is a drive to multiplex such assays. Multiplexed ELISAs, however, are time-consuming because of the need for multiple washing steps, use large sample volumes, and suffer from antibody cross-reactions, limiting their usefulness, reliability, and scalability (Theilacker *et al.* 2011). Homogenous immunoassays, such as the amplified luminescent proximity homogeneous assay (AlphaLISA), simplify assay procedures by eliminating wash steps, increase dynamic range, and are faster to perform but typically have limited multiplexing potential because single-color signals generated by the homogeneously distributed antibody-bead reagents cannot be spatially localized or spectrally resolved (Eglen *et al.* 2008). Here, we describe the use of micropatterned aqueous two-phase systems (ATPSs), composed of the phase-forming polymers polyethylene glycol (PEG) and dextran (DEX), to overcome these limitations and enable multiplexing of homogeneous immunoassays (Tavana *et al.* 2009).

In our approach, complementary pairs of AlphaLISA bead/antibody reagents that target specific antigens are co-localized within DEX microdroplets formed within a PEG solution. The incorporation of antigens in the PEG phase allows simultaneous delivery of antigens to all DEX droplets providing the multiplexing capability. Importantly, unlike conventional multiplexed assays where a cocktail of detection antibodies is delivered to all capture antibody spots, this

method localizes detection antibody reagents only to DEX droplets containing complementary capture antibody reagents. This reagent co-localization makes it possible to create spatially addressable homogeneous immunoassay arrays where amplified luminescent signals from different antigens are spatially resolved and the possibility of unwanted antibody cross-reactions are eliminated (**Fig. 2.1**). The assay method is very simple and an overview of the workflow is illustrated in **Fig. 2.2**. We validated our assay and demonstrated its versatility and clinical use potential by detecting 4 proinflammatory chemokines and cytokines, namely C-X-C motif chemokine 10 (CXCL10), C-X-C motif chemokine 9 (CXCL9), interleukin-8 (IL-8), and interleukin-6 (IL-6)] in cytokine-stimulated human lung carcinoma epithelial cell supernatants and plasma from 88 patients who underwent bone marrow transplantation (BMT). We chose this validation panel because these proinflammatory agents are typically elevated in chronic graft-versus-host disease (GVHD) (Croudace *et al.* 2012; Min *et al.* 2010; Westekemper *et al*. 2010). GVHD is a long-term, multi-organ disorder that afflicts 30% – 70% of allogeneic BMT patients who survive 100 days post-transplantation (Lee 2010).

2.2 Materials and Methods

2.2.1. Reagents

Antioxidant-free polyethylene glycol (PEG) (Mw. 35,000) was purchased from Fluka. Dextran (DEX) (Mw. 10,000) was purchased from Pharmacosmos. Rhodamine-Dextran (Mw. 10,000) was purchased from Sigma and AlphaScreen Omnibeads was purchased from Perkin Elmer.

2.2.2. AlphaLISA protocol

Human CXCL10 (AL259C), human CXCL9 (AL280C), human IL-8 (AL224C), and human IL-6 (AL223C) AlphaLISA immunoassay kits were purchased from Perkin Elmer and performed according to manufacturer's protocol. For cell culture supernatant samples, the assay buffer contained 25 mM HEPES, 50 mM NaCl, 10 mM sodium EDTA, 2 mg/ml Dextran (Mw. 500,000), 0.5% casein, and 0.05% Tween-20, adjusted to pH 7.4. For plasma samples, the assay buffer also contained 0.1% bovine gamma globulin (G-5009, Sigma Aldrich) and 0.2 mg/ml HBR1 (3KC533, Scantibodies). Standards, biotinylated detection antibodies, and acceptor bead solutions were prepared in assay buffer. The assays were performed in 384-well white polypropylene conical-bottom microplates (4307, Thermo Scientific). Two microliters of standards, cell culture supernatant or plasma sample were incubated with 10 μg/ml acceptor beads and 1 nM biotinylated detection antibody for 1 hour at room temperature. Streptavidin-coated donor beads (40 μg/ml) were added to the mixture and incubated for an additional 30 minutes. The plate was read on a PHERAstar FS reader (BMG LabTech) where the bead complex was excited at 680 nm for 1 second and emission signals were collected at 615 nm for 1 second after a 40-millisecond delay.

2.2.3. ELISA protocol

Human CXCL9/MIG duoset (DY392, R&D Systems) ELISA was performed, following manufacturer's specifications. Costar 96 well half-area plates were coated with 6 μg/ml capture antibody solutions and stored overnight at 4° C. Plates were washed 4 times with wash buffer (phosphate-buffered saline (PBS) containing 0.05% Tween-20) and blocked with 1% bovine

serum albumin (BSA) for 2 h. Plates were washed another 4 times and then 50 μl recombinant protein standard, cell supernatant, or 1:10 diluted plasma sample was added. After 2 h incubation, plates were washed again 4 times, incubated with 50 μl of 200 ng/ml detection antibody solution for 2 h, washed another 4 times, then incubated with streptavidin-conjugated horse radish peroxidase for 45 minutes. Finally, plates were washed 4 times and incubated with SuperSignal ELISA Femto Maximum Sensitivity Substrate (37074, Thermo Scientific). Chemiluminescent signal was detected using a FluorChem M (Protein Simple) imaging system.

2.2.4. Multiplex ATPS homogeneous immunoassay protocol

An 18 wt% PEG solution was prepared in 25 mM HEPES buffer containing 0.1% casein. An 18 wt% DEX was prepared in assay buffer specific to either cell culture supernatants or plasma samples. PEG was mixed with standards or sample solutions in a 4:1 volume ratio and the mixture was vortexed. For singleplex ATPS assays, 10 μl of the PEG-antigen mixture was dispensed into 384-well microplates such that each well contained approximately 2 μl of standard or sample and 8 μl of PEG. Acceptor beads (25 mg/ml) and biotinylated detection antibody (2.5 nM) were prepared in 18 wt% DEX. For multiplexed ATPS assays, 100 μl of the PEG-antigen mixture were dispensed into each PEG well. DEX solutions, containing acceptor beads and detection antibodies against 4 different antigens (CXCL10, CXCL9, IL-8 and IL-6) were dispensed into each of the four DEX micro-basins located in the common PEG well. Using a multipipettor, 1 μl of the DEX/antibody mixture was dispensed in each DEX micro-basin and the mixture was incubated at room temperature for 1 h. To prevent evaporation, the plates were sealed with sealing film. An 80 μg/ml solution of donor beads were prepared in 18% DEX. At

the end of the 1 h incubation, 1 μl of the DEX/donor bead solution was dispensed into each micro-basin and incubated for an additional 60 minutes. The assays were read on a PheraSTAR FS Plus after bead excitation for 1 second.

2.2.5. Plate fabrication

Multiplexed ATPS assays were performed in custom plates fabricated from black (Objet FullCure 870 Vero Black, Proto 3000) and white (Objet FullCure 830 Vero White, Proto 3000) resins using an Objet printer. In this design, white individual DEX micro-basins (2.5 mm x 2.5 mm x 2.5 mm) were located within a solid black plate matrix (well size 8 mm x 8 mm and 11.5 mm in height). Specifically, there are 96 sample wells, each containing 4 DEX microbasins. Generally, an all-white plate matrix has better reflectivity to maximize the emission signal, and is therefore commonly used for luminescent-based detection. In contrast, an all-black plate matrix absorbs light, minimizing background signals and optical crosstalk. Black plates are used primarily for fluorescent-based detection. In our custom plates, white micro-basins were designed to maximize amplified luminescent signal. Optical crosstalk was minimized between adjacent micro-basins because of presence of the black plate matrix. The micro-basins were arranged in a standard 384-well format (24 columns, 16 rows, 4.5 mm spacing) to comply with the custom plate specifications of the Society of Biomolecular Screening, and the plate was read using a narrow 2.0 mm aperture.

2.2.6. Protein and bead partitioning

AlphaLISA was used to determine protein partitioning. Solutions containing 2,500 pg/ml antigen were added to Eppendorf tubes containing 8.4 wt% PEG and 8.4 wt% DEX (total volume, 80

ml). Control tubes contained 5 μl PBS instead of the antigen. The contents of each Eppendorf tube were mixed by vortexing. The tubes were then centrifuged at 400 rcf at 4° C for 15 min. After centrifugation, the PEG and DEX phases were separated. Two microliters of the PEG phase or the DEX phase were assayed as described above. The partition coefficient was defined as the protein concentration in the PEG phase divided by the protein concentration in the DEX phase. For partitioning of Omnibeads, 5 μl of the separated PEG and DEX phases was directly dispensed into 384-well plates. Since beads contain all chemical components to generate luminescent signals, samples were directly excited at 680 nm for 1 second.

2.2.7. Detection antibody partitioning

Partitioning of the biotinylated detection antibodies was determined by dot blot. Five microliters of 500 nM detection antibodies was added to Eppendorf tubes, containing 8.4 wt% PEG and 8.4 wt% DEX (total volume of contents, 80 μl). Control tubes contained 5 μl PBS instead of the detection antibody sample. The contents of each Eppendorf tube were mixed by vortexing. The tubes were then centrifuged at 400 rcf at 4° C for 15 min. After centrifugation, the PEG and DEX phases were separated. Polyvinylidene fluoride (PVDF) membranes (Bio-Rad) were soaked in methanol for 15 seconds, water for 2 minutes, and finally PBS for 5 minutes. 0.3 μl of the PEG and DEX phases were dispensed onto the PVDF membranes, and membranes were blocked in 1% BSA for 1 h and washed 4 times with PBS containing 0.05% Tween-20. The membranes were then incubated with streptavidin-conjugated horseradish peroxidase for 1 h, washed 4 times, and incubated with SuperSignal ELISA Femto Maximum Sensitivity Substrate (37074, Thermo Scientific). Chemiluminescent signal was detected using the FluorChem M

(Protein Simple) imaging system. The partition coefficient was defined as the reagent concentration in the PEG phase divided by the reagent concentration in the DEX phase.

2.2.8. Cell culture

A549 human lung carcinoma epithelial cells were maintained in RPMI 1640 supplemented with 10% heat-inactivated FBS and 1% antibiotics within a humidified atmosphere containing 5% CO_2 at 37° C. Cells were seeded in 24-well tissue culture plates ($8x10^5$ cells per well) 24 h before use. At the start of experiments, medium was replaced with complete RPMI supplemented with 50 ng/ml IFN-γ, 50 ng/ml TNF-α, or 50 ng/ml IFN-γ/50 ng/ml TNF-α. Cell culture supernatants were collected at 0 h, 6 h, 12 h and 24 h. Recombinant human IFN-γ was purchased from Peprotech and recombinant human TNF-α was purchased from R&D systems.

2.2.9. Plasma samples

Heparinized plasma samples from 88 patients were acquired from a clinical study at the University of Michigan between 2000 and 2010. Samples were aliquoted without additives and stored at – 80 °C. Of these 88 samples, 20 samples were collected from patients who received autologous bone marrow transplantation, 59 samples were collected from patients who received allogeneic bone marrow transplantation (GVHD- = 27, GVHD+ = 32), and 9 samples were from healthy patients. The institutional review board at University of Michigan approved plasma samples collection. For AlphaLISA and multiplexed ATPS assays, plasma samples were diluted 1:4 in the appropriate assay buffer i.e. 5 µl plasma was diluted with 15 µl assay buffer.

2.2.10. Statistical analysis

Each experiment was repeated in triplicate, using 3 different plates. Results are expressed as as mean values +/- standard error of mean. Graph Pad Prism was used to fit standard curves with a four parameter logistic function to calculate sample values. The limit of detection (LoD) was computed as LoB + 1.645 ($SD_{low\ concentration\ sample}$), where SD is the standard deviation and LoB is the limit of blank. LoB was calculated from LoB = $mean_{blank}$ + 1.645 (SD_{blank}). The linear dynamic range (LDR) was calculated as the ratio of the maximum linear response versus the LoD (Armbruster *et al.* 2008). Student's t-test (two-tailed), one-way ANOVA with the Tukey's post-test, and Pearson's coefficient of correlation were used to assess significance between sample groups and between assay formats.

2.3 Results and Discussion

2.3.1. ATPS assay design characteristics

In our custom 96-well microplates (**Fig. 2.3A**), the DEX droplet size and location were constant over the course of the 2 h required to perform the assay (**Fig. 2.4A**). Each of the 96 wells contained four micro-basins for spatial patterning of 2 μl DEX assay droplets (**Fig. 2.3B-C**). ATPSs composed of 18 wt% PEG and 18 wt% DEX were used because these polymer concentrations favored antigen and antibody-bead reagent partitioning to the DEX phase, ensuring maximum antigen transport into, and retention of reagents within the DEX droplets over the course of the assay (**Table 2.1**). As seen in **Table 2.1**, regardless of antibody type, all IgG antibodies partition stably in the DEX phase. We also measured partitioning of IL-6 and

CXCL9 antigens in an ATPS composed of higher molecular weight DEX, specifically 5 wt% PEG and 6.4 wt% DEX 500. In this ATPS, IL-6 and CXCL9 had partitioning coefficients of 1.33 and 0.95, respectively. These values are significantly greater than the 0.28 paritioning coefficients reported for the DEX (Mw. 10,000) in Table 2.1. These data suggest that small chemokines and cytokines partition better to smaller molecular weight DEX, and indicate the importance of selecting the correct ATPS system for any given application.

In addition, increasing DEX concentration generally resulted in higher detection limits of singleplex IL-6 ATPS-AlphaLISAs, possibly due to inability of antigens to readily diffuse through and bind to antibody-bead pairs in more concentrated DEX (**Fig. 2.4B**).

The optimum assay incubation time was 2 h based on measurement of the 12 pg/ml limit of detection (LoD) of IL-6 and the steep gradient of the standard curve (**Fig. 2.4C-D**).

2.3.2. Comparison of singleplex ATPS and singleplex AlphaLISAs

Next, we assessed the effect of ATPS on AlphaLISA signals. Standard curves for CXCL10, CXCL9, IL-8, and IL-6 were similar in terms of linear dynamic range (LDR) and LoD for singleplex ATPS-AlphaLISA and conventional singleplex AlphaLISA (**Fig. 2.5A**). Moreover, the signal-to-noise ratios were comparable between assay formats for all tested antigens, even though the ATPS format assays consumed ten times less antibody and bead reagents. The LoD and LDR data, along with low statistical variation between measured signals, indicate that the chosen ATPS does not interfere with AlphaLISA signals.

2.3.3. ATPS prevents antibody cross-reactions in multiplexed AlphaLISAs

The importance and effectiveness of using ATPSs to localize antibody-bead reagents and generate a reliable signal is demonstrated in **Fig. 2.6**. In the absence of ATPS, any localized reagent dispensing effect is quickly lost by diffusion and convective circulation leading to no observable signal anywhere in the presence of 1,000 pg/ml of IL-6. On the other hand, when ATPS reagent localization is used, the DEX droplet that contains acceptor beads (AccBs) and biotinylated detection antibodies (Abs) bound to streptavidin-coated donor beads generates a strong signal whereas the other droplets containing only Ab, only AccB, or no reagent showed no signal. When the concentration of IL-6 was increased to 10,000 pg/ml, weak background signals were detected everywhere due to reagent crosstalk in the absence of ATPS whereas the ATPS assays showed a strong signal only in the droplet with all the required reagents (**Fig. 2.3D)**. A comparison of standard curves generated by attempting to multiplex AlphaLISA in conventional buffer versus curves generated by multiplexing AlphaLISA with ATPS further supports the critical importance of ATPS use (**Fig. 2.7**).

In some conventional multiplexed ELISAs, the assay sensitivity decreases by as much as 2- to 5-fold compared to corresponding singleplex assays because of antibody cross-reactions and high background signals (Kingsmore 2006). However, in our side-by-side comparison of individual singleplex ATPS and multiplex ATPS AlphaLISAs for CXCL10, CXCL9, IL-8, and IL-6 in custom 96-well microplates, the standard curves completely overlapped. These data indicate that there was no difference in sensitivity caused by antibody cross-reactions or increased background signals in our ATPS-multiplexed assays (**Fig. 2.8A-D**). Moreover, the LoD values for proinflammatory cytokines (10.3 pg/ml – 90 pg/ml) and LDR (~ 3 log units) were comparable between singleplex and multiplex ATPS AlphaLISAs (**Fig. 2.8E**). Assay

precision, as indicated by a coefficient of variation (CV) of less than 25%, is also an important consideration for immunoassays. Our ATPS-multiplexed assays had CVs less than 20% (**Fig. 2.8F**) (Chau *et al.* 2008).

2.3.4. ATPS-AlphaLISAs enable multiplexed protein detection in cell supernatants

One application of our multiplex ATPS assay is monitoring cytokine cascades in stimulated cells. Tumor necrosis factor-alpha (TNF-α) and interferon-gamma (IFN-γ) play important roles in pulmonary disease (Mukhopadhyay *et al.* 2006; Koch *et al.* 2006). We validated our assay by measuring 4 proinflammatory cytokines (CXCL10, CXCL9, IL-6, IL-8) in supernatants from A549 human pulmonary type II alveolar epithelial cells stimulated with TNF-α and IFN-γ alone or in combination (**Fig. 2.9**). As expected, stimulation with TNF-α or IFN-γ alone did not result in a pronounced release of CXCL10 or CXCL9 (Sauty *et al.* 1999; Pechkovsky *et al.* 2005). In agreement with other studies, our multiplex ATPS assay showed that IFN-γ alone was not sufficient to mediate IL-8 or IL-6 release in A549 cells, but that TNF-α alone or in combination with IFN-γ could mediate both IL-8 and IL-6 release (Boost *et al.* 2008; Smart *et al.* 1994; Crestani *et al.* 1994). In contrast, stimulation with combinations of TNF-α and IFN-γ caused dramatic increases in CXCL10, CXCL9, IL-8, and IL-6, although the level for IL-8 was similar to TNF-α alone. **Figure 2.10** shows correlation curves for CXCL10, CXCL9, IL-8, and IL-6 between ATPS-multiplexed AlphaLISA and conventional singleplex AlphaLISA. Our ATPS-multiplexed assay correlates well with singleplex AlphaLISA ($n > 33$), as indicated by Pearson's correlation coefficients greater than 0.7. We postulate that multiplex ATPS IL-8 assays have the weakest correlation (0.7) with conventional AlphaLISA because of the 4 measured cytokines, IL-8 partitions poorest to the DEX phase. CXCL9 values obtained from our ATPS-multiplexed

assay also correlate well with conventional singleplex CXCL9 ELISA (n = 19), as indicated by a Pearson's correlation coefficients of 0.93 (**Fig. 2.12A**).

2.3.5. ATPS-AlphaLISAs enable multiplexed GVHD biomarker detection in human plasma

Finally, we validated our assay for use with clinical samples by measuring the same four chemokines/cytokines in plasma from patients who received autologous and allogeneic bone marrow transplantation (BMT). Patients who receive allogeneic BMT usually become afflicted with chronic graft-versus-host disease (GVHD). Little is known of the pathophysiology of chronic GVHD, leading to a lack of effective diagnosis and treatment (Socie *et al.* 2010). We tested the potential use of the ATPS-multiplexed assays for monitoring and diagnosing chronic GVHD. In accordance with previous reports, both CXCL9 and CXCL10 were significantly elevated in GVHD+ patients compared to GVHD- patients (P < 0.05 by ANOVA), demonstrating the potential of these two cytokines as diagnostic GVHD biomarkers (**Fig. 2.11A,B**) (Westekemper *et al.* 2010, Imanguli *et al.* 2009; Croudace *et al.* 2012). Specifically, GVHD+ patients had mean CXCL9 values of 3,226 pg/ml while GVHD- had mean CXCL9 values of 843.3 pg/ml. Similarly, GVHD+ patients had mean CXCL10 of 2,463.4 pg/ml while GVHD- patients had mean CXCL10 values of 398 pg/ml. However, based on our requirement of diluting plasma 1:4 in assay buffer and the sensitivity of AlphaLISA we could not reliably detect IL-6 or IL-8 in plasma samples (Min *et al.* 2001; Tawara *et al.* 2011). It is also probable that IL-6 and IL-8 are not significantly elevated in chronic GVHD but only in acute GVHD. Again, the ATPS-multiplexed assay data correlated well with singleplex AlphaLISA (**Fig. 2.11C,D**). Similarly, CXCL9 data from our ATPS-multiplexed assay correlated well with singleplex CXCL9 ELISA (**Fig. 2.12B**). We also compared the individual area under the curve (AUC)

values for CXCL10 and CXCL9 between assay platforms (**Fig. 2.11E,F**). For both CXCL9 and CXCL10, AUC values were greater than 0.8, demonstrating that CXCL10 and CXCL9 distinguish between patient groups in our multiplex assay.

The technological specifications for an ideal multiplex protein assay are extensive: assays should be sensitive enough to detect antigens within the biological dynamic range; consume only small sample volumes; have similar precision to conventional singleplex assays; demonstrate high specificity due to lack of antibody cross-reactions; and require only short processing times (Kingsmore 2006). Current multiplexed assays, however, do not meet these requirements. As the number of antibody pairs in these multiplexed immunoassay increases, the likelihood of nonspecific antibody interactions increases exponentially (Gonzalez *et al.* 2008). To mitigate risks of cross-reactivity, tedious systematic evaluations of nonspecific interactions between each antibody and each measured protein must be performed to validate these assays (Gonzalez *et al.* 2008; Gaster *et al.* 2011; Schweitzer *et al.* 2002). Some methods circumvent antibody cross-reactions by performing multiple singleplex tests (sequential ELISA), where each singleplex test measures only one target protein at a time (Fiema *et al.* 2012). Other methods require surface modification, complicated microfluidic approaches or printing of reagents in dry environments, which causes reagent evaporation (Li *et al.* 2011; Gaster *et al.* 2011; Qin *et al.* 2009; Pla-Roca *et al.* 2012).

We eliminated many of these problems with our multiplexed, no-wash, ATPS-multiplexed AlphaLISAs. Confinement of antibody-conjugated beads within DEX droplets prevented the free circulation of beads and enabled, for the first time, multiplexing of homogeneous AlphaLISAs. ATPS-AlphaLISAs are inherently designed to prevent antibody cross-reactions; antibody-beads stably partition to DEX and therefore do not diffuse from one

DEX droplet to another. Because DEX is more hydrophilic and has a lower molecular weight than PEG, small cytokines and chemokines in the PEG-sample bath preferentially partition to DEX, and so are simultaneously delivered to all DEX droplets. Although non-target antigens can also diffuse into the DEX droplets, only target antigens that recognize matched pairs of high affinity, high specificity antibodies in DEX will elicit amplified luminescent signals. We achieved detection of CXCL10, CXCL9, IL-8, and IL-6 at concentrations of 10.3 pg/ml – 90 pg/ml in as little as 20 ml of 1:4 diluted plasma with dynamic ranges (2.5 – 3.5 log units) for the ATPS assay comparable to singleplex AlphaLISA and greater than most existing multiplex ELISA assays (Ikami *et al.* 2010). Compared to other multiplex bead-based assays, such as Luminex, ATPS-multiplexed AlphaLISAs do not require any wash steps nor specialized equipment other than a common plate reader to resolve signals from the bead complexes (Liu *et al.* 2005). In addition, the ATPS-multiplexed assays are scalable because there is no worry of antibody cross-reactions or increased background that typically accompanies multiplexed immunoassays that use detection antibody cocktails. Furthermore, in contrast to lengthy ELISA or Luminex assays, our assay can be completed in as little as 2 hours. Finally, we note that the ATPS-multiplexed assays reduce AlphaLISA reagent costs by tenfold, from $2.40/well of a 384-well plate to $0.24/assay droplet.

2.4 Conclusion

In summary, we have developed and validated a multiplex homogeneous bead-based assay that localizes reagents in solution by stable aqueous two-phase system partitioning. The reagent localization feature not only enables multiplexing of homogenous immunoassays but has the added advantage of eliminating unwanted antibody cross-reactions typical of other multiplexed

immunoassays. This is possible because spatial confinement of antibody-conjugated beads in ATPS droplets prevents any interactions between different detection antibodies. In other words, although we only demonstrate a 4-plex assay, there are little fundamental limitations for higher multiplexing. We do note that poor antigen partitioning can affect detection reliability but since the formulation for each DEX droplet can be distinct, such issues should be addressable by individualizing the DEX formulations, for example by addition of small amounts of DEX derivatives or adjusting salt content in DEX (Albertsson 1986). Our highly specific multiplex ATPS assay is sensitive enough to detect clinically relevant proinflammatory cytokines in both cell culture supernatant and plasma samples with minimal matrix interference. In addition, our no-wash assays enable researchers to detect a panel of proteins in only 2 hours while using small volumes of biological or clinical samples. With more extensive validation on larger patient sets, this ATPS-multiplexed assay is envisioned to be useful not only in research settings but also as a clinical diagnostic tool.

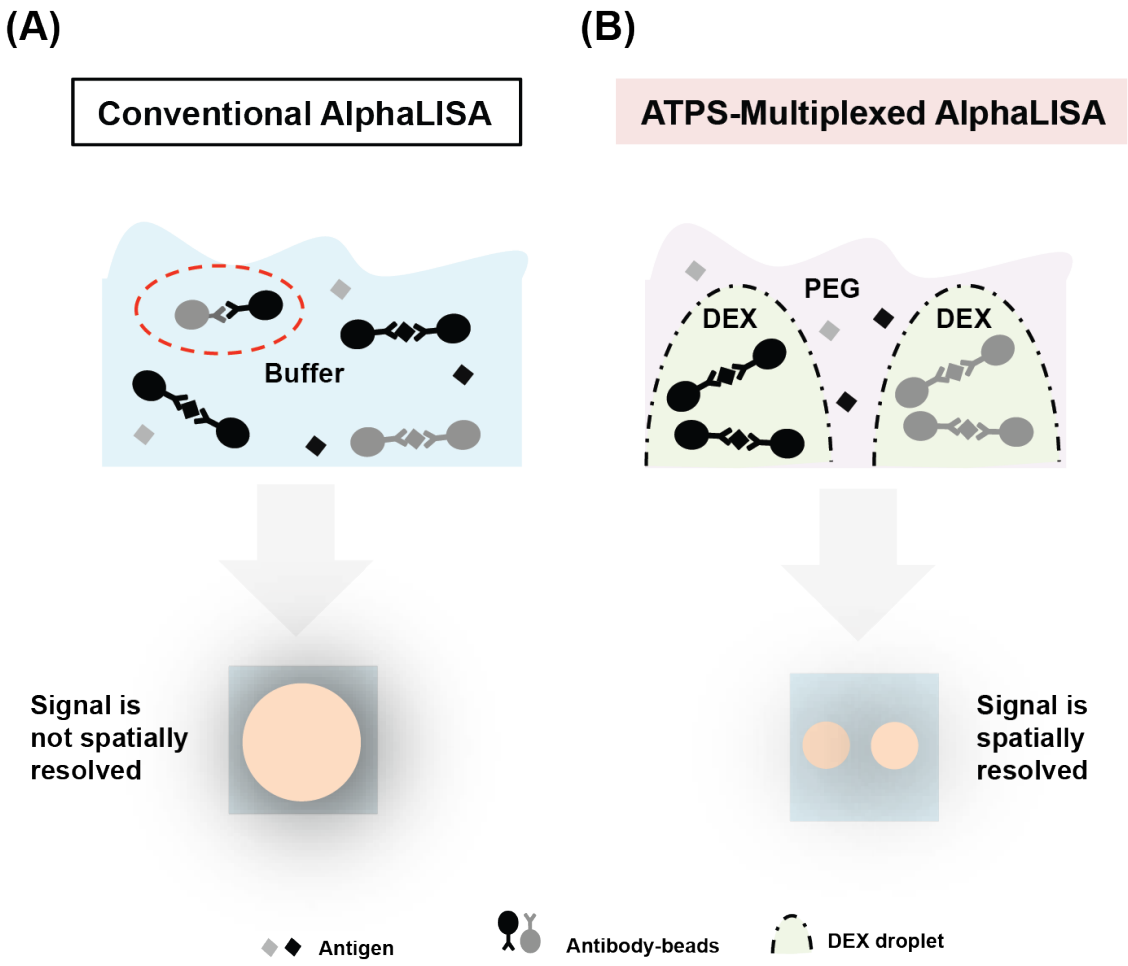

Figure 2.1: Schematic representation of ATPS-enabled multiplexed AlphaLISA. (**A**) Conventional AlphaLISA assays can perform no-wash singleplex antigen detection with wide dynamic ranges but cannot be multiplexed because antibody-bead complexes freely diffuse and circulate in the assay wells, making it impossible to resolve single-color luminescent signals from multiple biomarkers. Also the antibody-bead complexes may crosstalk (red circle), resulting in false positive detection. (**B**) In ATPS-multiplexed AlphaLISA, antibody-bead complexes are spatially confined in dextran droplets and biomarker specific readouts are spatially resolved, while eliminating antibody cross-reactions (PEG, polyethylene glycol; DEX, dextran).

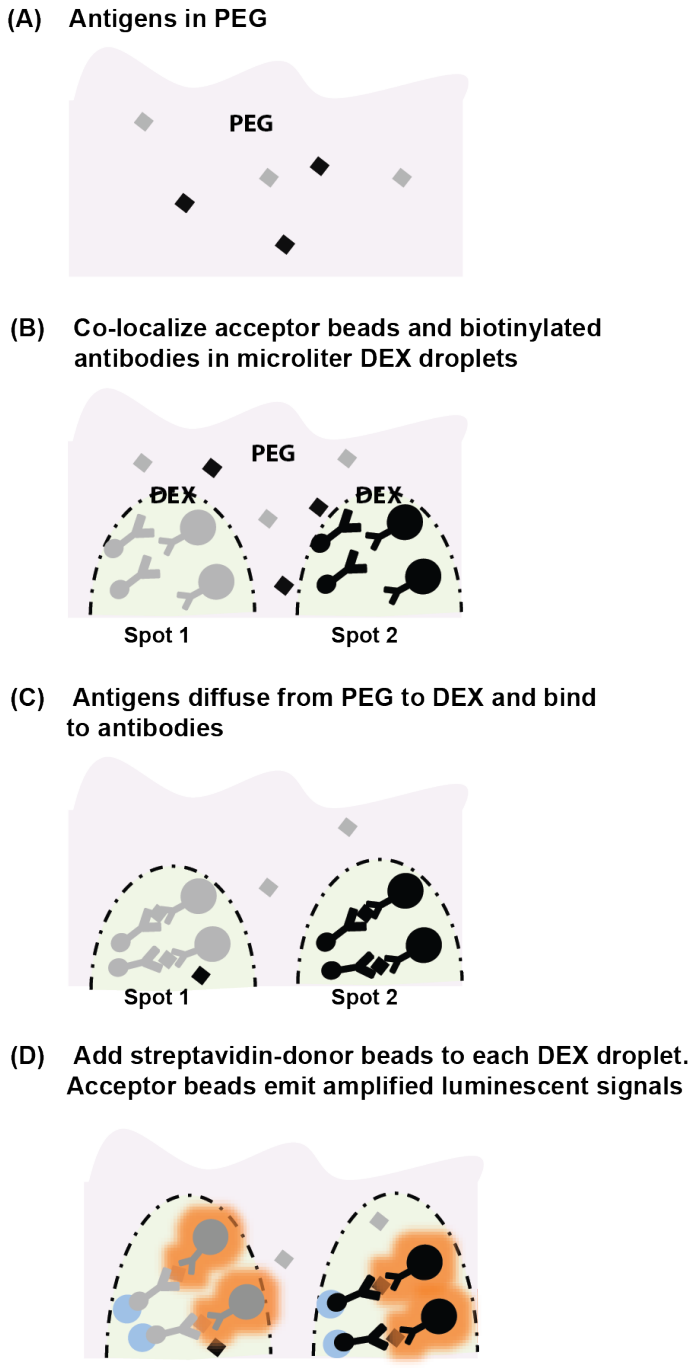

Figure 2.2: Schematic of workflow for ATPS-multiplexed homogeneous assay. (**A**) Samples, containing antigens, are mixed with PEG. (**B**) DEX droplets (1 μl), containing corresponding antibody-acceptor bead pairs are spatially dispensed into the bulk PEG phase. (**C**) During a 1-hour incubation, antigens diffuse from PEG into the DEX droplets, and bind to antibody-beads. (**D**) DEX droplets (1 μl), containing streptavidin-coated donor beads are introduced into the solution and incubated for another hour. Donor beads bind to biotinylated antibodies, eliciting amplified luminescent signals by acceptor beads. The resulting signal is spatially and spectrally resolved.

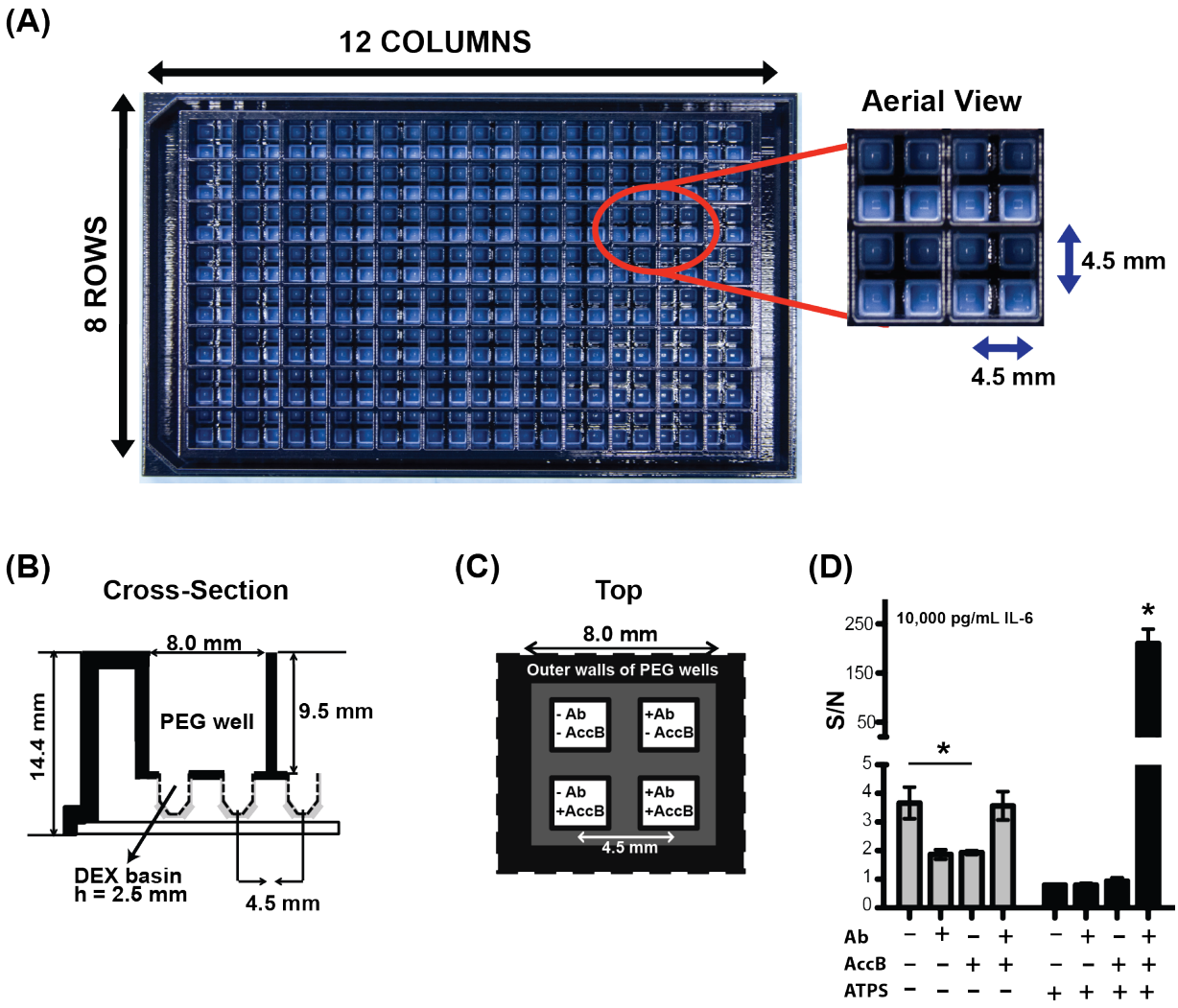

Figure 2.3: Custom microplates for ATPS-multiplexed assays. (**A**) A photograph of the custom 96-well microplate. Each of the 96 wells contains four white micro-basins for stabilizing four patterned dextran droplets within the black plate matrix. (**B**) A cross-sectional diagram of the custom plate showing micro-basins for DEX droplet stabilization. (**C**) A top-view diagram depicting the configuration of Ab-AccB complexes as used for the cross-reaction analysis in **D**. (**D**) In the presence of ATPS, background levels were low, no cross-reactions were observed, and maximum luminescent signal was detected only when both Ab & AccB were dispensed into the same microbasin (black bars). But in the absence of ATPS, background levels were high and significant cross-reactions occurred (grey bars) (*$P < 0.05$ by one-way ANOVA and Tukey's post-test). AlphaLISA signal was normalized to control experiments where the buffer or DEX respectively did not contain spiked IL-6. Error bars represent mean values ± SEM, over 3 replicates (Ab, detection antibody; AccB, acceptor beads).

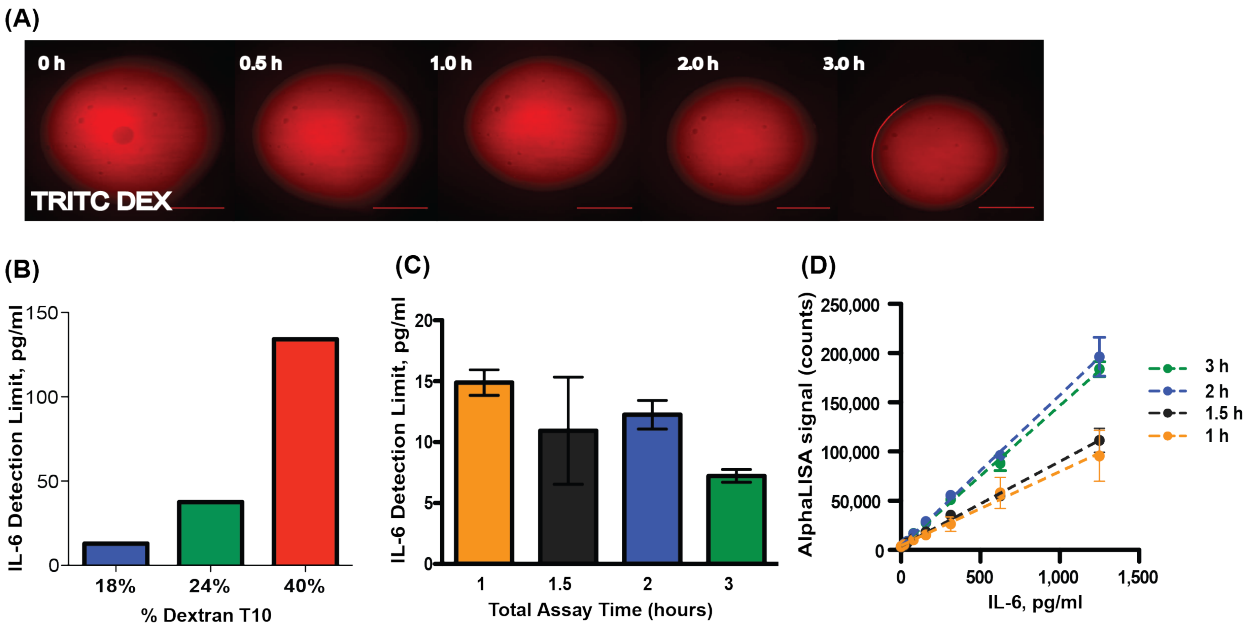

Figure 2.4: Optimizing ATPS assay incubation time. (**A**) Time lapse showing dextran droplet stability in the custom plates over the course of 3 hours at room temperature. Scale bar, 500 mm. (**B**) Mean limit of detection for singlplex IL-6 ATPS-AlphaLISA as a function of DEX (Mw. 10,000) concentration. (**C**) Mean limit of detection values for singleplex IL-6 ATPS-AlphaLISAs as a function of total assay time. The means were not significant upon analysis by one-way ANOVA and Tukey's post-test. (**D**) Standard curves for singlplex IL-6 ATPS assays indicate that 2-hour assay times have greatest AlphaLISA signal counts. Error bars represent means ± SEM.

Table 2.1. Partition coefficients of antigens and antibody-bead reagents in ATPS. Antigens and antibody-bead reagents partition to DEX in our ATPS assays. The partition coefficient (K_{part}) was defined as the concentration of reagent in PEG divided by the concentration of reagent in DEX.

	Detection Antibody Type	**Detection Antibody, K_{part}**	**Antigen, K_{part}**	**Bead, K_{part}**
CXCL10	Goat polyclonal	0.23	0.09	--
CXCL9	Goat polyclonal	0.30	0.28	--
IL-8	Mouse monoclonal Protein A purified	0.07	0.64	--
IL-6	Rat monoclonal	0.18	0.28	--
Omnibeads		--	--	0.01

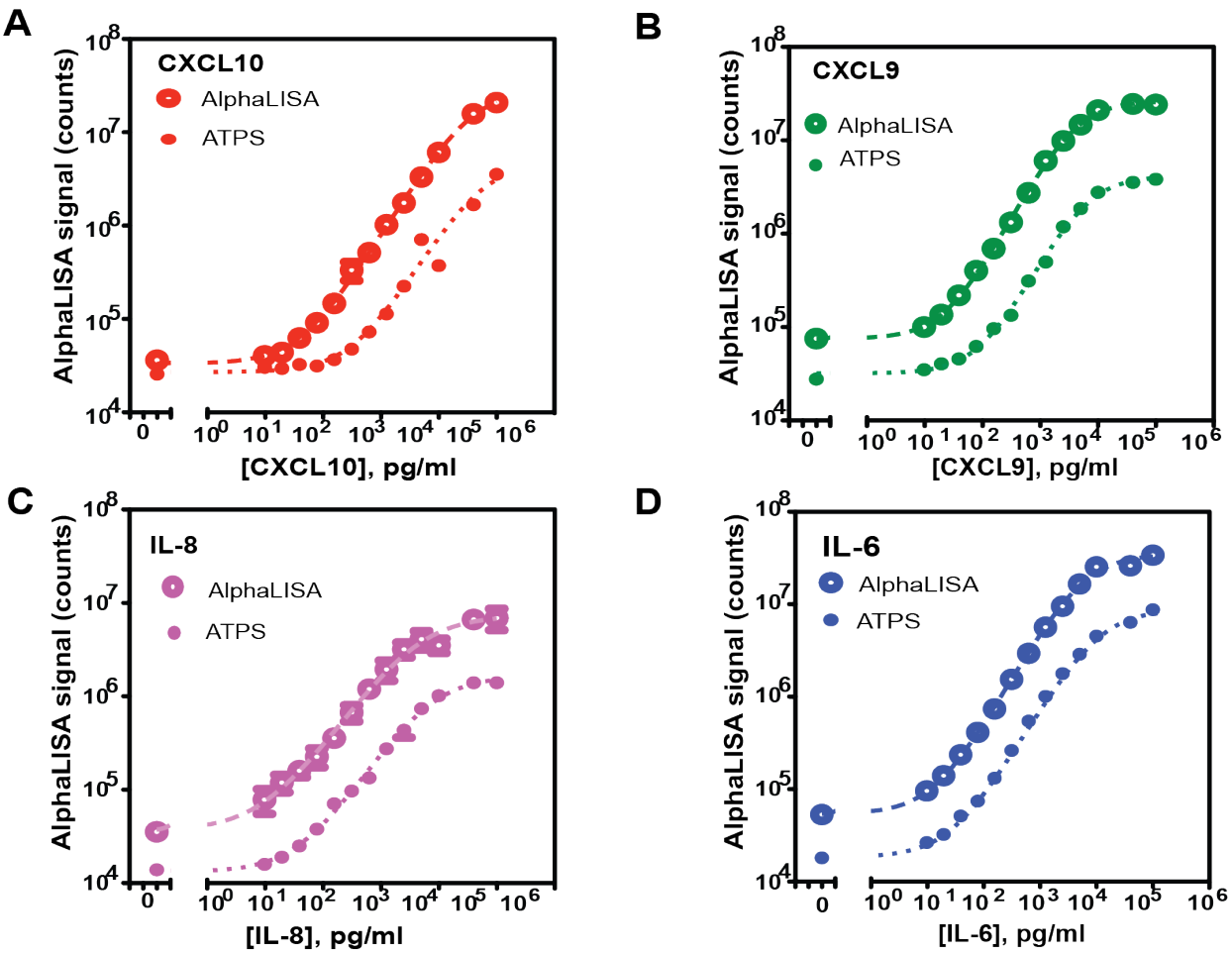

E

Detection Limits and Linear Dynamic Range (LDR)

		CXCL10	CXCL9	IL-8	IL-6
Singleplex ATPS	**LoD** **LDR**	89.8 pg/ml 2.5 logs	27.9 pg/ml 3.0 logs	11.5 pg/ml 3.4 logs	10.3 pg/ml 3.5 logs
AlphaLISA	**LoD** **LDR**	11.8 pg/ml 3.4 logs	21.8 pg/ml 3.1 logs	6.8 pg/ml 3.6 logs	6.2 pg/ml 3.7 logs

Figure 2.5: Comparison of limit of detection (LoD) and linear dynamic range (LDR) for singleplex ATPS assays (2 µl reagents) and conventional singleplex AlphaLISAs (20 µl reagents) (**A-D**). (**E**) Quantification of LoDs and LDRs. Error bars represent means ± SEM. The tenfold decrease in required antibody-beads accounts for the overall reduced AlphaLISA signal in the ATPS assays. Consequently ATPS standard curves are shifted downwards from the AlphaLISA curves in. However, the signal-to-noise ratios are comparable between both assay formats for all tested antigens.

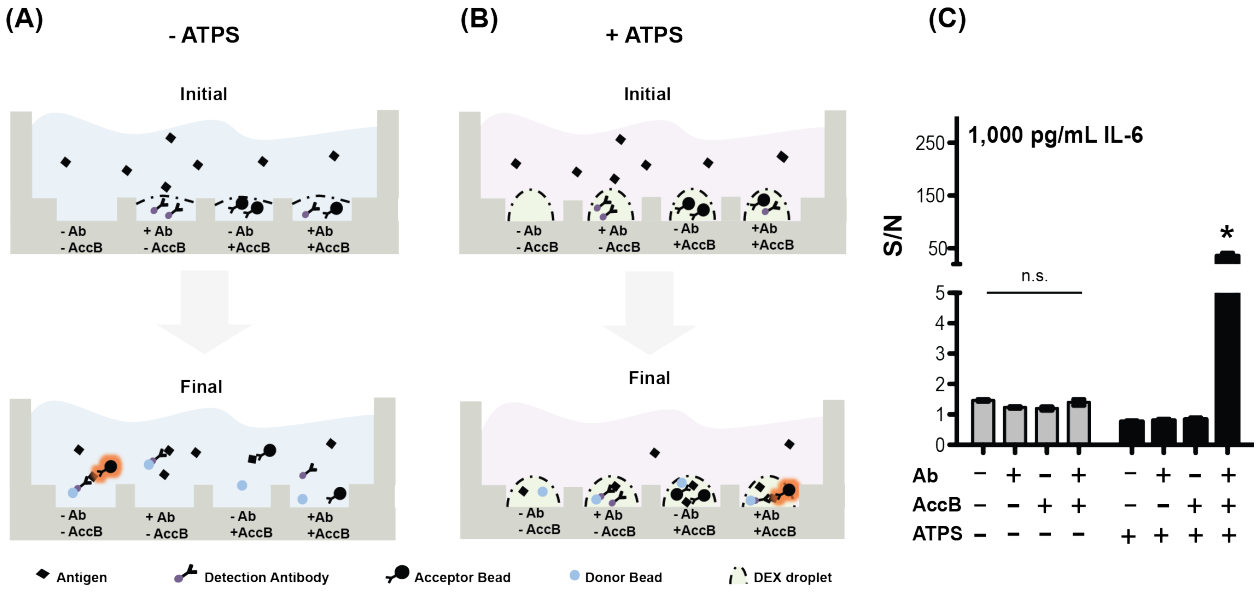

Figure 2.6: ATPS-multiplexed assays confine antibody-bead reagents and prevent reagent cross-reactions. (**A**) In the absence of ATPS, detection antibodies (Ab), acceptor beads (AccB), and donor beads freely circulate in assay buffer. (**B**) In the presence of ATPS, Ab, AccB, and donor beads remain localized in DEX droplets while antigens diffuse from the bulk PEG phase into DEX droplets. (**C**) In the absence of ATPS, droplets containing Ab only, AccB only or no reagent generated luminescent signals similar to the signal detected when both Ab and AccB were dispensed into the same microbasin (grey bars) (n.s. by one-way ANOVA and Tukey's post-test). But spotting Ab, AccB, and donor beads in DEX, confined the reagents at the correct working concentrations in the micro-basins, producing the expected level of luminescent signal for 1,000 pg/ml IL-6, without any enhancement of signal for the Ab only, AccB only or the Empty cases (black bars) (*$P < 0.05$ by one-way ANOVA and Tukey's post-test). Error bars represent mean values ± SEM, over 3 replicates.

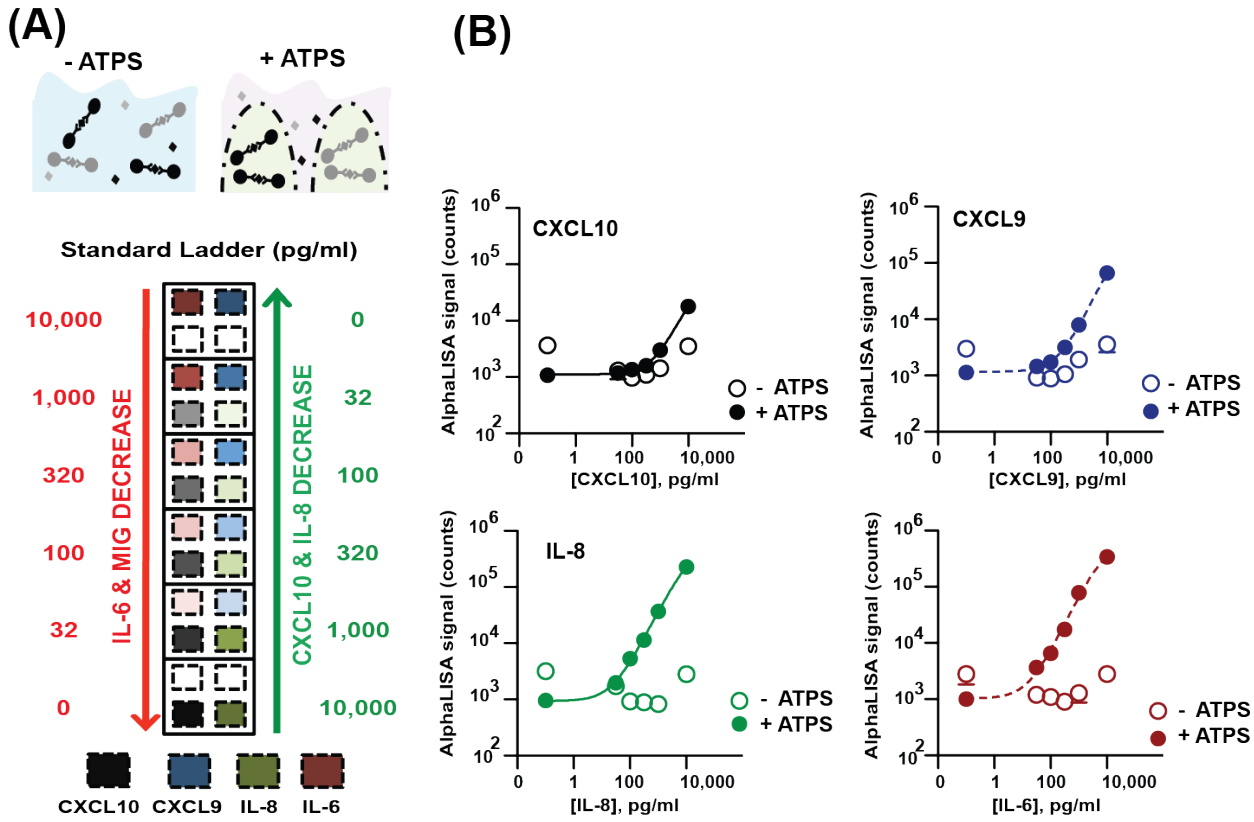

Figure 2.7: Co-localizing bead-based reagents in ATPS droplets is necessary to perform multiplexed homogeneous assays. (**A)** Protein levels in standard ladder decreased (IL-6 and CXCL9) while CXCL10 and IL-8 levels increased. (**B**) Higher background levels were noted in the multiplex standard curves in buffer only (no ATPS), indicating significant antibody cross-reactions. In contrast, lower background levels were observed when antibody-bead reagents were co-patterned in DEX (ATPS), validating the lack of antibody cross-reactions in ATPS-multiplexed AlphaLISA assays. Error bars represent means ± SEM.

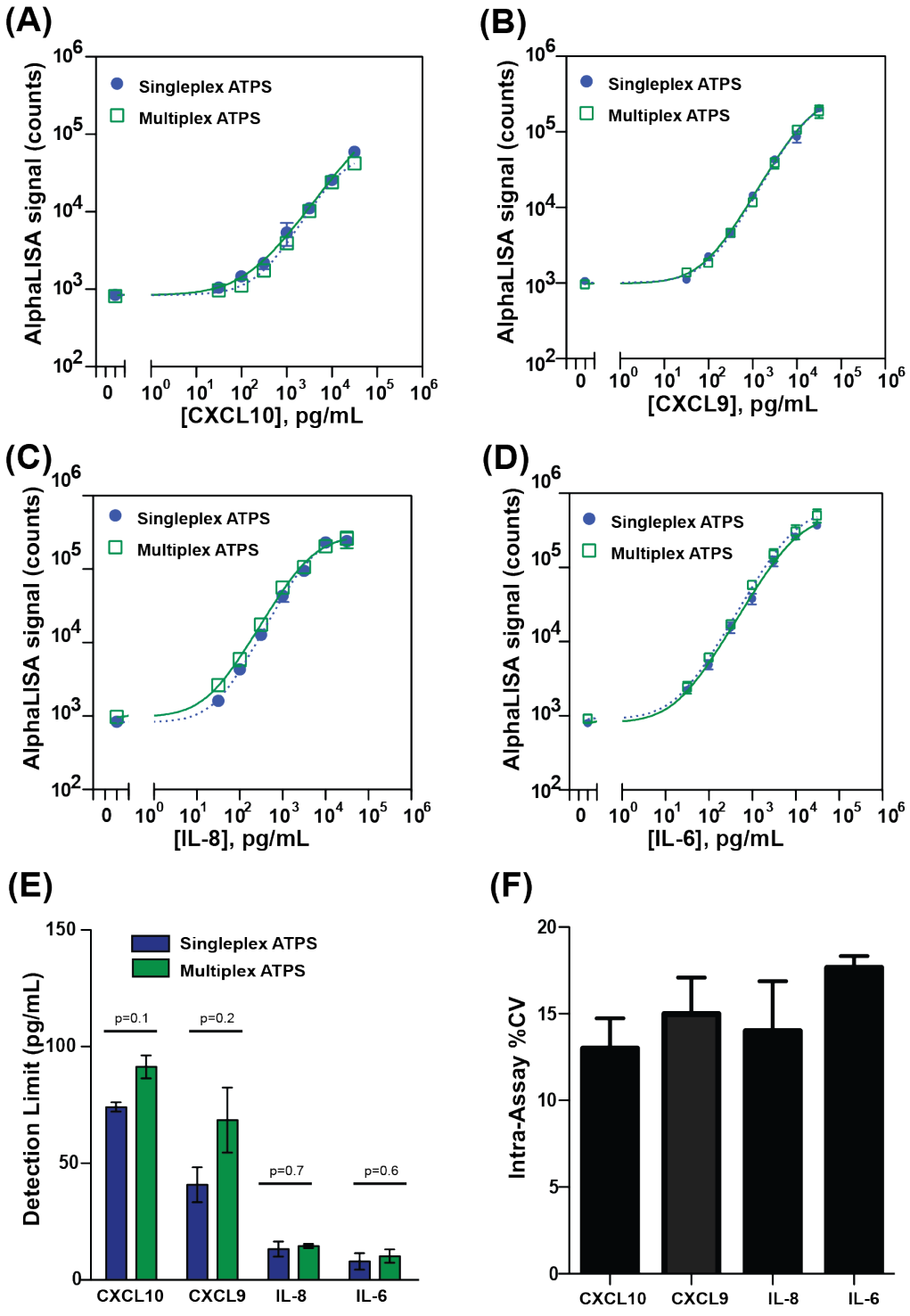

Figure 2.8: Correlation between ATPS-singleplexed and –multiplexed AlphaLISAs for four proinflammatory cytokines: (**A**) CXCL10, (**B**) CXCL9, (**C**) IL-8 and (**D**) IL-6. (**E**) Sensitivity of cytokine detection between singleplex and multiplex ATPS assays (p-values calculated by two-tailed t-tests). (**F**) Mean intra-assay CVs for ATPS-multiplexed AlphaLISA. Data in **A-D** were fitted with a four parameter logistic function. Error bars represent mean values ± SEM, over 3 replicates.

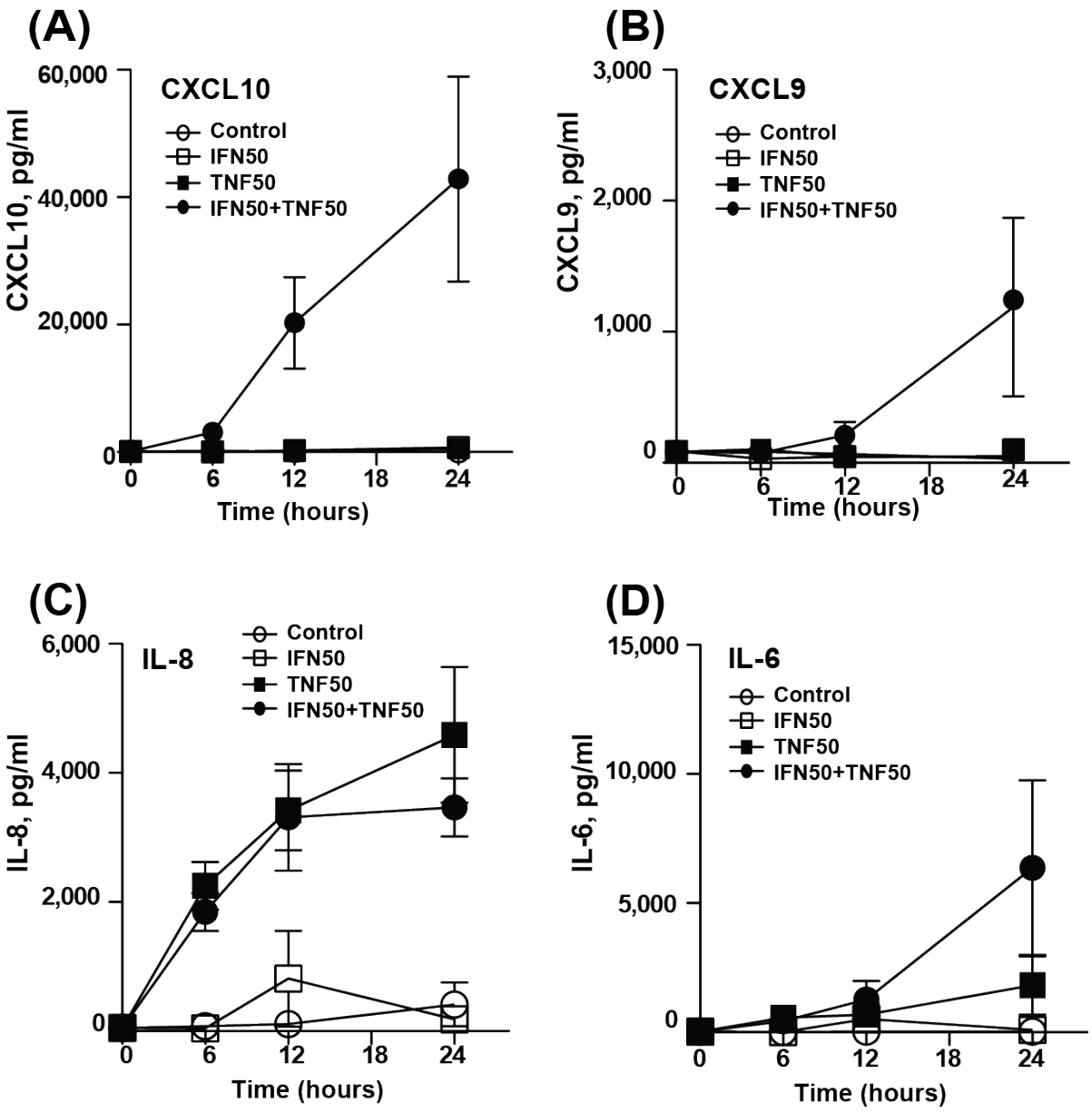

Figure 2.9: Dose and time-dependent effects of TNF-α and IFN-γ stimulated A549 cells on the release of proinflammatory cytokines: (**A**) CXCL10, (**B**) CXCL9, (**C**) IL-8 and (**D**) IL-6. Cells were stimulated at the indicated times with 50 ng/ml TNF-a (TNF50) alone, 50 ng/ml IFN-γ (IFN50) alone, or 50 ng/ml IFN-γ and 50 ng/ml TNF-α (IFN50 + TNF50). Protein levels measured via ATPS-multiplexed AlphaLISA. Error bars represent means ± SEM.

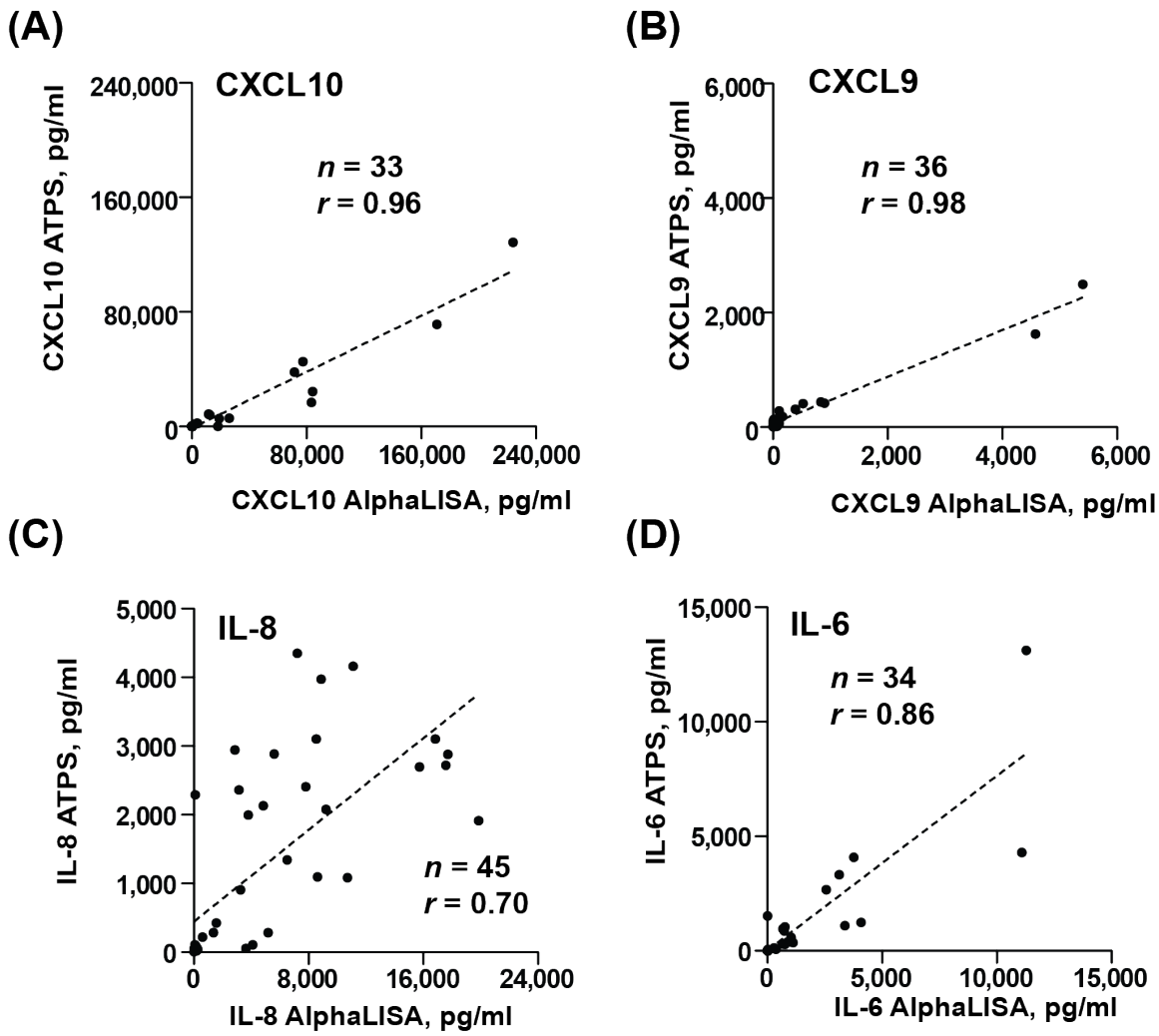

Figure 2.10: Correlation of measured values between the ATPS-multiplexed and conventional AlphaLISA assays for (**A**) CXCL10, (**B**) CXCL9, (**C**) IL-8, and (**D**) IL-6 in cell culture supernatants. Correlation is reported using the Pearson r correlation coefficient. Error bars represent means ± SEM.

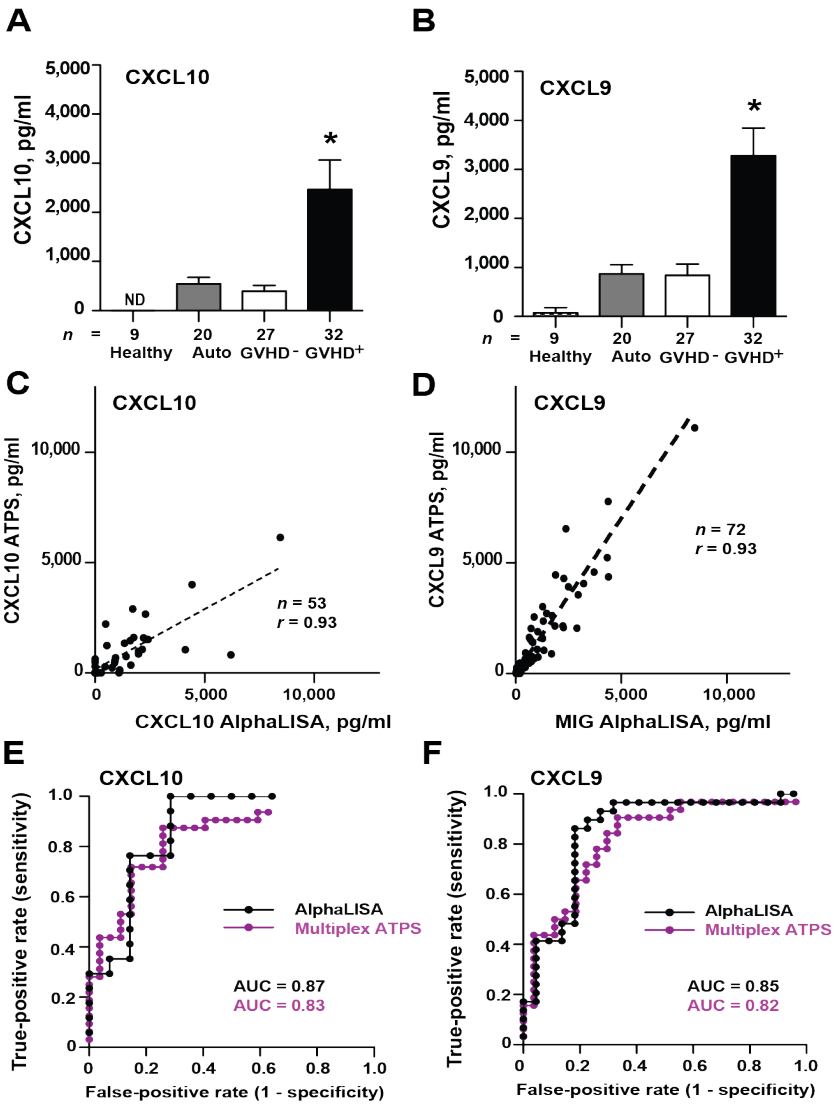

Figure 2.11: Multiplexed protein measurements in plasma of patients who had undergone bone marrow transplantation. (**A, B**) Mean values of CXCL10 and CXCL9 concentrations from 88 healthy, autologous, no GVHD, and chronic GVHD patients measured by ATPS-Multiplexed AlphaLISA assays. Samples were measured in triplicate on one plate and in 3 independent experiments. Both CXCL10 and CXCL9 were significantly elevated in GVHD+ patients compared to all other patient groups (*$P < 0.05$ by one-way ANOVA and Tukey's post test) (**C, D**) Correlation of measured values between the multiplex ATPS assay and conventional AlphaLISA for plasma samples. Correlation of protein levels in clinical patient plasma for CXCL9 and CXCL10 are reported using the Pearson r correlation coefficient. (**e-f**) Receiver operating characteristic (ROC) curves comparing CXCL10 and CXCL9 concentrations in patients without GVHD and patients with GVHD. ROC curves for ATPS-Multiplexed AlphaLISAs are compared to ROC curves obtained from singleplex AlphaLISA. All error bars represent means ± SEM. ND = Not Detectable.

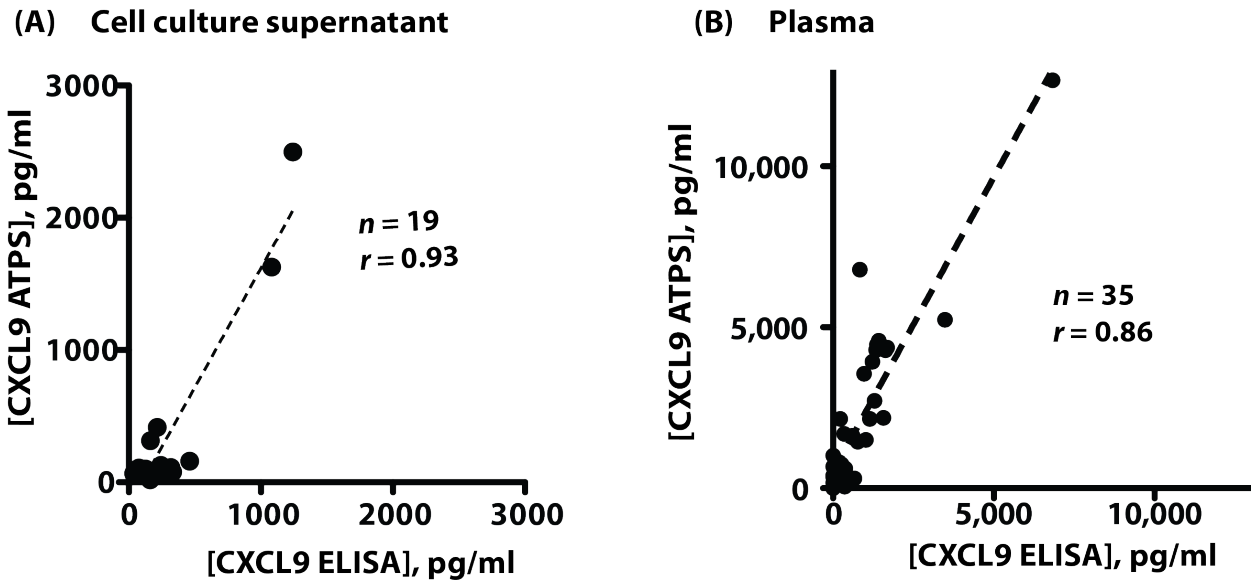

Figure 2.12: Correlation of measured CXCL9 values between the ATPS-multiplexed AlphaLISA and conventional singleplex ELISA for (**A**) cell culture supernatants and (**B**) plasma samples. Correlation of protein levels in clinical patient plasma for CXCL9 is reported using the Pearson r correlation coefficient.

2.5 References

Albertsson, P.-A. *Partition of Cell Particles and Macromolecules* 3rd edition (Wiley, 1986)

Armbruster, D.A. & Pry, T. Limit of blank, limit of detection and limit of quantitation. *Clin Biochem Rev* **29 Suppl 1**, S49-52 (2008).

Boost, K.A. et al. IFN-gamma impairs release of IL-8 by IL-1beta-stimulated A549 lung carcinoma cells. *BMC Cancer* **8**, 265 (2008).

Chan, S.M., Ermann, J., Su, L., Fathman, C.G. & Utz, P.J. Protein microarrays for multiplex analysis of signal transduction pathways. *Nat Med* **10**, 1390-1396 (2004).

Chau, C.H., Rixe, O., McLeod, H. & Figg, W.D. Validation of analytic methods for biomarkers used in drug development. *Clin Cancer Res* **14**, 5967-5976 (2008).

Crestani, B. et al. Alveolar type II epithelial cells produce interleukin-6 in vitro and in vivo Regulation by alveolar macrophage secretory products. *J Clin Invest* **94**, 731-740 (1994).

Croudace, J.E. et al. Chemokine-mediated tissue recruitment of CXCR3+ CD4+ T cells plays a major role in the pathogenesis of chronic GVHD. *Blood* **120**, 4246-4255 (2012).

Eglen, R.M. et al. The use of AlphaScreen technology in HTS: current status. *Curr Chem Genomics* **1**, 2-10 (2008).

Fiema, B. et al. High throughput sequential ELISA for validation of biomarkers of acute graft-versus-host disease. *J Vis Exp* (2012).

Gaster, R.S., Hall, D.A. & Wang, S.X. Autoassembly protein arrays for analyzing antibody cross-reactivity. *Nano Lett* **11**, 2579-2583 (2011).

Gonzalez, R.M. et al. Development and validation of sandwich ELISA microarrays with minimal assay interference. *J Proteome Res* **7**, 2406-2414 (2008).

Ikami, M. et al. Immuno-pillar chip: a new platform for rapid and easy-to-use immunoassay. *Lab Chip* **10**, 3335-3340 (2010).

Imanguli, M. et al. Increased T-bet+ cytotoxic effectors and type I interferon-mediated processes in chronic graft-versus-host disease of the oral mucosa. *Blood* **113**, 3620-3630 (2009).

Kingsmore, S.F. et al. Identification of diagnostic biomarkers for infection in premature neonates. *Mol Cell Proteomics* **7**, 1863-1875 (2008).

Kingsmore, S.F. Multiplexed protein measurement: technologies and applications of protein and antibody arrays. *Nat Rev Drug Discov* **5**, 310-320 (2006).

Koch, M. et al. Role of local pulmonary IFN-gamma expression in murine allergic airway inflammation. *Am J Respir Cell Mol Biol* **35**, 211-219 (2006).

Lee, S. Have we made progress in the management of chronic graft-versus-host disease? *Best Pract Res Clin Hematol* **23**, 529-535 (2010).

Li, H., Leulmi, R.F. & Juncker, D. Hydrogel droplet microarrays with trapped antibody-functionalized beads for multiplexed protein analysis. *Lab Chip* **11**, 528-534 (2011).

Liu, M.Y. et al. Multiplexed analysis of biomarkers related to obesity and the metabolic syndrome in human plasma, using the Luminex-100 system. *Clin Chem* **51**, 1102-1109 (2005).

Min, C.K. et al. The kinetics of circulating cytokines including IL-6, TNF-alpha, IL-8 and IL-10 following allogeneic hematopoietic stem cell transplantation. *Bone Marrow Transplant* **28**, 935-940 (2001).

Mukhopadhyay, S., Hoidal, J.R. & Mukherjee, T.K. Role of TNF-alpha in pulmonary pathophysiology. *Respir Res* **7**, 125 (2006).

Paczesny, S. et al. A biomarker panel for acute graft-versus-host disease. *Blood* **113**, 273-278 (2009).

Pechkovsky, D.V. et al. CCR2 and CXCR3 agonistic chemokines are differently expressed and regulated in human alveolar epithelial cells type II. *Respir Res* **6**, 75 (2005).

Pla-Roca, M. et al. Antibody colocalization microarray: a scalable technology for multiplex protein analysis in complex samples. *Mol Cell Proteomics* **11**, M111.011460 (2012).

Qin, L., Vermesh, O., Shi, Q. & Heath, J.R. Self-powered microfluidic chips for multiplexed protein assays from whole blood. *Lab Chip* **9**, 2016-2020 (2009).

Sauty, A. et al. The T cell-specific CXC chemokines IP-10, MIG, and I-TAC are expressed by activated human bronchial epithelial cells. *J Immunol* **162**, 3549-3558 (1999).

Schweitzer, B. et al. Multiplexed protein profiling on microarrays by rolling-circle amplification. *Nat Biotechnol* **20**, 359-365 (2002).

Smart, S.J. & Casale, T.B. Pulmonary epithelial cells facilitate TNF-alpha-induced neutrophil chemotaxis. A role for cytokine networking. *J Immunol* **152**, 4087-4094 (1994).

Socie, G., Ritz, J. & Martin, P.J. Current challenges in chronic graft-versus-host disease. *Biol Blood Marrow Transplant* **16**, S146-151 (2010).

Tavana, H. et al. Nanolitre liquid patterning in aqueous environments for spatially defined reagent delivery to mammalian cells. *Nat Mater* **8**, 736-741 (2009).

Tawara, I. et al. Interleukin-6 modulates graft-versus-host responses after experimental allogeneic bone marrow transplantation. *Clin Cancer Res* **17**, 77-88 (2011).

Theilacker, N., Roller, E.E., Barbee, K.D., Franzreb, M. & Huang, X. Multiplexed protein analysis using encoded antibody-conjugated microbeads. *J R Soc Interface* **8**, 1104-1113 (2011).

Westekemper, H. et al. Differential chemokine expression in chronic GVHD of the conjunctiva. *Bone Marrow Transplant* **45**, 1340-1346 (2010).

Chapter Three

Aqueous Two-Phase System Patterning for Crosstalk-free, Multiplexed, Heterogeneous Enzyme-Linked Immunosorbent Assays

This chapter describes the use of aqueous two-phase systems to prevent the antibody crosstalk problem – the key limitation of current multiplexed heterogeneous immunoassays. Detection antibodies were spatially localized in aqueous microdroplets. Data from this crosstalk-free multiplexed ELISA correlated strongly with data from conventional singleplex ELISAs. Notably, these innovative crosstalk-free assays allow robust multiplexing of any reliable singleplex ELISA. Therefore, there is no need to cross-validate reagents every time new candidate biomarkers are available or reagents change.

3.1 Introduction

Protein biomarkers assess the physiological state of the human body and their concentrations change as a result of microbial infection, inflammation, or malignancy. Hundreds of potential disease-specific biomarkers have been reported; however because of the complexities of the body, individual biomarkers cannot truly identify many diseases (Vasan 2006; Paczesny 2009). Thus, there is a need for simultaneous protein biomarker analysis, or so-called multiplexed biomarker assays. Many multiplexed biomarker tests exist but these tests suffer from the nonspecific binding of detection antibodies to non-target biomarkers, i.e. antibody crosstalk. Antibody crosstalk increases assay background levels, reduces sensitivity, limits quantification accuracy, and increases false positive signals. Technological advances that eliminate antibody crosstalk in multiplexed biomarker tests will inevitably overcome these inherent test limitations.

We have eradicated the problem of detection antibody crosstalk by using an aqueous two-phase system (ATPS) composed of polyethylene glycol (PEG) and dextran (DEX) to confine detection antibodies to regions where the corresponding capture antibodies are patterned (Tavana *et al.* 2009, Tavana *et al.* 2010, Frampton *et al.* 2013). This new method, referred to as ATPS-ELISA, works on three principles: 1) droplets of the denser DEX solution sink in the PEG solution and remain in contact with the assay plate during incubation; 2) interfacial tensions between DEX-PEG and DEX-assay plate cause the DEX droplet to assume a dome shape that remains in place; and 3) antibodies are retained in the DEX phase due to partitioning effects, i.e. they are less susceptible to diffusion from their original location. We demonstrate that this approach is effective at simultaneously detecting at least four different chemokines and cytokines associated with acute graft-versus-host disease (GVHD), a disease that requires multiple biomarker analysis for definitive diagnosis and prognosis (Paczesny *et al.* 2009; Paczesny *et al.*

2010). Our measurements were free from antibody crosstalk and required less antibody and patient sample than conventional ELISA.

3.2 Materials and Methods

3.2.1. Reagents

ATPSs were prepared from DEX solutions of various molecular weights and concentrations (10 kDa and 500 kDa (Pharmacosmos), and 40 kDa (Sigma)), with 35 kDa PEG of various concentrations (Sigma). Phycoerythrin-conjugated mouse anti-human CD184 IgG2α (cat # 555974, BD Pharmingen) and 500 kDa fluorescein-dextran (cat # D7136, Molecular Probes) were used to assess droplet stability and antibody localization over time. ELISA kits for human sTNFR1 (cat # DY225), human IL-2 Rα (cat # DY225), human ST2 (cat # DY523), human trappin-2/elafin (cat # DY1747), and human HGF (cat # DY294) were purchased from R&D Systems and SuperSignal ELISA Femto Substrate (cat # 37074) was purchased from Thermo Scientific.

3.2.2. ELISA Protocol

Manufacturer specifications for ELISA assays were followed, with several modifications. Briefly, polystyrene plates of various formats were coated with either a mixture of capture antibodies or separate capture antibody spots reconstituted in PBS. The plates were then wrapped in Parafilm to limit evaporation and stored at 4 ˚C overnight. Plates were washed five times with wash buffer (PBS, containing 0.05% Tween-20), and blocked with 3.0 wt% casein for 1 h. After blocking, the plates were washed five times and incubated with sample solutions for 2 h.

Following antigen application, plates were washed five times and incubated for 2 h with detection antibody in either a traditional ELISA or ATPS-ELISA format. For conventional multiplexed ELISAs, detection antibodies were bath applied according to manufacturer specifications. For ATPS-ELISAs, the plate was first filled with a solution of PBS containing PEG and 0.1 wt% casein. DEX droplets containing the appropriate biotinylated detection antibody were then pipetted into the PEG. Following detection antibody incubation, the plates were washed eight times followed by incubation with streptavidin-conjugated horseradish peroxidase for 1 h. Plates were then washed five times and incubated with SuperSignal ELISA Femto Maximum Sensitivity Substrate (37074, Thermo Scientific). Chemiluminescent signal was detected using either a ChemiDoc XRS (BioRad) or FluorChem M (Protein Simple) imaging system.

3.2.3. Plate fabrication

Untreated polystyrene plates were used for both ATPS-ELISAs and conventional multiplexed ELISAs. To reduce the volume of sample required to perform the assay, several methods were used to customize the plates. In the alpha prototypes of the custom plate, sample volumes were contained by attaching a hydrophobic tape stencil to the plate surface. To aid in localization of capture antibody spots and DEX droplets containing detection antibody an indented array was fabricated as a feature of the plate surface by drilling into the surface of the polystyrene. The resulting indentations were ~2 mm in diameter and ~1-2 mm in depth. Beta prototypes of the custom plate were designed in AutoCAD (Autodesk) and SolidWorks (Dassault Systemes). Aluminum molds, containing a 9x9 array of 6.5 mm diameter sample wells that each contained four 1.5 mm diameter DEX-antibody wells, were fabricated using precision CNC

micromachining (Protomatic, Inc., Dexter, MI). Polystyrene dishes were heated above their glass transition temperature and the aluminum mold was stamped into the dish to mold the plate to its final dimensions.

3.2.4. Plasma samples

Heparinized plasma samples were collected from patients who received allogeneic bone marrow transplantation at the University of Michigan between 2000 and 2010. Plasma samples were collected under protocols approved by the University of Michigan Institutional Review Board and stored at the University of Michigan. To mitigate effects associated with mismatch between the standard diluent and plasma sample several approaches were taken. First, an appropriate dilution of plasma was determined for each biomarker. Next, spike and recovery and linearity of dilution for the standard and sample diluents containing FBS, BSA and/or healthy pooled plasma were investigated. Finally, a standard diluent of 10% healthy pooled plasma and 1% FBS, and a sample diluent of 10% patient plasma and 1% FBS were selected and used for all patient sample analyses.

3.2.5. Statistical analysis

All plots and statistical analyses were carried out in either Sigmaplot with Sigmastat (Systat Software) or Graphpad. Standard curves were fitted using a four parameter logistic function that was used to predict unknowns. The limit of detection (LoD) was determined from the equation $LoD = LoB + 1.645\ (SD_{low\ concentration\ sample})$, where SD is the standard deviation and LoB is the limit of blank. LoB was calculated from $LoB = mean_{blank} + 1.645\ (SD_{blank})$ (Armbruster and Pry

2008). Linear dynamic range (LDR) was determined using LDR = Maximum linear response/ LoD. To compare ATPS-ELISA values with conventional ELISA values, a Pearson product-moment correlation test was used with values of |0.3-0.5| and |0.5-1.0| considered to be medium strength and strong correlations respectively.

3.3 Results and Discussion

3.3.1. Optimizing ATPS parameters for multiplexed ELISAs

ATPS-ELISA (**Fig. 3.1A**) is performed using similar steps to conventional sandwich ELISA (**Fig. 3.1B**). The main difference is that ATPS-ELISAs use detection antibody solutions that are deposited in DEX droplets over pre-arrayed capture antibody spots. Localization of detection antibodies in dextran droplets prevents antibody cross-reactions because interaction of multiple detection antibodies as well as non-target antigen recognition by detection antibodies is hindered.

We studied the effect of chemiluminescent ELISA signal as a function of polymer concentrations (**Fig. 3.2A-B**). We observed that signal area decreased as polymer concentration increased for each phase system tested. This is in part due to the increased interfacial tension and viscosity at higher polymer concentrations, which prevent dextran droplets from spreading. To demonstrate that detection antibodies are retained within the DEX phase during ATPS-ELISAs, we performed time-lapse studies of phycoerythrin (PE)-IgG in DEX over the course of 2 h (**Fig. 3.1C**). DEX-confinement of the fluorescent detection antibodies over this time period indicated that detection antibodies partitioned stably in the DEX phase. We selected the 20% DEX 500K/20% PEG 35K system for multiplexed ELISAs because this ATPS produced the smallest signal area for a given DEX volume.

3.3.2. ATPS is necessary to prevent antibody cross-reactions

To confirm that an ATPS was required to localize the antibodies, we spotted the detection antibody on a dry well that had been treated with capture antibody and antigen (**Fig. 3.3A**). The detection antibody spread across the well, producing a large signal area that would prevent multiplexing. In contrast, in ATPS, a pronounced discrete chemiluminescence signal was observed (**Fig. 3.3B**). Finally, if the detection antibody was introduced into a PEG bath with a PBS carrier solution, the detection antibody could not come into contact with the plate and no signal was observed (**Fig. 3.3C**). These experiments demonstrate that a PEG/DEX system is absolutely necessary for localizing detection antibodies in our multiplexed ELISA format.

Next, we systematically proved that ATPSs prevented detection antibody crosstalk (**Fig. 3.4**). First, we deposited closely spaced droplets of capture antibodies: a mouse anti-human antibody recognizing tumor necrosis factor receptor (TNFR1) and an anti-goat antibody recognizing the goat anti-human TNFR1 detection antibody. After incubating with a solution containing TNFR1, the goat detection antibody was spotted above the mouse capture antibody-antigen complex in DEX. Upon analysis it was clear that there was no cross-reactivity signal for the ATPS format (**Fig. 3.4A**), while significant cross-reactivity was observed during conventional bath application of the detection antibodies (**Fig. 3.4B**). We next performed a duplex experiment with capture and detection antibodies for TNFR1 and ST2, where both the capture and detection antibodies were spotted in ATPS. We observed differential signal intensity between the two spots, again demonstrating that crosstalk did not occur (**Fig. 3.4C**). When the detection antibodies were bath applied in the same solution, this differential signal intensity was not observed, indicating the existence of crosstalk between these pairs of antibodies (**Fig. 3.4D**).

Finally, we produced partial overlap of the capture and detection antibodies (**Fig. 3.4E**). We observed a "cat eye"-shaped signal area, which is only possible if the detection antibody is perfectly retained in the DEX droplet, again demonstrating that our system can prevent crosstalk. A circular spot was observed when the detection antibody was bath applied, demonstrating that the "cat eye" was not an artifact of poor capture antibody spotting (**Fig. 3.4F**).

3.3.3. ATPS-multiplexed ELISAs can detect chemokines and cytokines in human plasma

In custom plates (**Fig 3.5A**), we generated standard curves for four GVHD biomarkers (HGF, Elafin, ST2 and TNFR1) in multiplexed format either with ATPS detection antibody spotting (solid lines in **Fig. 3.5C-F**) or in indivual singleplex ELISAs (dashed lines in **Fig. 3.5C-F**). With ATPS, we obtained linear dynamic ranges (LDR: HGF, 2.0; Elafin, 0.8; ST2, 2.0; and TNFR1, 1.6) and limits of detection (LoD: HGF, 96 pg/ml; Elafin, 1,437 pg/ml; ST2, 103 pg/ml; and TNFR1, 87 pg/ml) that were acceptable for prediction of GVHD in patient plasma. Multiplex ATPS-ELISAs generally out-performed singleplex ELISAs in terms of LDR (HGF, 1.7; Elafin, 0.1; ST2, 1.4; and TNFR1, 2.2 for singleplex ELISA) and LOD (LoD: HGF, 124 pg/ml; Elafin, 2,298 pg/ml; ST2, 431 pg/ml; and TNFR1, 62 pg/ml; values for singleplex ELISA). These observations are consistent with the observations of others and suggest that small spot sizes and assay volumes produce superior LoD and LDR values (Kai 2012).

We have demonstrated a 4-plex immunoassay against biomarkers of acute graft-versus-host-disease (GVHD) and performed tests on plasma of cancer survivors with and without GVHD. We compared three groups: healthy donors (n=20), allogeneic bone marrow transplant patients who did not get GVHD (GVHD-; n=19, median 28 days post-transplant) and allogeneic bone marrow transplant patients who had been diagnosed with acute GVHD (GVHD+, n=32,

median 100 days post-transplant). As expected, we measured significantly higher levels of HGF, Elafin, ST2, and TNFR1 in GVHD+ patients as compared to healthy donors and GVHD- patients (**Fig. 3.6A-D**). We compared our multiplexed values with single biomarker ELISA values and observed identical trends in the mean concentration of biomarkers between GVHD and non-GVHD patients (**Fig. 3.7A-D**). Notably, single biomarker ELISAs were performed in 384-well plates instead of 96-well plates, not only to conserve patient plasma but also because the signal spot size between 384-well single ELISAs was comparable to our ATPS-AlphaLISA. ATPS-ELISA chemiluminescence values correlated well with individual sandwich ELISAs by Pearson product-moment correlation (ρ=0.86, 0.72, 0.71, and 0.68), providing evidence that our ATPS-ELISA system is in accordance with conventional ELISA (**Fig. 3.8A-D**). Receiver operating characteristic (ROC) analysis indicated that our test was sensitive and specific for all four biomarkers, as determined by measuring the area under the curve (**Fig. 3.9A-B**). We postulate that the ATPS-ELISAs generally had better ROC curves than single biomarker ELISAs because: (i) washing small 384-wells for single ELISAs was difficult and poor washing may have resulted in higher background signals, (ii) we observed some optical crosstalk in signals obtained in standard ELISAs, which could also have increased our background signals, and (iii) difficulty in pipetting into small 384 wells may have resulted in uneven distribution of the chemiluminescent substrate in assay wells and also result in large signal variability. Collectively, these results indicate that the multiplexed ATPS-ELISA system can be used to detect complex diseases, such as acute GVHD, by simultaneously measuring the levels of multiple plasma biomarkers.

We developed a method that enables crosstalk-free multiplexing of commercially available ELISA kits. Confinement of detection antibodies in ATPS droplets effectively prevents antibody crosstalk. We validated the clinical utility of our system by detecting acute GVHD

biomarkers in recipients of allogeneic bone marrow transplants. Our results demonstrate that the ATPS-ELISA system can discriminate between acute GVHD patients and healthy transplant recipients with a low rate of false-positives, suggesting that this will be a clinically useful tool for GVHD diagnosis. Our assay offers several advantages over conventional singleplex ELISAs including use of small plasma volumes (10 µl of diluted plasma for four biomarkers), one hundred-fold less detection antibody consumption, and most importantly complete lack of antibody crosstalk in the multiplexed format. Other potential benefits that enhance the multiplexed ATPS-ELISAs include microscale surface localization effects that enhance detection antibody binding, more effective washing due to the shallow well profiles, and less depletion of chemiluminescent substrate, all of which can affect LoD and LDR.

3.4 Conclusions

In summary, we engineered a unique crosstalk-free multiplexed ELISA platform that prevents antibody crosstalk and produces high quality data with sensitivity similar to or better than existing singleplex ELISAs. Fewer wash steps minimize user error and allow faster time-to-first results. No specialized readers are needed, allowing substantial cost savings to researchers (chemiluminescent-based imagers or even light sensitive film can be used for readouts). Most importantly, the microscale patterning technology allows robust multiplexing of any ELISA that can be reliably performed in singleplex format. There is no need to cross-validate reagents every time a panel member changes or reagents change.

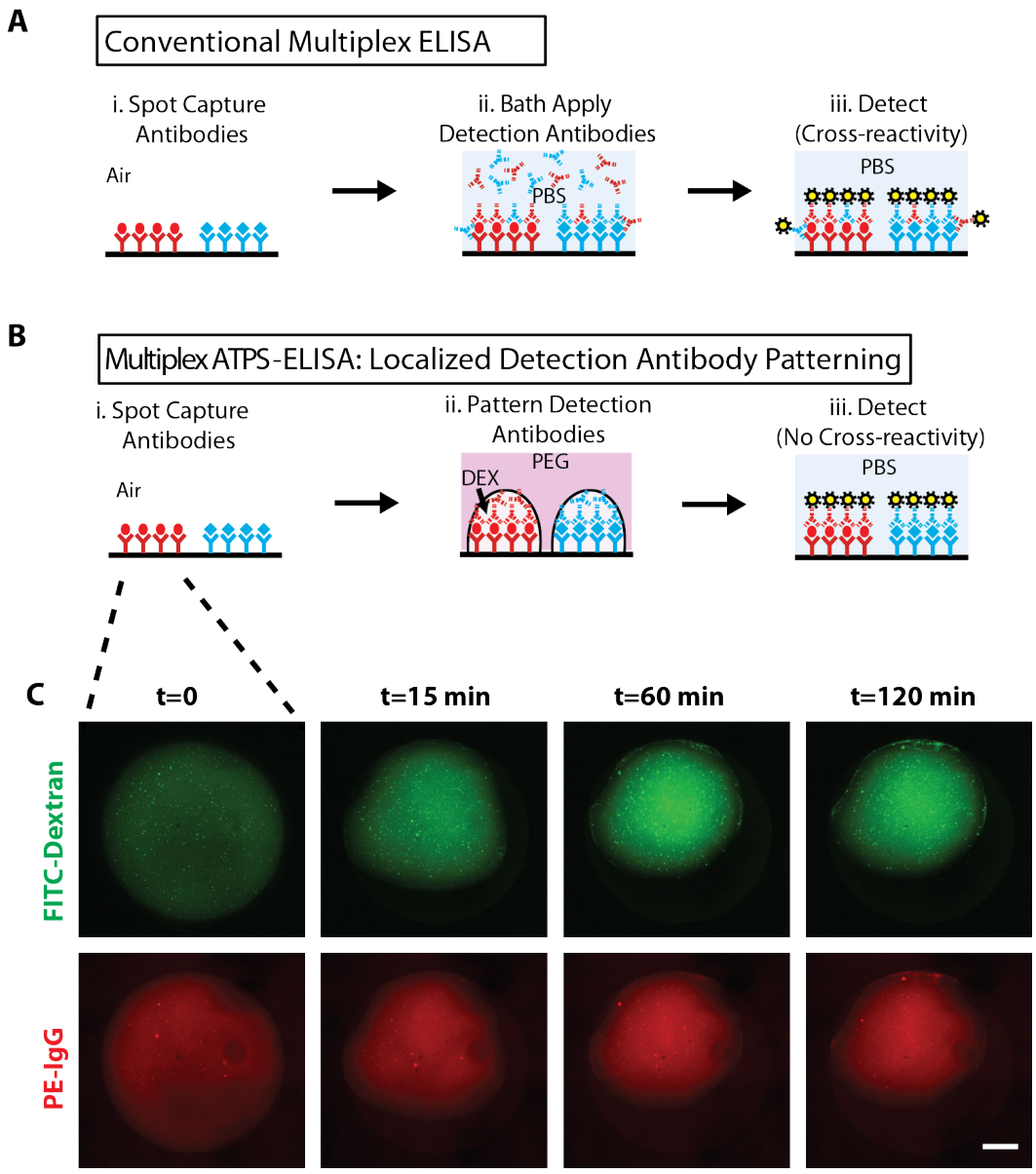

Figure 3.1: Schematic of (**A**) conventional multiplex ELISA and (**B**) multiplex ATPS-ELISAs. (**C**) Time-lapse fluorescent images, showing detection antibodies partition stably in dextran droplets in multiplexed ATPS-ELISAs.

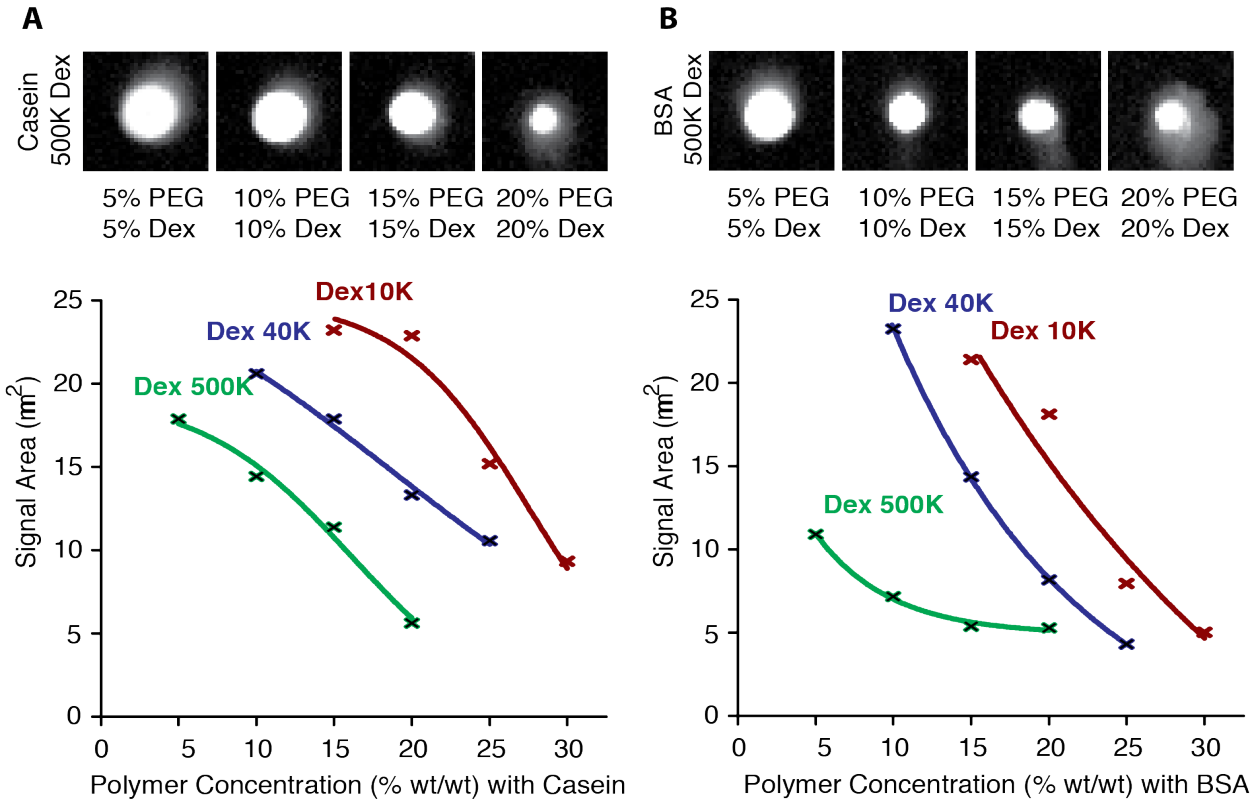

Figure 3.2: Effect of polymer concentrations and polymer molecular weights on signal area of chemiluminescent ELISA signals. Multiplex ATPS assays were blocked with either (**A**) casein or (**B**) bovine serum albumin (BSA).

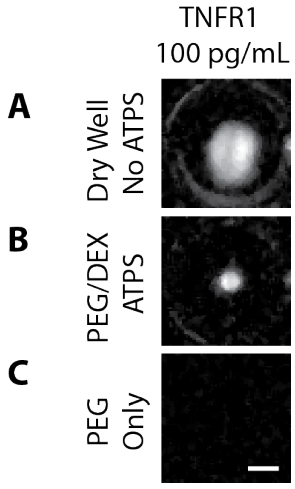

Figure 3.3: ATPS is necessary for localized chemiluminescent signals in multiplex ATPS-ELISAs. (**A**) In dry wells, without ATPS, signal spreads throughout well of 96-well plate. (**B**) In PEG/DEX ATPS, the chemiluminscent signal is localized. (**C**) In PEG only, no chemiluminscent signal is observed.

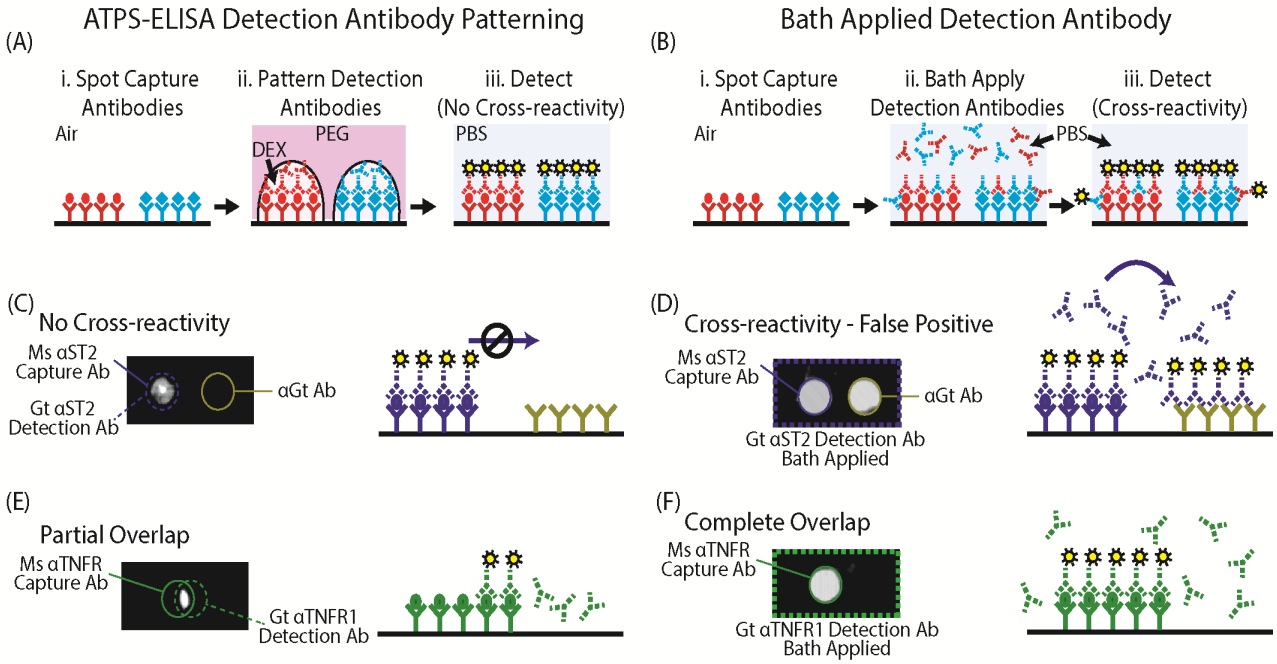

Figure 3.4: Localized ATPS-ELISA detection antibody patterning eliminates antibody cross-reactions (**A, C, E**) while bath application of detection antibody in conventional multiplexed ELISAs demonstrates significant antibody crossreactions (**B, D, F**).

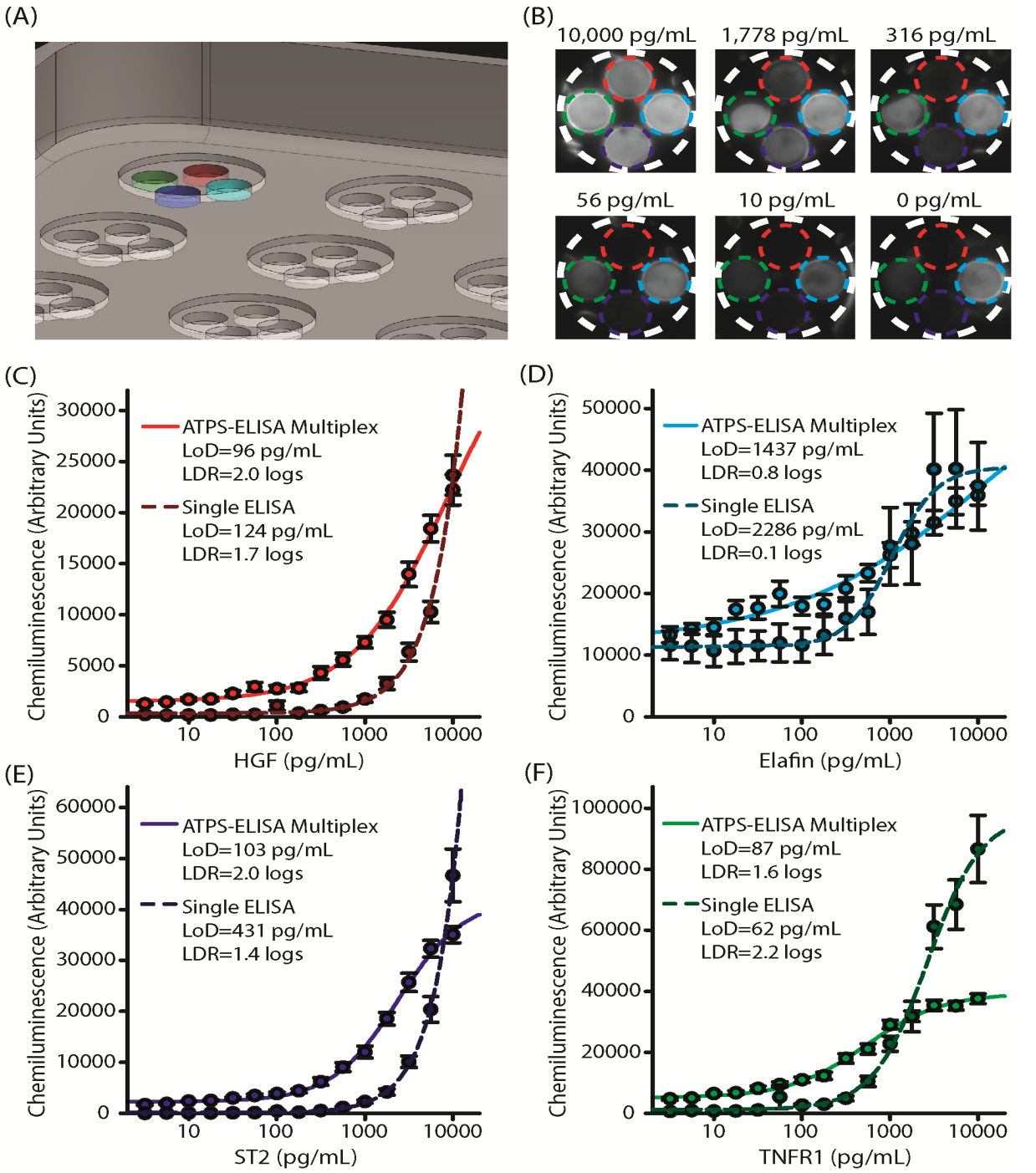

Figure 3.5: Multiplexed ATPS-ELISA for GVHD biomarkers. (**A**) Three-dimensional image showing custom plate design consisting of 4 DEX/antibody insets within a common shallow sample well. (**B**) Representative images of chemiluminescent standards. (**C-E**) Standard curves for all four GVHD biomarkers in PBS generated by densitometric quantification of chemiluminescence images compared to individual sandwich ELISAs (dashed lines). Error bars represent standard error of the mean.

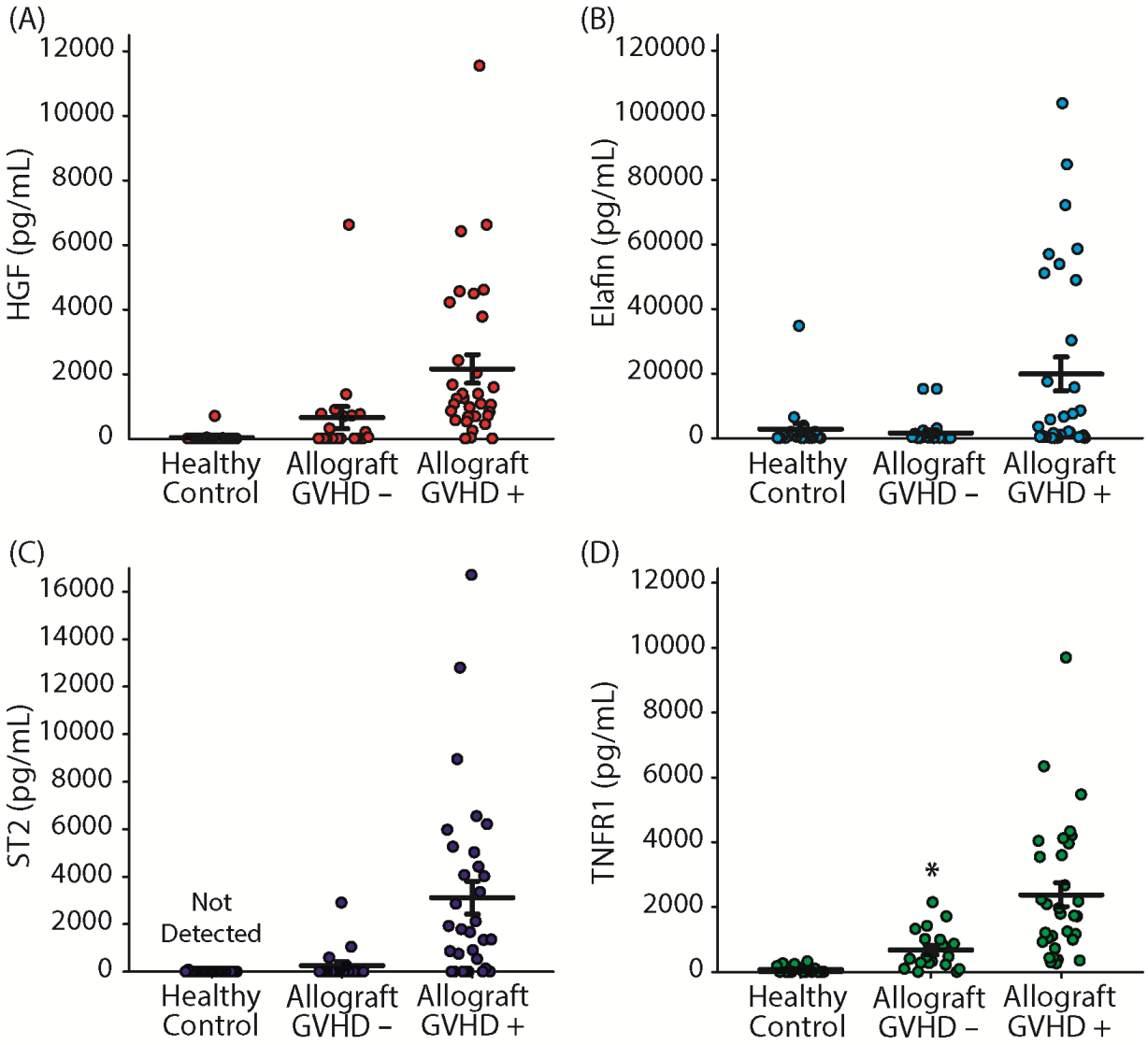

Figure 3.6: Multiplexed ATPS-ELISA detection of (**A**) HGF, (**B**) Elafin, (**C**) ST2, and (**D**) TNFR1 in plasma from patients who underwent bone marrow transplantation. The GVHD+ group displayed significantly high levels of all four biomarkers compared to the GVHD – and healthy control groups ($p<0.05$ by one-way ANOVA with Dunn's multiple comparison test). Error bars represent standard error of the mean.

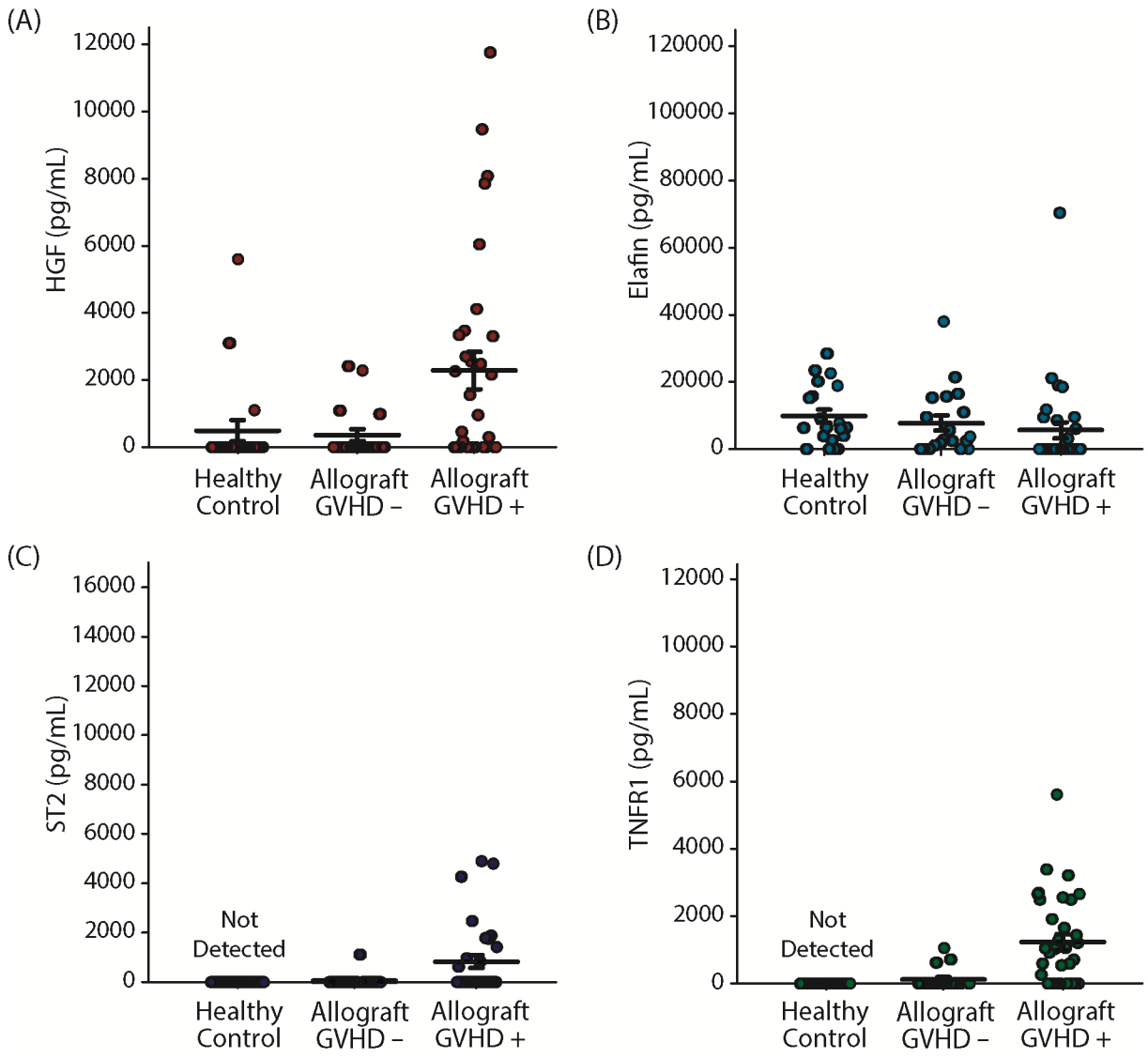

Figure 3.7: Measurement of (**A**) HGF, (**B**) Elafin, (**C**) ST2, and (**D**) TNFR1 from patient plasma using individual sandwich ELISAs. Significance between the GVHD+ group and the GVHD- and healthy control groups was obtained for HGF and TNFR1 ($p<0.05$ by one-way ANOVA with Dunn's multiple comparison test), but not for elafin or ST2, although ST2 values for the GVHD+ group tended to be higher than the other groups. Error bars represent standard error of the mean.

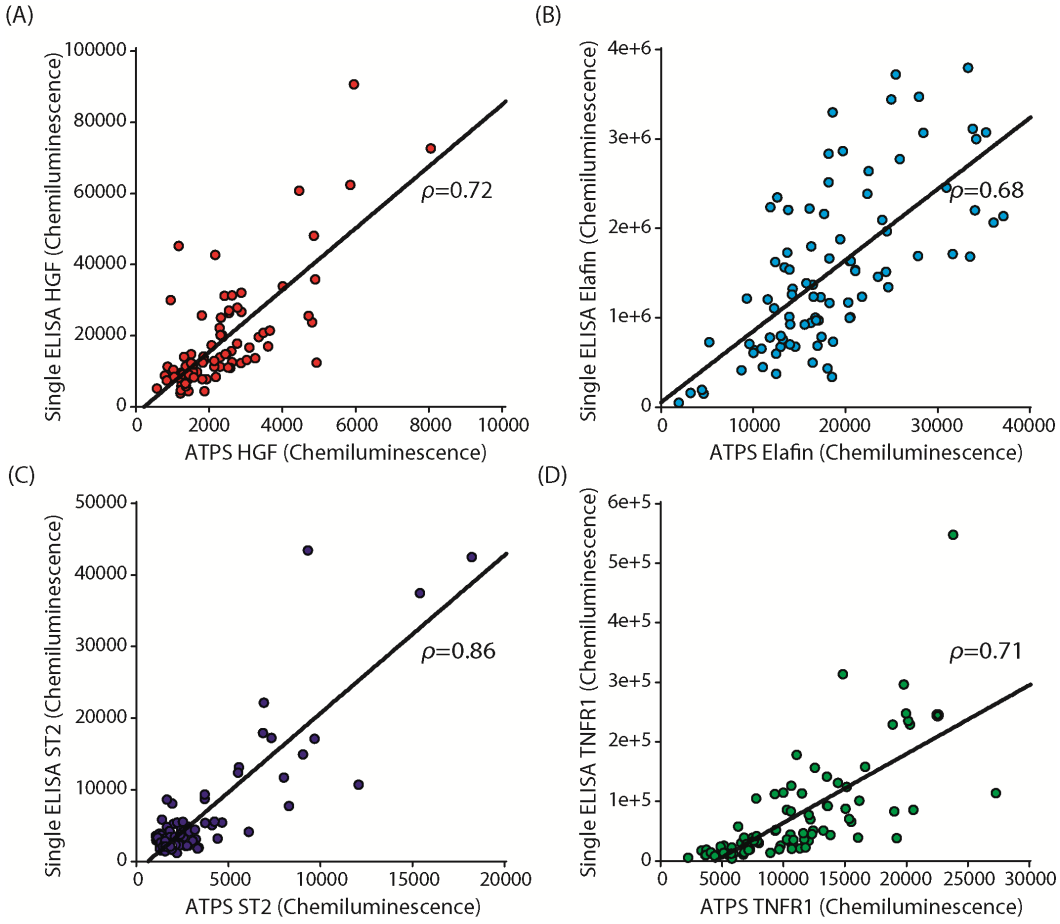

Figure 3.8: Scatter plots showing correlation between patient sample measurements for ATPS-ELISA (x-axis) and single sandwich ELISAs (y-axis) for (**A**) HGF, (**B**) Elafin, (**C**) ST2, and (**D**) TNFR1. Pearson's coefficient (ρ) is listed next to each linear regression fit.

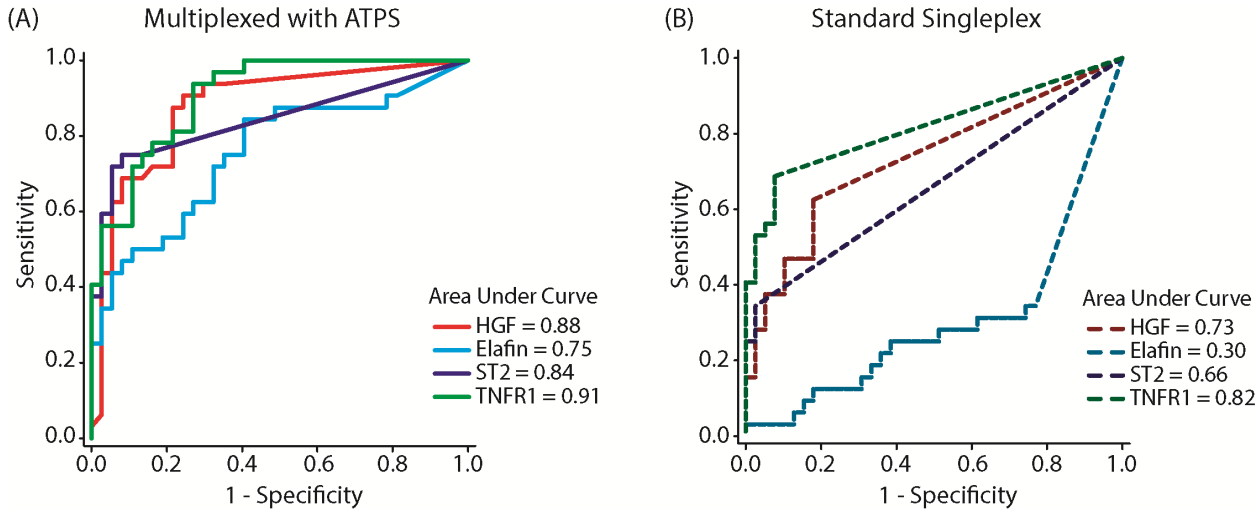

Figure 3.9: Receiver operating characteristic (ROC) curves for multiplexed ATPS-ELISA (**A**, solid lines) demonstrate that the assay has high sensitivity and specificity for determining GVHD status from biomarker levels in patient plasma. Single sandwich ELISAs (**B**, dashed lines) were less sensitive and specific due to their higher LoD and lower LDR values.

3.5 References

Armbruster, D.A. & Pry, T. Limit of blank, limit of detection and limit of quantitation. *Clin Biochem Rev* **29 Suppl 1**, S49-52 (2008).

Frampton J et al. Aqueous two-phase system patterning of microbubbles: localized induction of apoptosis in sonoporated cells. *Advanced Functional Materials* (2013).

Kai J. et al. A novel microfluidic microplate as the next generation assay platform for enzyme-linked immunoassays (ELISA). *Lab Chip* **12**, 4257-4262 (2012).

Paczesny, S. et al. A biomarker panel for acute graft-versus-host disease. *Blood* **113**, 273-278 (2009).

Paczesny, S. et al. Elafin is a biomarker of graft versus host disease of the skin. *Sci Transl Med* **2**, 13ra2 (2010).

Tavana, H. et al. Nanolitre liquid patterning in aqueous environments for spatially defined reagent delivery to mammalian cells. *Nat Mater* **8**, 736-741 (2009).

Tavana H, Mosadegh B, Takayama S. Polymeric aqueous biphasic systems for non-contact cell printing on cells: engineering heterocellular embryonic stem cell niches. *Advanced Materials* **22**, 2628-2631 (2010)

Vasan, R. Biomarkers of cardiovascular disease. Circulation **113**, 2335-2362 (2006).

Chapter Four

Conclusions and Future Directions

4.1 Summary

Many multiplex protein biomarker tests exist but these tests (i) are time- and labor-intensive to develop, (ii) have poor specificity due to antibody cross-reactions, (iii) have high sample and reagent consumption, and (iv) require expensive, specialized equipment (ELISA Trends 2010). The innovative, crosstalk-free, homogeneous and heterogeneous, multiplexed immunoassays developed in this dissertation research successfully solve all four challenges faced by these commercially available platforms.

In fact, we enabled, for the first time, multiplexing of amplified luminescent proximity homogeneous assays (AlphaLISAs) by co-localizing antibody-bead reagents in droplets of immiscible aqueous polymers (**Chapter 2**). It is this microscale reagent patterning technique that allows our no-wash, multiplexed assay to also prevent the antibody cross-reactivity problem that plagues many current multiplexed protein assays. In previous methods, these antibody cross-reactions result in false positive detection, reducing test specificity. Not only is our assay highly specific and highly sensitive, with a wide dynamic range of 3.5 log units, but it is also inexpensive because we use tenfold less antibody-bead reagents than standard AlphaLISAs. In addition, our assay can be completed in 2 hours and can be read using standard 384-well microplate readers. We demonstrated the potential of C-X-C motif chemokine 9 (CXCL9) and C-X-C motif chemokine 10 (CXCL10) as diagnostic biomarkers for chronic graft-versus-host

disease by quantifying these proinflammatory chemokines in plasma from 88 patients who underwent bone marrow transplantation. In addition, we quantified the levels of IL-6, IL-8, CXCL9 and CXCL10 in antigen-stimulated cell cultures of human pulmonary type II alveolar epithelial cells. These experiments indicated that our assay is a valuable alternative detection method to AlphaLISA and enzyme-linked immunosorbent assay (ELISA) for protein quantification in cell culture supernatant and human plasma.

Similarly, our heterogeneous, crosstalk-free, multiplex ELISA is one of only two ELISA-based technologies that prevent antibody cross-reactions, ensuring that life scientists can detect proteins more accurately in biological samples. In conventional multiplex ELISAs, a cocktail of detection antibodies is introduced into assay wells, and these antibodies bind nonspecifically to each other leading to antibody crosstalk. In contrast, in multiplex ATPS-ELISAs described in **Chapter 3**, detection antibodies are localized within spatially, discrete dextran droplets. Thus, each detection antibody is matched only with its corresponding pre-spotted capture antibody. The other ELISA-based technology that claims to prevent antibody crosstalk is called the antibody co-localization array; however, these arrays are disadvantageous because droplets of detection antibody solutions are printed in dry environments and so may easily evaporate before test completion (Pla-Roca *et al.* 2012). Instead in ATPS-ELISAs, detection antibody solutions are printed in hydrated ATPS environments; hence, there is no risk of evaporation. Like our ATPS-AlphaLISAs, the ATPS-ELISAs use less sample and less antibodies than conventional immunoassays. Specifically, ATPS-ELISAs only requires 1 μl neat plasma, which is 50 times less the sample volume used in standard ELISAs. This savings in sample consumption is particularly advantageous in pediatric testing when patient sample size is small to begin with. And, compared to traditional ELISAs, ATPS-ELISAs use 100-fold less antibodies, providing

huge cost savings to researchers.

We expect that both crosstalk-free multiplex immunoassay platforms will revolutionize the life science research and clinical diagnostics markets because these platforms are the only current technologies that eradicate antibody cross-reactions in multiplex protein tests. By preventing antibody crosstalk, our assays do not detect false positive signals and so enable more accurate protein biomarker detection and diagnoses. Currently the research market is crowded with key players, namely RayBiotech Inc., Luminex, Quansys, and Meso Scale Discovery (MSD), who were all interviewed in the 2012 National Science Foundation Innovation-Corps Program. However, none of their multiplexed assays can be completed without wash steps or/and without antibody crosstalk (**Table 4.1**).

Table 4.1: Comparison of ATPS-multiplexed assays to commercial multiplexed assays.

	Luminex	Meso Scale Discovery	R&D Systems	ATPS-ELISAs	ATPS-AlphaLISAs
Eliminates false positive signals	NO	NO	NO	**YES**	**YES**
Cost of required instrument	HIGH	HIGH	LOW	**LOW**	MODERATE
Number of Wash Steps	MANY	MANY	MANY	MANY	**NONE**
Total Assay Time	> 6 hours	5 – 6 hours	> 6 hours	> 6 hours	**2 hours**

There are many emerging technologies that are entering in the multiplexed immunoassay space. For example, single molecule arrays (Simoas), sold by Quanterix Corporation, boast of femtomolar detection limits. In Simoas, analytes in the sample fluid are concentrated into very small chambers such that the concentration of analyte molecules in the chambers is greater than the bulk sample solution. This concentration-by-microcompartmentalization technique explains why Simoas are able to achieve orders of magnitude higher sensitivities. However, Simoas also

suffer from antibody crosstalk due to use of detection antibody cocktails; hence, the technology can only multiplex up to 10-plex.

Given the significant across-the-board cuts per the recent government sequestration, researchers are receiving less federal funding. Less research funding drives researchers to seek inexpensive, alternative technologies. Since our ATPS-multiplexed assays reduce antibody costs by 10- to 100-fold, we expect that life science researchers will be incentivized to adopt these technologies. Furthermore, no specialized readers are needed, allowing substantial cost savings to researchers. Instead, common lab instruments such as digital chemiluminescent-based imagers (Western blot readers) and 384-well microplate readers can be used.

4.2 Future Directions

While this dissertation research has been instrumental in the development and validation of crosstalk-free multiplexed immunoassays, additional experiments can be performed to demonstrate the broad applicability of these assays. In particular, future directions can be aimed at (i) detecting biomarkers in various sample matrices, (ii) increasing assay plexing level, (iii) increasing dynamic range, and (iv) making assays user-friendlier.

4.2.1. Detecting biomarkers in additional sample matrices

In this work, biomarkers quantified by both ATPS-multiplexed assay platforms were limited to two sample matrices: cell culture supernatants and human plasma. However, other biological fluids like serum, cell lysates, broncho-alveolar lavage fluid (BALF), and urine are often used to measure biomarkers. Since plasma is more complex than most other sample matrices, we expect

that our ATPS-multiplexed assays are robust enough to enable reliable and accurate biomarker quantification in all other sample matrices.

4.2.2. Increasing assay plexing level

To date, we have successfully developed 4-plex ATPS-AlphaLISAs and 4-plex ATPS-ELISAs. Typically, multiplex immunoassays that allow simultaneous detection of less than 10 biomarkers are beneficial for disease diagnosis, in part, because the algorithm used to diagnose patients can be made simple (Brand *et al.* 2011; Daly *et al.* 2013). Assays that enable multiplexed detection of more than 10 biomarkers are used for biomarker discovery and studying signal transduction pathways. Mass spectrometry, for example, is used extensively in biomarker discovery because it provides high throughput multi-analyte analysis. The drawbacks are mass spectrometry is very expensive and it is not sensitive enough to detect low abundance biomarkers (detection limit, 2 μg/ml) (Addona 2009). Luminex platforms are also used for biomarker discovery and a custom 50-plex cytokine panel is offered by Stanford's Human Immune Monitoring Center. Since our crosstalk-free multiplex assays are inexpensive compared to both Luminex and mass spectrometry, and have greater sensitivies than mass spectrometry, developing 16- or 100-plex ATPS-AlphaLISAs or ATPS-ELISAs will be extremely advantageous. In the current format, ATPS-AlphaLISAs may be limited to 16-plex because most plate readers are constrained to reading 1536-well plates. ATPS-ELISAs, however, can theoretically detect 100-plex and higher because chemiluminescent detection is obtained via digital imagers. In addition, since both ATPS-AlphaLISAs and ATPS-ELISAs inherently prevent antibody crosstalk, any singleplex AlphaLISA or ELISA can be added into the respective ATPS-multiplexed format without extensive characterization of antibody crossreactivity between detection antibody pairs.

4.2.3. Increasing assay dynamic range

Methods to increase the dynamic range of our crosstalk-free multiplexed assays can also be explored. Biomarkers in the blood span a concentration range of 11 orders of magnitude. Therefore, some biomarkers may be present in pg/ml concentrations while others may be present in μg/ml or mg/ml concentrations (Anderson and Anderson 2002). To increase the dynamic range of ATPS-AlphaLISAs, the following parameters can be optimized for each measured biomarker: antibody concentrations, antibody affinity, and charge of dextran. Increasing acceptor bead concentrations means there are more capture antibodies per bead, ensuring maximal capture of target biomarkers. However, since acceptor beads elicit the chemiluminescent signal, increasing acceptor bead concentrations result in higher background levels. An optimum acceptor bead concentration is therefore crucial. Use of high affinity antibodies also ensures that maximal target biomarkers are sandwiched between acceptor beads and biotinylated antibodies. Although we may carefully design assays so that antibodies and acceptor beads partition strongly to dextran assay droplets, if antibodies have low affinities for the target biomarker, detection limits will be higher and dynamic range will be reduced. It is well known that partitioning of proteins in an ATPS is dependent on the ionic composition of the phase-forming polymers (Albertson 1986). Thus, the influence of individual dextran-charged droplets, pH adjustments, or salt additions can be studied to determine the condition for best biomarker partitioning. Optimum biomarker partitioning leads to increased biomarker captured by antibody-beads, increasing dynamic ranges.

For ATPS-ELISAs, use of high affinity antibodies as well as optimum antibody concentrations per biomarker may also help increase assay dynamic range. However, one

disadvantage of our chemiluminescent ATPS-ELISAs is the inability to manipulate the exposure per measured biomarker. Some biomarkers give strong signals and some give weak signals at the same exposure. Consequently, it is difficult to discriminate between weak signals, reducing assay dynamic range. To overcome this, ATPS-ELISAs can be adapted into a fluorescent readout by use of multi-color Cy3/Cy5/FITC-conjugated detection antibodies. In this fluorescent format, it will be relatively easy to adjust the exposure of each measured biomarker because a different labeled detection antibody will detect each biomarker. This should increase the dynamic range of ATPS-ELISAs.

4.2.3. Improve assay's ease-of-use: rehydratable antibody microarrays

Efforts can also be pursued to make assays user-friendlier or/and automated. Since custom microplates for the multiplexed ATPS-AlphaLISAs satisfy the Society of Biomolecular Screening standards for 384-microwell plates, liquid handlers (e.g., CyBi®-Well, CyBio, Inc.) can be used to automatically dispense dextran/donor beads during the second step of our assay. It may also be possible to reduce the number of pipetting steps in multiplexed AlphaLISAs by creating rehydratable antibody microarrays (**Fig. 4.1**).

In this format, antibody-conjugated beads are co-localized in dextran droplets, then dried by evaporation or lyophilization. When the sample solutions (mixed with PEG) are bath applied to the dried droplets, the dextran droplets rehydrate and enable no-wash, multiplexed detection of cytokines and chemokines. This potential rehydratable assay format is indeed simpler and positions our multiplexed ATPS-AlphaLISA to be more readily adopted by lab technicians. The rehydration of DEX droplets in PEG is illustrated in **Fig. 4.2**. We have, in fact, recently demonstrated the feasibility of rehdyratable ATPS-AlphaLISAs by performing singleplex IL-6

ATPS-AlphaLISAs. Differences in detection limits for assays with normal hydrated (wet), evaporated (dehydrated), and freeze-dried (lyophilized) formats are statistically insignificant, indicating the feasibility of this approach (**Fig. 4.3A-B**). For dehydrated assays, DEX droplets were evaporated at room temperature for 2 hours, then stored overnight at 4 °C. For lyophilized-reagent assays, DEX droplets contained 5% D-sorbitol (Sigma), and were stored at -80 deg C for at least 2 to 3 hours prior to lyophilizing overnight. It is well known that polymers (e.g., dextran) and sugars (e.g., sorbitol) are used to stabilize proteins during freeze-drying and freeze-thawing (Wang 2000; Sun and Davidson 2001; Lovgren *et al.* 1996; Koskinen *et al.* 2005). On the following day, PEG-sample mixtures were bath applied to the dehydrated or lyophilized DEX droplets, and droplets rehydrated as shown in **Fig. 4.2**. Since singleplex rehdyratable ATPS-AlphaLISAs can be performed, we expect that multiplex rehdyratable ATPS-AlphaLISAs are also feasible.

Notably, the described rehydratable assays still require individual additions of 1-microliter dextran/donor beads into each of the 4 microbasins within a sample well of custom microwell plates. We determined that all antibody-bead reagents could not be present initially in DEX. If strepatividin donor beads are added directly to biotinylated detection antibodies in DEX, large antibody-bead complexes form because of the strong binding between streptavidin and biotin (McMullen and Banaszak-Holl 2011). We postulate that these large complexes block antigen-binding sites and prevent antigens from sandwiching between antibodies and acceptor beads. Based on manufacturer's specifications of antibody-bead reagents: (i) each biotinylated detection antibody has between 4-13 biotin molecules, (ii) each donor bead has 1000 streptavidin molecules, (iii) each streptavidin molecule has 3 biotin-binding sites instead of the typical 4 because one site is blocked by geometry, and (iv) each acceptor bead has 300 capture antibody

molecules. Clearly, one-step rehydratable ATPS-AlphaLISAs that contain all antibody-bead components initially in DEX, is only possible if detection antibodies are made with only one biotin molecule. This will ensure that each detection antibody can only bind to one streptavidin molecule on the donor beads, limiting formation of complex antibody-bead aggregates.

Instead of individual additions of 1-microliter dextran/donor beads into each of the 4 microbasins within a sample well, with some optimization, it may be possible to just add a single aliquot of donor beads in assay buffer to the sample well (**Fig. 4.4A**). If the latter is possible, the end-user only has 2 manual pipetting steps per sample well, or 2 automated pipetting steps per plate: bath application of sample in PEG, then single aliquot addition of donor beads in buffer. Alternatively, it may be possible to lyophilize the bulk PEG phase as well as dextran/antibody droplets (**Fig. 4.4B**). Consequently, end-users only need to add the sample. Both the PEG and DEX phases will rehydrate, and antigens in the sample should easily diffuse into the DEX phase.

ATPS-multiplexed ELISAs can also be made user-friendlier if both capture and detection antibodies are first pre-spotted and dried onto custom well plates. Antigen samples would be bath applied in PEG to dehydrated DEX-immobilized antibodies. DEX antibodies would then rehydrate upon addition of PEG. This format is advantageous to the end-user because not only does it eliminate user addition of capture and detection antibody solutions, but it also eliminates some washing steps. Consequently, the total assay time will reduce. In the proposed format, precise layered printing of capture and detection antibodies is absolutely necessary. This format is very challenging because it requires the printing of DEX layers in such a way that does not cause mixing prior to rehydration with PEG. Each time an additional DEX layer is spotted on an existing layer, there is a possibility of partial rehydration of the underlying DEX layer. Partial rehydration will promote untimely mixing and may also cause problems with protein stability by

causing multiple rounds of evaporative drying, denaturing proteins in solution. If, however, this challenge can be overcome, then this assay format will be extremely beneficial to translational researchers.

4.2.4. Commercialization potential

We participated in the 2012 National Science Foundation Innovation-Corps (NSF I-Corps), a fast-paced set of programs that allow researchers to evaluate the commercialization potential for their technology. We interviewed nearly 100 potential customers in hospitals, diagnostic labs, research labs, contract research organizations, and pharmaceutical companies. Clinicians expressed sincere interest in using our crosstalk-free multiplexed assays as a point-of-care device, particularly for the diagnosis of neonatal sepsis. Currently clinicians use 3 – 5 ml sample volumes for their studies, so a test that only requires a few microliters of blood is a major advancement. Before a point-of-care assay can be developed for sepsis, two major improvements to our ATPS-AlphaLISAs must be completed: 1) use of whole blood instead of blood plasma, and 2) 20 to 30 minute total assay time instead of 2 hours.

Translational researchers in academic institutions also value the rapid customizability of our crosstalk-free multiplexed platforms. No systematic analysis of all possible nonspecific interactions is necessary to develop and validate new biomarker panels because of the inherent ability of our assay to prevent antibody cross-reactions. Therefore, any singleplex ELISA or AlphaLISA can be included in our ATPS-multiplexed assays. No commercial technologies can customize and validate assays so rapidly. In fact, some multiplexed immunoassay companies charge as much as $20,000/protein added to in the multiplex test. This means that a custom 4-plex assay will cost at least $80,000 to develop in sometimes as much as 12 months. However,

by eliminating the need for lengthy optimizations of reagent and assay conditions, our custom crosstalk-free assays can potentially be developed in one-tenth the time. Furthermore, being the first-to-publish drives academics, so waiting 12 months for a custom assay may make researchers lose their window of opportunity. In addition, researchers cannot afford these high costs for custom assay development. Our ATPS-multiplexed assays are beneficial to researchers because reagent costs are reduced by 10- to 100-fold.

Life scientists at pharmaceutical companies also value our highly customizable, crosstalk-free multiplexed assays. Rapidly developed custom biomarker assays that prove or disprove drug efficacy is extremely valuable to pharmaceutical companies. Eliminating candidate drugs earlier in clinical trials will save pharma billions of dollars and reduce time-to-market.

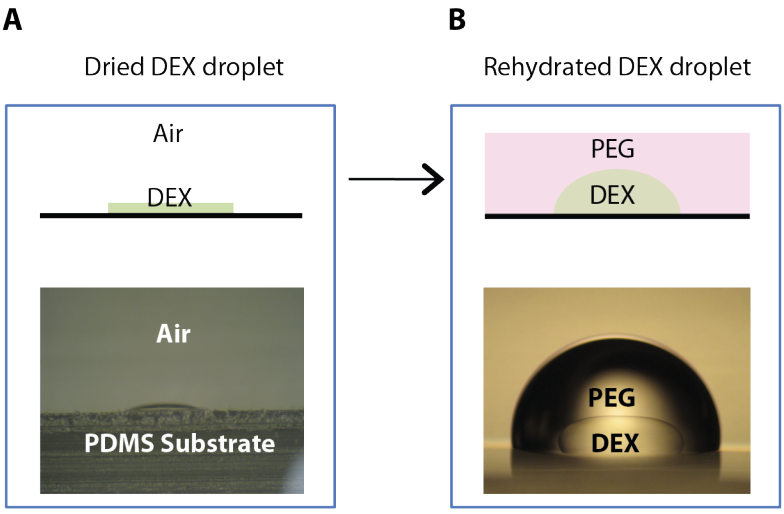

Figure 4.1: (**A)** Dried dextran (DEX) droplets become (**B**) rehydrated when PEG is applied.

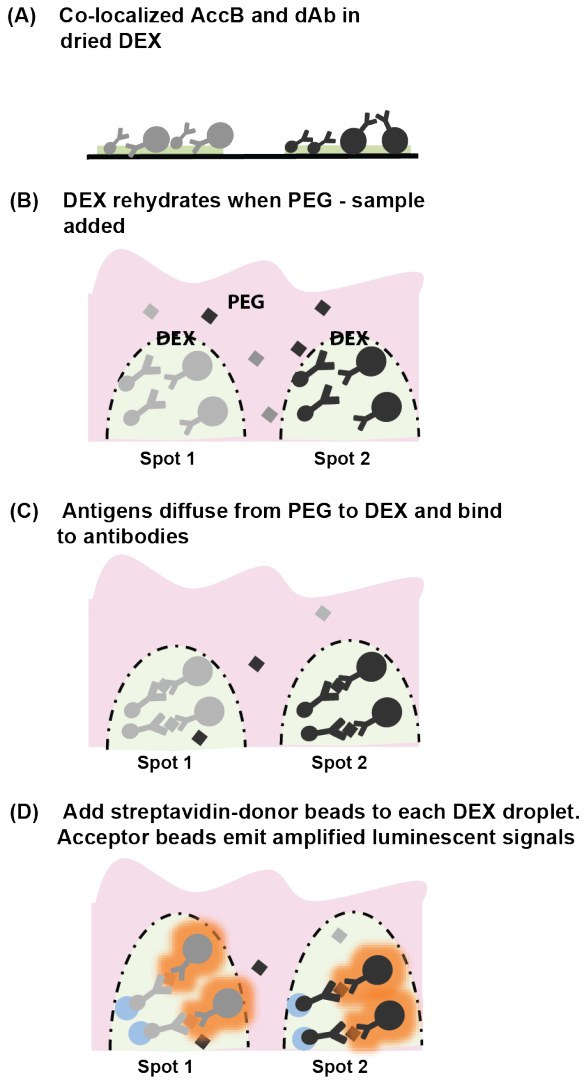

Figure 4.2: Schematic of workflow for rehydratable multiplexed ATPS-ALphaLISAs. (**A**) DEX droplets (1 µl), containin co-localized antibody-bead reagents, are air-dried or freeze-dried. (**B**) PEG-sample mixture is bath applied. (**C**) During a 1-hour incubation, antigens diffuse from PEG into the DEX droplets, and bind to antibody-beads. (**D**) DEX droplets (1 µl), containing streptavidin-coated donor beads are introduced into the solution and incubated for another hour. Donor beads bind to biotinylated antibodies, eliciting amplified luminescent signals by acceptor beads. The resulting signal is spatially and spectrally resolved.

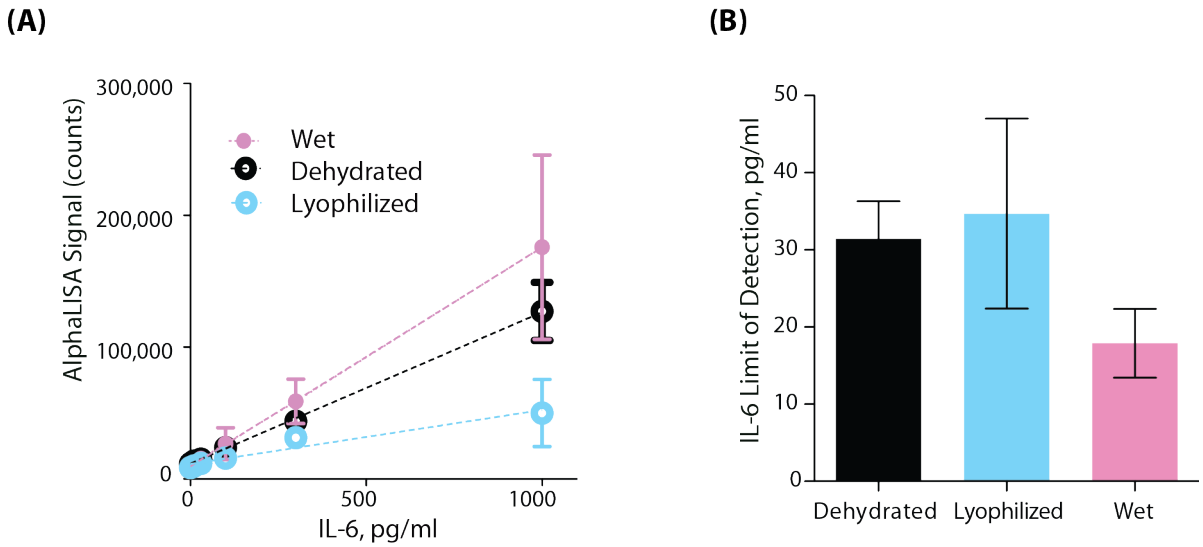

Figure 4.3: Rehydratable singleplex IL-6 ATPS-AlphaLISA. (**A**) Standard curves comparing wet, dehydrated, and lyophilized DEX assays. (**B**) Limit of detection of IL-6 in wet, dehydrated, and lyophilized DEX assays.

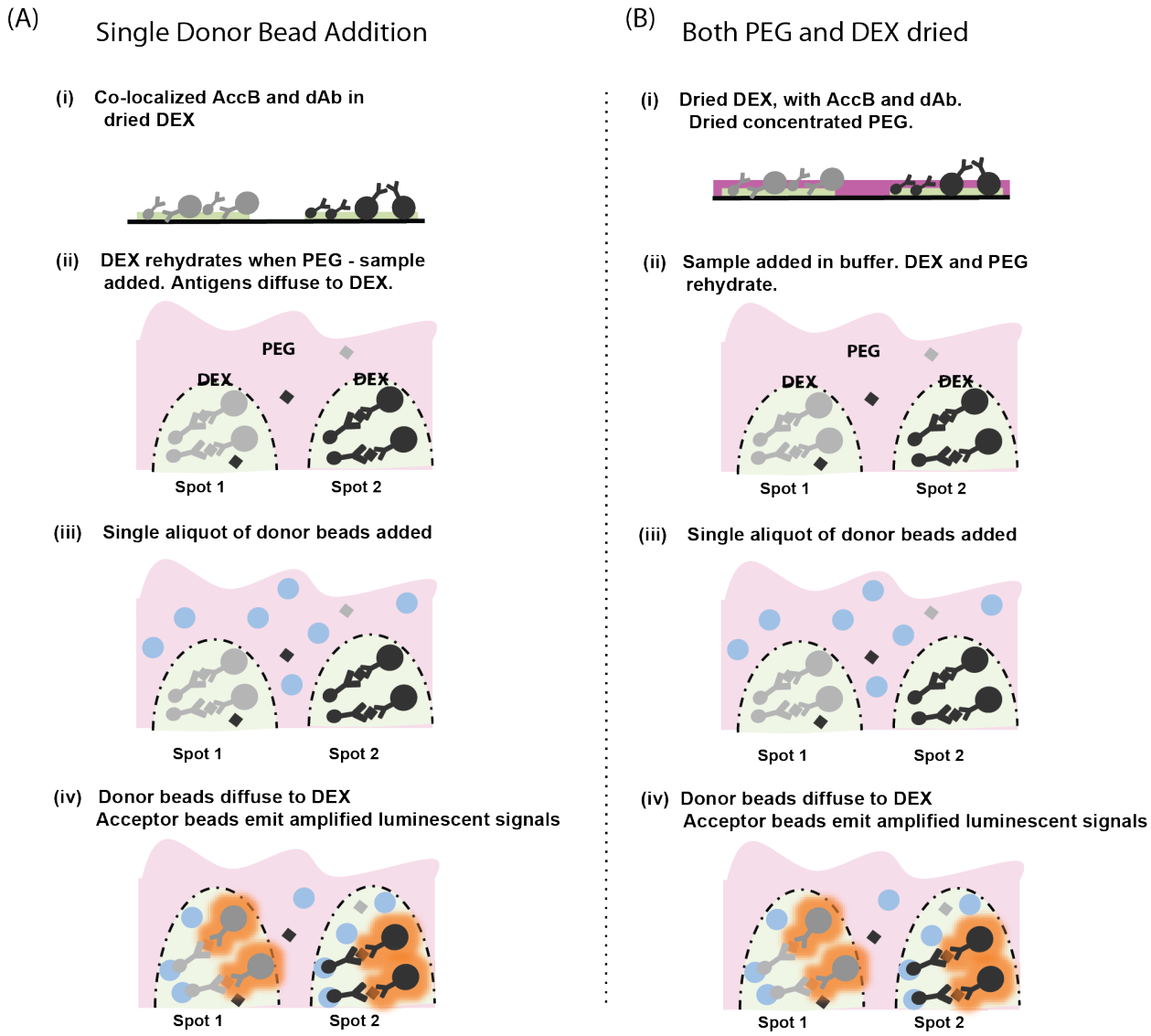

Figure 4.4: Two methods to reduce pipetting steps in ATPS-multiplexed AlphaLISAs: (**A**) single donor bead addition and (**B**) starting with dried PEG and DEX, which rehydrate upon sample addition.

4.3 References

Addona, T. et al. Multi-site assessment of the precision and reproducibility of multiple reaction monitoring-based measurements of proteins in plasma. *Nat. Biotech* **27**, 633-641 (2009).

Albertsson, P. *Partition of cell particles and macromolecules*. John Wiley & Sons, Inc. (1986).

Brand, R. et al. Serum biomarker panels for the detection of pancreatic cancer. *Clin Cancer Res* **15**, 805-816 (2011).

Daly, S et al. Development and validation of a plasma biomarker panel for discerning clinical significance of indeterminate pulmonary nodules. *J Thorac Oncol* **8**, 31-36 (2013).

Koskinen, J. et al. A lab-on-a-chip compatible bioaffinity assay method for human α-fetoprotein. *Lab Chip* **5**, 1408-1411 (2005).

Lovgren et al. One-step all-in-one dry reagent immunoassays with fluorescent europium chelate label and time-resolved fluorometry. *Clin Chem* **42**, 1196-1201 (1996).

McMullen, D. and M. Banaszak-Holl. Heterogeneous ligand-nanoparticle distributions: a major obstacle to scientific understanding and commercial translation. *Acc Chem Res* **11**, 1135-1145 (2011).

Sun, W. and P. Davidson. Effect of dextran molecular weight on protein stabilization during freeze-drying and storage. *Cryo Lett* **22**, 285-292 (2001).

Wang, W. Lyophilization and development of solid protein pharmaceuticals. *Int J Pharm* **203**, 1-60 (2000).

Part 2

This section describes the utility of phase-forming polymers for localized induction of apoptosis in sonoporated cells as well as microscale patterning of contractile collagen gels.

Chapter Five

Aqueous Two-Phase System Patterning of Microbubbles: Localized Induction of Apoptosis in Sonoporated Cells

This chapter describes an innovative high throughput method to study cell apoptosis. In this method, gas-filled microbbubbles were localized within microliter droplets of immiscible polymer solutions. Typically, these microbubbles float in aqueous environments so antibody-conjugated microbubbles are needed to anchor microbubbles to cell membranes. In our study, by simply confining these microbubbles in dextran droplets, microbubbles were maintained in close proximity to cell membranes. When ultrasound was applied, pores were generated in cell membranes, causing calcium influx into the cells and subsequently induce cell apoptosis. The simplicity of patterning microbubbles in dextran droplets over cell monolayers enables the highly combinatorial study of the effect of ultrasound pressure and duration on *in vitro* cell apoptosis.

5.1 Introduction

Microscale patterning is used extensively in tissue engineering and biomedical engineering for high-throughput cell assays and investigation of interactions among cell populations. Patterning is typically achieved by depositing materials on a substrate prior to cell attachment (e.g., microcontact printing, stenciling and inkjet printing) or by localizing reagents over a preexisting cell monolayer (e.g., laminar flow patterning or microelectromechanical system (MEMS)- based culture platforms) (Hook *et al.* 2006, Takayama *et al.* 2001, Takayama *et al.* 2003, Jain and Muthuswamy 2007, Valley *et al.* 2009). However, these strategies can be difficult to translate to widespread use in the life sciences because they often use custom fabricated devices that require a high degree of user expertise to operate.

To overcome these limitations, we recently developed a user-friendly, non-contact, cell-compatible method to pattern cells and deliver biomolecules to discrete cell populations. This method involves the localization of biomolecules within the dextran phase (DEX) of a polyethylene glycol (PEG)/DEX aqueous two-phase system (ATPS) (Tavana *et al.* 2010, Tavana *et al.* 2010, Yaguchi *et al.* 2012). Here, we use an ATPS to pattern lipid-coated, gas-filled microbubbles to discrete regions on a cell monolayer, where they can be excited by ultrasound and induce localized cell apoptosis.

It is well known that after ultrasound application, microbubbles rapidly expand and contract, and/or collapse, and disrupt cell membranes (Marmottant and Hilgenfeldt 2003, Postema *et al.* 2004, Prentice *et al.* 2005, Ohl *et al.* 2006, van Wamel *et al.* 2006). The membrane disruption mediated by ultrasound excitation of microbubbles, referred to as sonoporation, has found applications both *in vitro* and *in vivo*, emerging as a valuable, noninvasive tool for transiently disrupting cell membranes to allow entry of membrane

impermeable exogenous agents into cells or to induce cell death (Ohl *et al.* 2006, Miller *et al.* 2002, Kudo *et al.* 2009). However, sonoporation is limited by a lack of control over microbubble location with respect to cells, often resulting in variable treatment outcomes and suboptimal efficiencies. Gas-filled microbubbles easily float to the surface of the cell culture medium *in vitro*, far from where they can exert their effects on adherent cells.

To circumvent the microbubble buoyancy problem, microbubbles are encapsulated with antibodies/ligands that target them to the surface of cells (Ferrara *et al.* 2009, Klibanov 2009, Linder 2004). These targeted microbubbles attach to cell membranes, and facilitate membrane disruption (Warram *et al.* 2012). Application of antibody-conjugated microbubbles to *in vitro* cell monolayers, however, results in microbubbles binding to the entire monolayer. Such systems do not provide the spatial selection that is required to target subpopulations of cells within a monolayer. Furthermore, expensive antibodies/ligands are needed to attach the microbubbles to the cells.

In this study, we address these limitations by spatially patterning microbubbles (without expensive antibodies) using ATPSs, and confining them to user-defined regions on a cell monolayer. Application of ultrasound results in localized sonoporation in patterned microbubble regions. This localized sonoporation cannot be achieved by any current methods. Moreover, the patterned microbubbles allow both the experimental treatments and the control (where cells within different regions are exposed to the same ultrasound condition without microbubbles nearby) to be simultaneously performed, in one step, in a single cell culture dish. By patterning microbubbles at multiple sites, multiple ultrasound conditions can be tested within the same culture dish, providing a multiplexed platform for efficient investigation of ultrasound-mediated sonoporation and downstream effects on cells, including induction of apoptosis.

5.2 Materials and Methods

5.2.1 ATPS Formulation

ATPSs were formulated from DEX (ranging in molecular weight from 3.5 kDa to 500 kDa; Pharmacosmos, Denmark) and PEG 35 kDa (Sigma, St. Louis, MO). These polymers were reconstituted as aqueous solutions in various buffered media. The initial formulations tested were near critical point concentrations of 9% DEX 3.5 kDa/10% PEG 35 kDa, 7% DEX 10 kDa/7% PEG 35 kDa, and 3.2% DEX 500 kDa/2.5% PEG 35 kDa in their fully equilibrated forms. For experiments that required additional reagents in the ATPS solutions, concentrations slightly higher than the critical points were used (e.g., stock solutions of 16% DEX 10 kDa/16% PEG 35 kDa, corresponding to a solution of approximately 8% DEX 10 kDa/8% PEG 35 kDa after full equilibration. ATPSs formed from stock solutions of 8% DEX 10 kDa/16% PEG 35 kDa and 4% DEX 10 kDa/16% PEG 35 kDa were also tested.

5.2.2 Microbubble Partitioning

Two types of commercially available ultrasound contrast agent microbubbles were used in this study: Definity (Lantheus Medical Imaging, Billerca, MA) and Targestar-SA (Targeson, San Diego, CA). Definity microbubbles are composed of a C3F8 gas core, encapsulated by a phospholipid shell. Targestar-SA is a perfluorocarbon microsphere, encapsulated with a lipid shell coated with streptavidin, which permits biotinylated ligands to bind to its surface via biotin-streptavidin conjugation chemistry. The affinities of different microbubbles for the above phase systems were tested by mixing stock solutions of microbubbles in equal concentrations of twice-concentrated solutions of PEG and DEX in a microcentrifuge tube. The phase systems were then

allowed to separate by gravity at room temperature. Once the phase systems reached equilibrium (~10 min), samples were taken from the top (PEG) and bottom (DEX) phases along with the PEG/DEX interface and diluted below the critical point (1:10 in PBS) to remove any residual PEG/DEX droplets that could be mistaken for microbubbles. Microbubbles were placed on a hemocytometer and imaged under brightfield illumination using a 10x objective. Images were imported into imageJ and numbers of microbubbles were automatically quantified using the automated nuclei counting plugin (Center for Bio- Image Informatics, UCSB). Partitioning was measured for Definity lipid coated microbubbles, Targestar-SA microbubbles (without antibody) and Targestar-SA microbubbles conjugated to biotinylated IgG by counting the numbers of microbubbles in each phase. Partitioning was also investigated by placing the microbubbles within non-equilibrated twice-concentrated solutions of DEX, which were then deposited into PEG as 1 μl droplets. The movement of microbubbles within the DEX droplets was monitored using video microscopy.

5.2.3 Cell Culture

Human umbilical vein endothelial cell (HUVEC) preparations (passage number 3-7) were plated one day prior to the experiment onto tissue culture treated 35 mm^2 glass bottom dishes. NIH3T3, MDA231 and HeLa cells were cultured under standard conditions and then either seeded separately or as mixtures (co-cultures) in HUVEC medium in 35 mm^2 glass bottom dishes one day prior to the experiment. A seeding density of 200 cells/mm^2 was used to ensure ~80% confluence the following day. Cultures were maintained in a humidified incubator at 37°C, with 5% CO2. For experimental treatments, cultures were removed from the incubator, covered with a solution of 16% PEG, patterned with DEX/microbubbles and immediately treated by ultrasound.

After 10 min incubation, the ATPS was removed through 3-5 consecutive washes in PBS. The cells were then either reintroduced to culture medium and returned to standard incubation conditions for later analysis or immediately stained and imaged.

5.2.4 Microbubble Preparation and ATPS Micropatterning

Microbubbles (~1×10^9 particles/ml) were incorporated into the DEX phase by mixing a solution of 32% DEX 10 kDa with an equal volume of microbubbles to obtain a solution of ~0.5×10^9 microbubbles/ml in 16% DEX, representing the optimal microbubble concentration. Solutions with 10-fold and 100-fold lower microbubble concentrations were also tested. The microbubble solutions were loaded into capillary needles that were positioned above the PEG coated cells. Capillary tips were lowered into the PEG and droplets of DEX containing microbubbles (~0.05–0.1 μl in volume) were dispensed in the desired patterns above the cells. These droplets sank vertically in the PEG solution, where they came into contact with the cells and spread on the cell monolayer. Once the final droplet was in place, the micropatterned cultures were ready for ultrasound exposure.

5.2.5 Experimental Setup for Ultrasound Application

The experimental setup consisted of a microscope equipped with a non-focused circular ultrasound transducer (center frequency 1.25 MHz, active element diameter 0.6 cm) (Advanced Devices, Wakefield, MA, USA) that was driven by a function generator (33250A, Agilent Technologies, Palo Alto, CA, USA) and an amplifier (75A250, Amplifier Research, Souderton, PA, USA). The transducer was calibrated in free field in water using a calibrated 40 μm needle

hydrophone (HPM04/1, Precision Acoustics, Dorchester, UK). The transducer was positioned at 45 degrees (to avoid standing wave buildup and accommodate simultaneous microscopic imaging) with its active surface ~7.5 mm (Rayleigh distance) from the cell culture surface such that the maximum ultrasonic pressure was focused on the cells. This configuration allowed us to simultaneously apply ultrasound and microscopically observe microbubbles. Ultrasound excitation of microbubbles was monitored by a high-speed camera (Photron FASTCAM SA1, San Diego, CA) at a frame rate of 20 000 frames per second. A cooled CCD camera (Photometrics QuantEM, Tucson, AZ, USA), a monochromator with 5 nm bandpass (DeltaRAM X, PTI, Birmingham, NJ, USA) and a polychroic filter (73000v2, Chroma, Rockingham, VT, USA) were used to perform ratiometric epifluorescence and standard epifluorescence imaging of molecules delivered by sonoporation. The ultrasound treatments were applied either as single 8 μsec pulses or as continuous (30 s) wave forms that varied in peak acoustic pressure from 0.05 MPa to 0.6 MPa.

5.2.6 Apoptosis and Calcium Influx

To investigate whether calcium influx during sonoporation plays a role in sonoporation-triggered apoptosis in our system, we used PEG solutions containing various calcium concentrations either in a buffer designed to mimic the intracellular ion concentration of cells (Cytomix) or in PBS/DPBS (van den Hoff *et al.* 1992). Calcium concentrations ranged from 0 to 20 mM. Cells were exposed to either 0.3 or 0.6 MPa peak acoustic pressures and allowed to recover for 15 min at room temperature before washing in PBS. Cells were then washed in annexinV binding buffer and incubated with a solution containing Alexa 488-annexinV (Invitrogen) and PI to detect apoptosis. Regions with microbubbles were compared to regions without microbubbles and the

total number of PI-positive and annexinV-positive cells was quantified as before for each condition, with the exception that PI was added after ultrasound treatment and used as a dead cell marker. Ratiometric imaging using Fura-2 AM (Invitrogen) was used to confirm that changes in intracellular calcium had occurred following ultrasound treatment. For ratiometric calcium imaging, cells were loaded with Fura2-AM before ultrasound by incubating the cells with Fura2-AM and Pluronic F-127 (0.05% v/v of 10% w/v) for 60 min at 37 °C. The cells were then washed 3 times to remove extracellular Fura-2AM (Fan *et al.* 2010). To quantify intracellular calcium concentration following ultrasound, the ratio of signal at 340/380 nm was calculated for each treated cell.

5.2.7 Viability Assays

To analyze cell viability as a function of ultrasound/ calcium-induced apoptosis, we used several independent tests. PI staining, applied after ultrasound treatment, revealed cells that were not able to reseal their membranes after sonoporation, while annexinV labeling was used as an early stage marker for apoptosis. Phase contrast images were used to quantify the total number of cells in each image and the percentage of annexinV- and PI-positive cells was calculated for various ultrasound and calcium conditions. Phase contrast and PI images also allowed us to qualitatively inspect the status of cells in terms of general morphology, membrane features and nuclear morphology. JC1 ratiometric staining (Invitrogen) was used to confirm that mitochondrial membrane potential was disrupted in the apoptotic cells. Cell Event caspase stain (Invitrogen) was used to confirm that cells entered the late stages of apoptosis.

5.2.8 Data Analysis

Image J and MetaFluor Analyst (Molecular Devices, Downingtown, PA, USA) photometric software were used for image analysis. Mosaic and live cell images were captured, compiled and stitched using Zeiss Axiovision software. Statistical analyses were carried out using Sigmaplot with Sigmastat. All graphs are presented as mean values ± standard error of the mean.

5.3 Results and Discussion

5.3.1 Microbubble patterning

We achieved microbubble patterning by dispensing droplets of DEX, containing microbubbles, through a glass capillary needle onto a cell monolayer immersed in PEG. Before dispensing the microbubbles, we broke the tip of the capillary to prevent clogging and shearing of the bubbles during the dispensing process. Use of a capillary needle instead of a micropipettor enabled us to dispense smaller droplets of DEX (~0.05–0.10 μl) (**Fig. 5.1A-C**). Since DEX is denser than PEG, DEX droplets sink and deposit on the cell monolayer. Once in contact with the cell monolayer, DEX droplets spread over some cells and the DEX-localized microbubbles are brought in close proximity to the cell surface. Using this non-contact microbubble patterning method, multiple, discrete DEX droplets can be deposited within the same monolayer and even generate arbitraty patterns (**Fig. 5.1G**). After patterning the DEX droplets, additional PEG was carefully added to the dish without disturbing the patterning. Additional PEG must be added to ensure the active element at the tip of the ultrasound transducer (which was focused on the cells on the dish) was immersed. Next, ultrasound was applied to excite microbubbles and generate cavitation, or rapid expansion and contraction of the microbubbles, resulting in bursting or

shrinking of the microbubbles near the cells (**Figure 5.1D–F**), confirming that the microbubbles in DEX behaved similarly as they do in cell culture medium (Fan *et al.* 2012). Ultrasound excitation disrupted cell membranes and induced cell death in discrete regions, as indicated by the staining pattern for annexinV (apoptosis) and propidium iodide (PI) (membrane disruption) in the microbubble-patterned regions (**Figure 5.1H**).

We observed that commercially available microbubbles patterned differently in the PEG/DEX system (**Fig. 5.2A**). Definity microbubbles partitioned primarily to the PEG and interface phases because the non-polar lipid shells of the Definity microbubbles were more compatible with PEG. Targestar-SA microbubbles partitioned primarily to the interface and DEX phases. A greater proportion of microbubbles were observed in the DEX phase for lower DEX molecular weights (3.5 and 10 kDa), most likely because proteins such as streptavidin display stronger partitioning to DEX at low DEX molecular weights. This was true regardless of the presence of conjugated antibody. Partitioning to the interface was not only dependent on microbubble chemistry and size, but was also caused by buoyancy of the microbubbles in DEX.

We confirmed microbubble partitioning by mixing microbubbles in DEX, and then dispensing DEX/microbubble droplets into a PEG bath (**Fig. 5.2B**). Definity microbubbles rapidly moved to the interface, with some crossing the interface and entering the PEG. In contrast, Targestar-SA microbubbles remained well distributed in the DEX droplet. These experiments allowed us to monitor the distribution of microbubbles in DEX droplets and showed that Targestar-SA microbubbles remained in the DEX droplets in spite of their buoyancy.

Next, we studied the ability of various DEX/microbubble combinations to disrupt cell membranes upon ultrasound application in the presence of the cell impermeable dye PI (**Fig. 5.2C**). As expected, no PI staining was observed with ultrasound application to patterned DEX

droplets containing Definity microbubbles because these microbubbles rapidly escaped from the DEX phase and floated to the surface of the PEG, where they had no effect on the cells. Patterned droplets containing Targestar-SA microbubbles, however, were able to disrupt cell membranes allowing entry of PI into cells in the patterned microbubble regions, even without antibody conjugation of the microbubbles to the cells. This finding is important because it demonstrates the ability of micropatterned DEX droplets to spatially confine the microbubbles to the cell surface for sonoporation without the need for coupling to expensive antibodies.

For subsequent experiments we chose the DEX 10 kDa/PEG 35 kDa phase system with unconjugated Targestar-SA microbubbles, since this formulation displayed reasonable partitioning properties, and had polymer concentrations and viscosities low enough for use with cells. In addition, DEX 10 kDa showed more spreading on cells than DEX 500 kDa, ensuring that bubbles floating to the interface would still remain in close proximity to the cells.

5.3.2 Effects of polymer and microbubble concentration, and cell type on cell sonoporation

We used our DEX/microbubble patterning system to investigate cell membrane disruption and death as a function of ultrasound pressure, polymer concentration, microbubble concentration and cell type. We used PI (applied after ultrasound) as a marker for cell membrane disruption and cell death. Since microbubbles could be arrayed with various spacing and number of treated regions, this allowed us to test multiple ultrasound conditions in parallel (e.g., different numbers of pulses and pressure amplitudes), essentially multiplexing the ultrasound treatment (**Fig. 5.3A**). Without ATPS localization (spatial scale of ~0.75 mm^2 or less with ATPS), this type of multiplexing would not have been possible, since the ultrasound excitation covers a treatment area several times larger than the ATPS microbubble patterns.

Next, we studied the effect of DEX concentration in the 16% PEG 35 kDa/DEX 10 kDa system. Both the DEX and PEG used in our system are biocompatible and noncytotoxic; therefore, the polymers themselves had little to no direct effect on cell apoptosis. In fact, the intracellular cytocompatibility of these polymers has been demonstrated using lipofection as a membrane disruption method, as well as through numerous studies that have used cell microinjection of fluorophore-conjugated polymers such as dextran for cell tracing. For these experiments, a single ultrasound pulse was applied (8 μs duration and 0.4 MPa peak negative pressure) to excite the microbubbles. A DEX concentration of 16% was optimal for maintaining an even distribution of microbubbles on the cells. Solutions of 8% DEX and 4% DEX produced clusters of microbubbles on the cells, resulting in uneven microbubble distribution, inefficient microbubble activation and reduced efficiency of cell membrane disruption (**Fig. 5.3B**). The clustering effect was likely due to equilibration of the DEX droplets in PEG, which caused the DEX solution to decrease dramatically in volume, resulting in microbubble aggregation.

Using the 16% PEG 35 kDa/16% DEX 10 kDa system, we tested the effect of microbubble concentration on membrane disruption. The highest concentration of microbubbles we tested was ~0.5×10^9/ml, which was determined by the maximum concentration of microbubbles provided by the manufacturer (~1.0×10^9/ml) and the maximum concentration of DEX 10 kDa that could be easily prepared (32%) mixed in equal parts (0.5X microbubble condition). We also tested microbubble concentrations that were 10-fold and 100-fold lower (0.05X and 0.005X microbubble conditions). The efficiency of cell membrane disruption decreased dramatically as microbubble concentration decreased (**Fig. 5.3C**).

Notably, the use of small ATPS volumes enables us to use much higher microbubble concentrations (~0.5×10^9/ml) than what is typically used for sonoporation. Using these

conditions in conventional sonoporation is, however, prohibitive because of the cost associated with consuming large amounts of this reagent. Although it is expected that high bubble concentrations should generate the strongest sonoporation effects on cells, we have observed interactions among microbubbles (due to the secondary radiation force or Bjerknes force) at high microbubble concentrations (Bjerknes 1906). This increased level of microbubble-microbubble interaction may influence their ability to produce direct effects on the cells during sonoporation. Thus, attempts to use microbubble concentrations much higher than those used in this study are unlikely to further enhance the efficiency of sonoporation.

Finally, we examined the effect of cell types on membrane disruption, using the 0.5X microbubble condition and the 16% PEG 35 kDa/16% DEX 10 kDa system. Of the five cell types we tested, (HUVEC, NIH3T3, MDA 231, HeLa and HUVEC/NIH3T3/MDA231 co-cultures), HUVECs were most sensitive to membrane disruption, but the overall level of cell death was similar among all other cell types (**Fig. 5.3D**). These results were expected because HUVECs, as with other types of primary cells, are typically more sensitive to physical or chemical disruption than immortalized cell lines and cancer cells. Cell death was less than 5% in control regions without microbubbles for all of the cell types we tested. Time lapse imaging of the ultrasound treated microbubble sites revealed that dead cells remained in place after treatment. Over the course of 48 h, surviving cells from the treated regions and healthy cells from the surrounding regions frequently interrogated the dead cells (**Fig. 5.3E**), eventually displacing the dead cells through active removal of cell debris, migration and proliferation.

5.3.3 Platforms for Testing Cell Physiology: Apoptosis

Most platforms for wound healing research involve either physical damage/displacement or chemical ablation that completely removes the cells (Liang *et al.* 2007, Keese *et al.* 2004). However, many types of injuries in vivo do not result in complete removal of cells from the tissue all at once. Rather, cells undergo a more complex removal process where they die from direct trauma (necrosis) or initiate their own death in response to unfavorable environmental factors (apoptosis) and must then be cleared by immune cells in the surrounding tissue. Thus, a physiological model for tissue damage should involve both necrotic and apoptotic modes of cell death, where the damaged/dying cells remain in place throughout the process. As demonstrated by the results presented in **Fig. 5.3E**, ultrasound excitation of patterned microbubbles can effectively generate cells death in targeted regions without removal of cells. Patterning microbubbles to control the location of this injury provides an ideal platform for investigating the physiology of the damaged cells and surrounding healthy regions.

Therefore, we next investigated the mechanism of sonoporation induced cell death. Using patterned microbubbles, we induced cell death in well-defined regions of the cell culture and stained with annexinV (to assay the appearance of phosphatidylserine on the cell surface) and PI (applied after ultrasound, to indicate loss of membrane integrity) (**Fig. 5.4A**). The annexinV-positive cells displayed a variety of morphologies indicative of apoptosis including changes in membrane appearance (roughening/ruffling), appearance of vacuoles and blebs and changes in nuclear morphology (**Fig. 5.4A**) (Fink and Cookson 2005, Ziegler and Groscurth 2004). We tested the effects of two ultrasound regimes on cell apoptosis in our system. The first regime consisted of a low-pressure ultrasound treatment over a long period (30 s) (**Fig. 5.4B**). This

treatment resulted in a low rate of acute apoptotic cell death, reaching a maximum of ~20% at 0.1 MPa as determined by PI/annexinV labeling. The second regime consisted of a high pressure, short (8 μs) pulse of ultrasound (**Fig. 5.4C**). This treatment increased apoptotic cell death to ~70% at 0.6 MPa.

In contrast to other forms of apoptosis, our treated cells were immediately positive for both the apoptosis marker annexinV and the secondary necrosis marker PI, with both markers generally localized to the same cells. This staining pattern may be due to the ability of microbubbles to simultaneously disrupt the plasma membrane and initiate apoptosis, as early apoptotic cells without membrane disruption would normally exclude PI. We hypothesized that apoptosis was initiated by an influx of extracellular calcium through ultrasound-induced membrane disruptions. We tested the effects of the levels of extracellular calcium on loss of cell viability/apoptosis in regions exposed to ultrasound treatment (**Fig. 5.5A-D**). Higher acoustic pressure (0.6 MPa) resulted in a higher percentage of cells labeled with PI and annexinV, as compared to lower acoustic pressure (0.3 MPa) (**Fig. 5.5A,B**). This could be due to the fact that at higher acoustic pressures, more microbubbles were excited to initiate necrosis and apoptosis in more cells than at lower acoustic pressures. This is because smaller microbubbles usually require a higher acoustic pressure for cavitation to occur.

The extracellular calcium concentration had an important impact on both the percentage of PI positive cells and the percentage of annexinV positive cells. The percentage of dead cells (both PI- and annexinV-labeled) was markedly higher when the extracellular calcium concentration was increased to more than 5 mM, indicating the existence of a threshold for extracellular calcium above which there is an increase in the percentage of apoptotic cells. Interestingly, at lower calcium concentrations (≤2 mM) and at 0.6 MPa ultrasound pressure, the

percentage of PI-positive cells (~60–65%) (**Fig. 5.5A**) was greater than the percentage of annexinV-positive cells (~40– 45%) (**Fig. 5.5B**). This indicates that there is a pool of cells that die directly from microbubble trauma (acute cell death) without initiating apoptosis. This trend was also observed at lower ultrasound pressures (0.3 MPa), where the percentage of PI-positive cells (~20–38%) was greater than the percentage of annexinV-positive cells (~12%). However, at high enough calcium concentrations (e.g., ≥5 mM), almost all of the cells that were PI-positive were also annexinV-positive, suggesting either that increased extracellular calcium helped to reduce the number of cells with acute necrotic death, possibly by facilitating membrane repair for some cells, in accordance with what has been observed in other studies, or more likely, that elevated extracellular calcium concentration increased the number of cells undergoing apoptosis (Zhou *et al.* 2008). This was true for both high and low pressure ultrasound conditions. Finally, at high calcium concentrations (≥5.0 mM), low ultrasound pressures (0.3 MPa, 8 μs) were nearly as effective as high ultrasound pressures (0.6 MPa, 8 μs) at killing cells.

We performed ratiometric calcium imaging using Fura-2AM to confirm that calcium entered the cells as a result of micro- bubble excitation (**Fig. 5.5E**). In the presence of extracellular calcium, there was a dramatic increase in the 340/380 nm ratio (corresponding to intracellular calcium concentration) that was observed immediately after the onset of ultrasound applica- tion, indicating that calcium was entering the cells driven by its concentration gradient. One consequence of rapid calcium influx is a loss of mitochondrial membrane potential, followed by further release of calcium from intracellular mitochondrial and endoplasmic reticulum stores, leading to propagation of intracellular pro-apoptotic signals (Orrenius *et al.* 2003). We confirmed that this occurred in the cells within the microbubble patterned regions by applying the JC1 ratiometric stain for mitochondrial mem- brane potential (**Fig. 5.5F**). An

increased level of green signal in the mitochondria indicated that mitochondrial function was disrupted by ultrasound induced calcium entry. Finally, to prove that cells entered the late stages of apoptosis, we assayed caspase activity using the Cell Event apoptosis detection kit (**Fig. 5.5G**). Several hours after ultrasound treatment, almost every cell dis- played a staining pattern indicative of caspase activity (cleavage of the Cell Event dye which subsequently labeled the nucleus). These results suggest a model whereby ultrasound excitation of microbubbles in the presence of high extracellular calcium leads to cell death that is almost exclusively apoptotic in nature. Our data also suggests that apoptosis is most likely mediated by influx of calcium into the cells which triggers the apoptosis cascade. Cells are unable to survive as this cascade initiates, resulting in simultaneous loss of membrane integrity with onset of apoptosis.

We developed a new method for patterning microbubbles for controlled ultrasound-mediated cell membrane disruption (i.e., sonoporation). Our approach is easy to perform, can be applied to cells growing on a variety of substrates and offers the ability to apply multiplexed ultrasound/microbubble treat- ments to a small number of cells. We tested two types of commercially available microbubbles and found that streptavidin-coated (Targestar-SA) microbubbles performed better within our system. Although both Definity and Targestar-SA microbubbles possess a perfluorocarbon gas core bounded by a lipid shell, the difference in partitioning can be explained by the fact that the streptavidin on the surface of Targestar-SA microbubbles partitions to dextran. The ability to spatially pattern microbubbles enabled controlled and effective ultrasound treatment of cells. We demonstrated that patterning of micro-bubbles can be used to disrupt cell membranes of various cell types within defined regions, allowing intracellular entry of otherwise cell impermeant agents such as PI. The targeted areas could be monitored over several days to observe the cell responses in the damaged regions. We

also demonstrated that the patterned microbubbles selectively induced apoptosis in subpopulations of cells following ultrasound treatment. This is relevant for researchers interested in apoptosis and useful as a testing platform for ultrasound/microbubble tissue disruption.

5.3.4 Patterning of Microbubbles with ATPS

Patterning techniques are frequently used in biomedical research for performing cell co-cultures, migration assays, wound healing assays, therapeutic targeting experiments and high throughput analyses. A variety of approaches have been developed for controlling placement of cells, including selective patterning of substrate materials, and direct cell printing with inkjets, and more recently ATPSs (Ringeisen *et al.* 2006, Wright *et al.* 2007, Tavana *et al.* 2009, Tavana *et al.* 2010). These technologies are useful for spatially organizing cells, but some cell types require patterning in situ (i.e., they are already growing on a surface). This is often the case for primary cells that have strict substrate requirements and a limited potential to divide *in vitro*. There are relatively few technologies that permit patterning on cells already growing as monolayers. ATPS micropatterning is capable of this type of patterning due to its biomolecule and particle partitioning ability (Tavana *et al.* 2009, Albertsson 1986). Here, we demonstrated that ATPSs can be used to deliver microbubbles to preformed monolayers of cells.

Physical disruption of the plasma membrane can be achieved by microinjection, hydrodynamic delivery, magnetotransfection, laser poration, ballistic delivery and electroporation, in addition to sonoporation (Villemejane and Mir 2009). Among these methods, electroporation and sonoporation are two of the most effective physical methods for disrupting membrane integrity (Wells 2010). However, neither technique is traditionally amenable to patterning. We demonstrated that spatial patterning of sonoporation could be achieved using

ATPSs to confine microbubbles, which are known to be highly effective sonoporation facilitators.

Our ATPS microbubble patterning strategy provides several advantages for sonoporation. First, it provides an easy way to precisely place microbubbles in close vicinity to cells, thereby providing a controlled sonoporation platform. In our system, the microbubbles reside directly above the cells and are well dispersed in the XY dimensions, as confirmed by brightfield microscopy and our observations that microbubbles are in nearly the same focal plane as cells. This allowed us to overcome one of the main challenges in sonoporation research, the inherent unpredictability associated with free-floating micro- bubbles and controlling their impact on cells. Conventionally, sonoporation experiments have been conducted in centrifuge tubes or Petri dishes, where microbubbles are freely floating in the bulk solution (Zhong *et al.* 2011). In these systems, the relative locations of the microbubbles and the cells are random and cannot be controlled. In some sonoporation experiments, cells are cultured inside thin chambers (e.g., Opticell). To ensure microbubbles are in contact with the cultured cells, these thin chambers are positioned upside down so that microbubbles float up to the adherent cells (Meijering *et al.* 2009). However, this approach often leads to clustering of microbubbles at the boundaries of cells due to differences in the height of cells across the cell monolayer. In these systems, it is difficult, if not entirely impossible, to target a small region or sub-population of cells.

In our approach, the microbubbles can be easily positioned on any target cell population at controlled spatial locations. In most types of ultrasound experiments, long sonoporation treat- ment durations are used to maximize the chance of free-floating microbubbles impacting the cells. Since our approach mini- mizes free-floating microbubbles, we used short (microsecond)

ultrasound durations; therefore, the microbubble dynamics are better controlled without large translational movements due to effects such as microstreaming.

Our system can be used for cells that grow on virtually any substrate, making this approach more versatile and adaptable. The ATPS medium itself imposes no acoustic discontinuity above the cells while confining the bubbles within a fluid (this is problematic for most microdevices). In addition, our approach reduces the amount of reagent and the number of microbubbles by as much as 10 000-fold because microbubbles are confined in 0.1 μl DEX droplets instead of 10 ml solutions used in conventional sonoporation experiments in a dish or similar container. Since we use small amounts of microbubbles and can generate well-defined patterns, this approach is highly amenable to multiplexing ultrasound parameters, the microbubble type/ concentration, and the concentration and type of biomolecule present in the extracellular space. The final advantage of our system relates to the need for antibody/microbubble conjuga- tion. For targeted microbubble applications, antibody conjuga- tion is needed to ensure microbubble targeting and attachment to the cell surface. Our approach does not require antibodies for targeting cells because the DEX droplets confine the microbubbles at the cell surface. This allows the same microbubbles to be used with any cell type without any modification.

5.3.5 Implications for Apoptosis Research

Patterning of microbubbles using ATPSs provides a novel system with great potential for new bioapplications. In this study, we used ATPS microbubble patterning for selectively inducing apoptosis. A number of studies have shown sonoporation induced apoptosis in cells, although the mechanisms are not completely understood (Zhong *et al.* 2011, Honda *et al.* 2004, Hassan *et al.*

2010). Moreover, in sonoporation-mediated gene delivery experiments, a large number of cells are often damaged or killed by ultrasound-activated microbubbles, although the number of dead cells and the mechanism of their death (i.e., apoptosis vs necrosis) are not always clearly reported in the literature. In our study, the spatial localization and patterning of microbubbles using ATPS enabled detailed investigation of ultrasound excitation of microbubbles and their effects on the cells. With ATPS microbubble patterning, we induced a high proportion of cells to enter apoptosis in targeted areas within a monolayer by inducing calcium influx into the cells during sonoporation. Based on our previous experiments using DEX as a delivery vehicle for lipofection agents, the DEX and PEG polymers have little to no effect on cell viability. Therefore, apoptosis was mediated by microbubble-induced membrane damage and cal- cium influx, as evidenced by a dose response to extracellular calcium. This example illustrates that our technology of ATPS microbubble patterning may be used as a potential platform for studying apoptosis through transmembrane delivery of ionic or chemical initiators of apoptosis. Since our technique facilitates multiplexing of both microbubble condition and ultra- sound treatment for testing the effects of sonoporation on cell viability, this may be useful for studying localized cell injury or apoptosis, while testing a wide range of treatments or acquiring a large number of independent observations (Douville *et al.* 2011).

Apoptotic cells are recognized and removed by resident macrophages in tissue; whereas damage caused by necrotic injury is not recognized by the immune system and can lead to toxicity in the surrounding tissue (Wickman *et al.* 2012). Since apoptosis is highly localized to specific cell populations in our system, ATPS microbubble patterning for ultrasound excitation may serve as a useful test system for investigating the interactions of apoptotic cells with surrounding cells, including the ability of healthy cells to migrate into apoptotic regions and

remove debris. The effect that dying cells have on neighboring healthy populations can also be readily investigated in our system. Furthermore, by using ATPS and microbubbles to locally kill cells it will be possible to perform well-controlled wound healing assays without physical removal of the damaged region. In our system, the wounded region consisting of both apoptotic and necrotic cells may represent a more physiologically relevant in vitro model for wound healing.

5.4 Conclusion

It will be useful to design easier to use setups to dispense the DEX droplets and apply ultrasound excitation to microbubbles. Development of new microbubbles that partition better in DEX can also help to improve and expand this technology. Finally, our technology may serve as a useful high throughput testing platform to investigate the mechanisms for various microbubble-potentiated ultrasound applications such as ultrasound mediated drug delivery for cancer treatment, as well as ultrasound tissue ablation, where fractionation, necrosis and enhanced apoptosis have been identified as factors beneficial for treatment (Czarnota *et al.* 2012, Kennedy 2005).

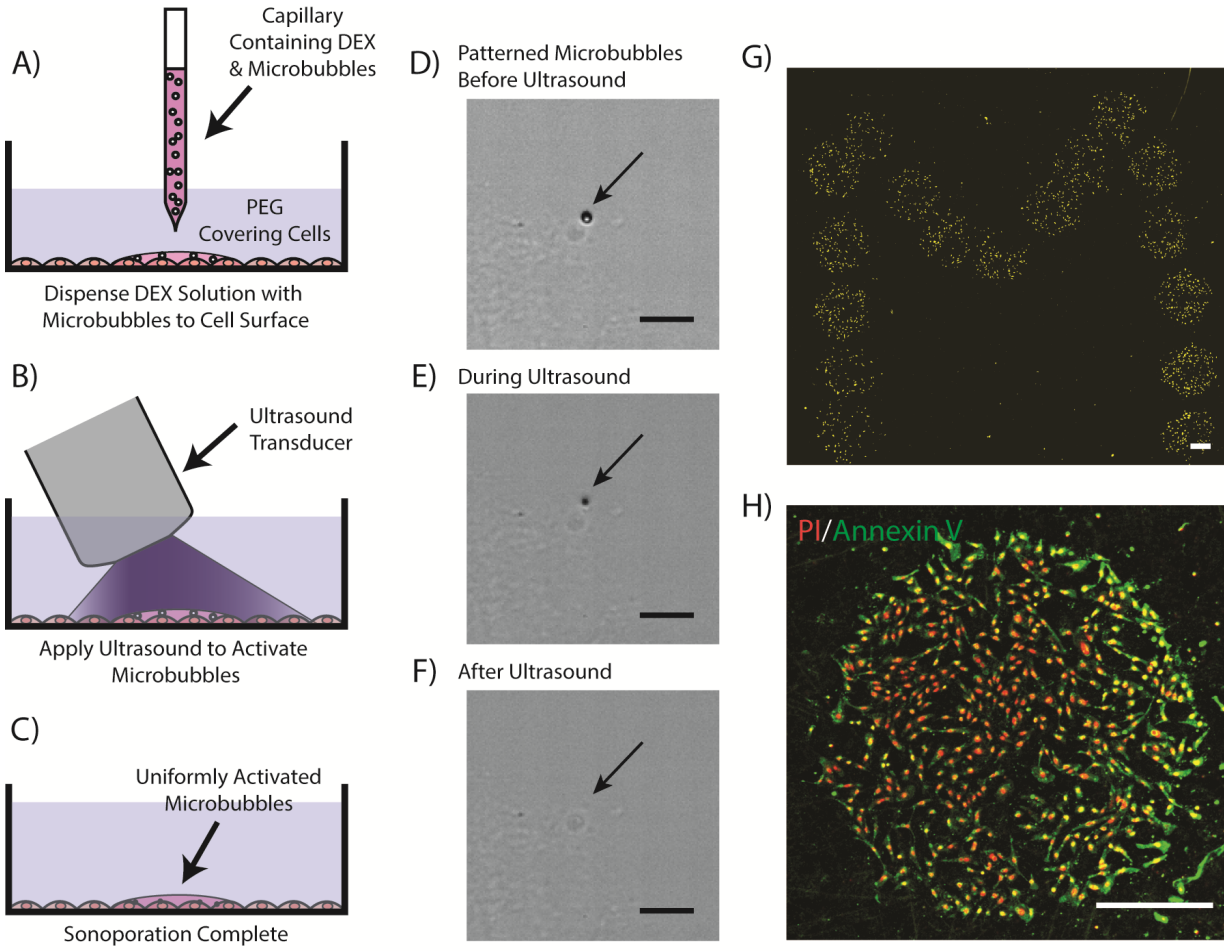

Figure 5.1: Patterned sonoporation is achieved by depositing DEX droplets, containing microbubbles on cell monolayers in a PEG/DEX ATPS. (**A**) Microbubbles are dispensed onto cells in PEG using a glass capillary needle. (**B-C**) The ultrasound transducer is used to activate the bubbles, which are contained within the DEX phase. (**D-F**) High magnification images of a single microbubble in DEX attached to a single cell (as indicated by the black arrows) before, during, and after ultrasound application captured with a high speed camera. This bubble was activated upon ultrasound treatment, undergoing rapid expansion and contraction, which resulted in bursting/shrinking on the cell, as visualized using ultrafast videomicroscopy. As microbubbles expand and contract during ultrasound application at 1.25 MHz, halos appear around the microbubbles due to rapid volume (**E**). After microbubble activation, the microbubbles disappear or become smaller in size (**F**). (**G**) Microbubbles can be patterned with various user-defined array geometries, as indicated by patterning of a Michigan "M", visualized with intracellular PI staining after microbubble excitation. (**H**) Apoptosis was selectively induced in the microbubble patterned regions treated with ultrasound (0.6 MPa, 8 µsec pulse) as indicated by annexinV (green) and PI (red) staining after ultrasound treatment. All images are for non-conjugated Targestar-SA microbubbles. Scale bars are ~5 µm in (**D-F**) and ~300 µm in (**G**) and (**H**).

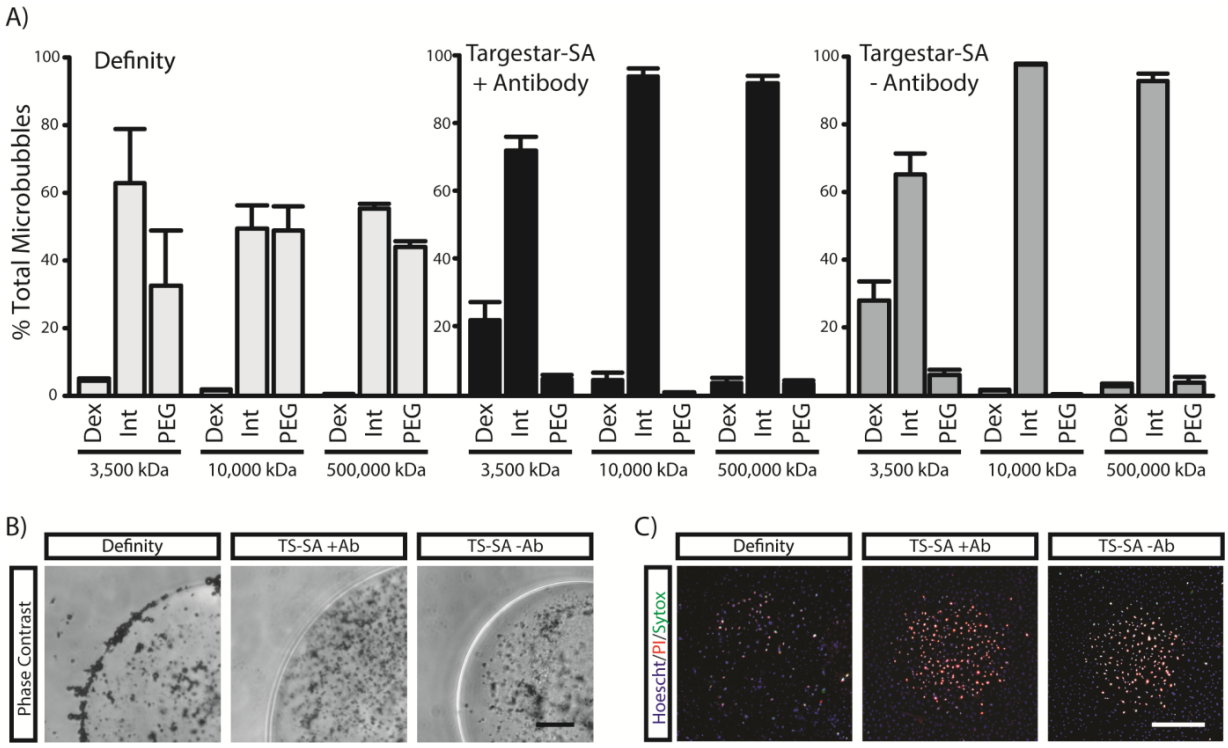

Figure 5.2: Partitioning of microbubbles. (**A**) The percentage of microbubbles present in DEX, at the PEG/DEX interface and in PEG was calculated for various ATPS formulations with different DEX molecular weight. Definity™ microbubbles localized to the interface and the PEG phase, whereas Targestar-SA microbubbles localized to the interface and the DEX phase for lower molecular weight of DEX. Bars denote mean ± SEM. (**B**) Microbubbles that were deposited within DEX droplets and tracked by video microscopy confirmed the results in (**A**). Definity™ bubble collected at the PEG/DEX interface and eventually crossed the interface to enter the PEG phase. Targestar-SA microbubbles were well-retained in DEX. Scale bar ~ 60 µm. (**C**) Droplets of DEX containing Definity™ microbubbles could not mediate transmembrane delivery of PI in HUVECs. Droplets with Targestar-SA microbubbles mediated PI delivery with high efficiency in HUVECs, even without antibody targeting. Scale bar ~ 300 µm.

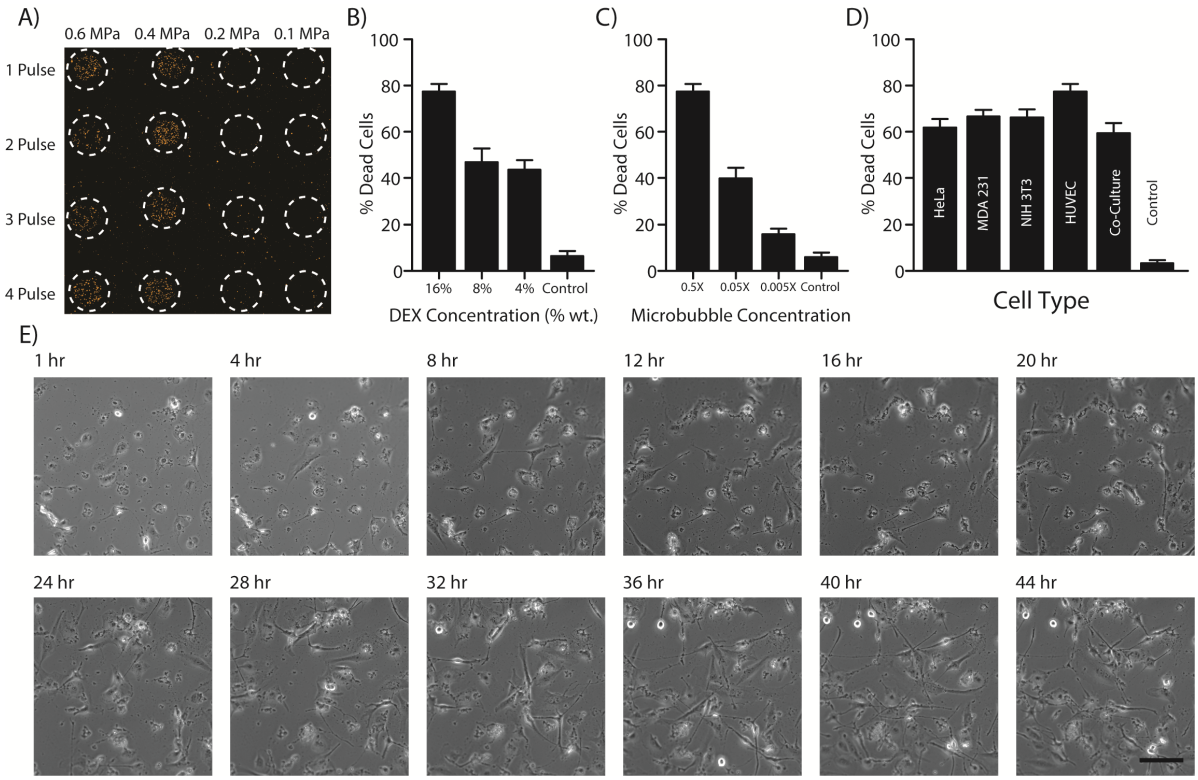

Figure 5.3: Optimization of ultrasound and microbubble conditions for targeted cell killing. (**A**) Placing DEX droplets in an array allows multiplexed testing of ultrasound parameters such as number of pulses (down) and pressure amplitude (across). The array image is a reconstructed mosaic from high magnification brightfield and PI images. Scale ~ 500 μm. Cell death was minimal at low pressures (0.1 and 0.2 MPa). Multiple low pressure pulses (3 or 4 pulses) resulted in a slight increase in cell death for the 0.2 MPa ultrasound condition. Pressures of 0.4 and 0.6 MPa resulted in a high proportion of cells dying in the patterned areas, with little effect from additional pulses. (**B**) Decreasing the DEX concentration resulted in microbubble aggregating. Cell death was markedly reduced at 8% and 4% DEX concentrations. (**C**) The proportion of dead cells decreased with decreasing microbubble concentrations. (**D**) HUVECs were most sensitive to microbubble excitation, but cell death was similar among all the cell types we tested. Control regions without microbubbles showed minimal cell death (data compiled for all cell types). Bars in (**B-D**) denote mean ± SEM for n= 3 independent experiments. (**E**) Time lapse imaging of microbubble targeted co-cultures of MDA231, NIH 3T3 and HUVECs showed that cell debris was gradually removed over the course of several days as the treated regions became repopulated by cells from surrounding untreated areas. Scale ~ 60 μm.

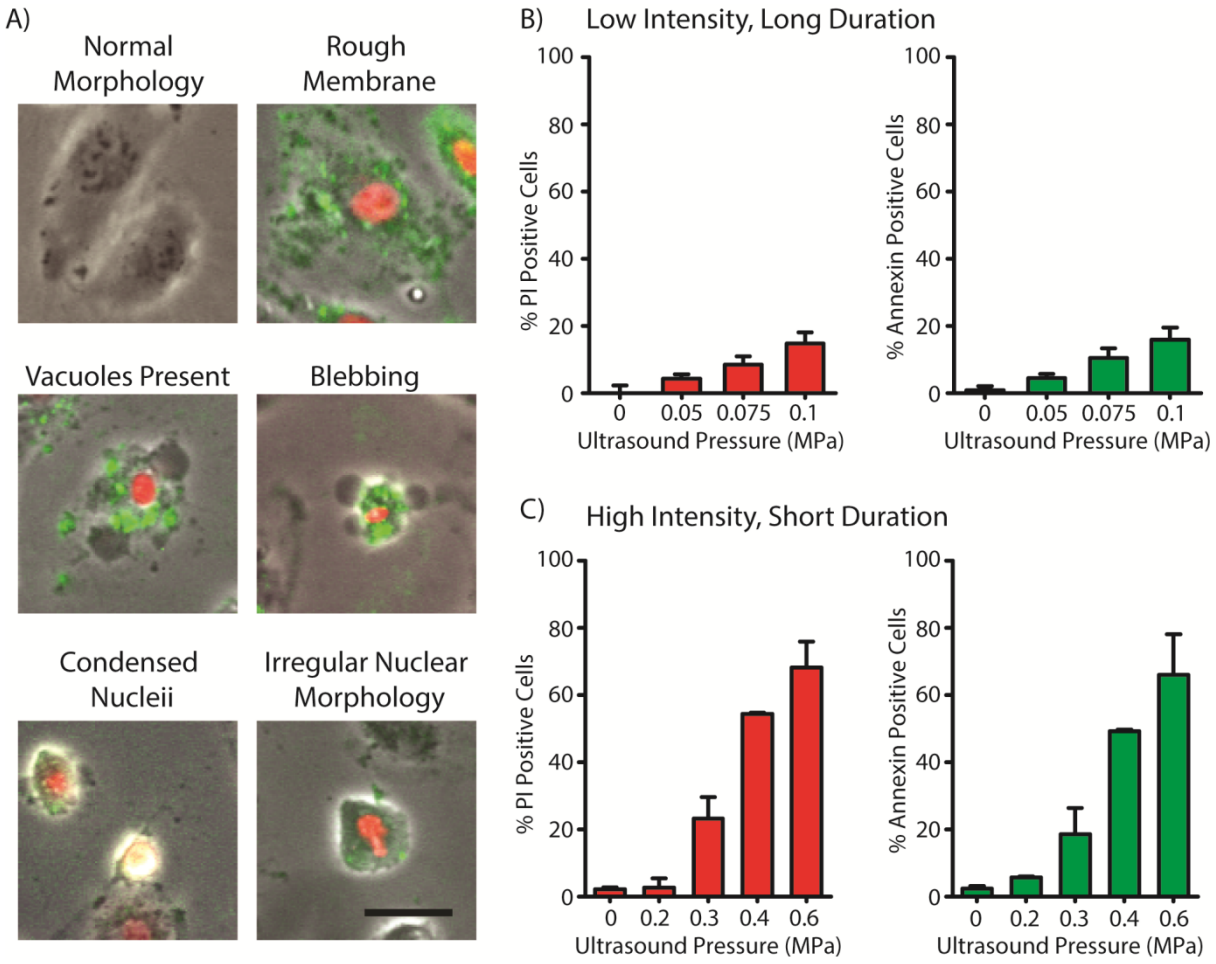

Figure 5.4: Effects of ultrasound excitation of microbubbles on HUVECs. (**A**) Treated cells displayed a variety of apoptotic morphologies. Red signal corresponds to PI nuclear staining and green signal corresponds to annexinV staining. (**B**) Ultrasound activation with low pressure (e.g. < 0.3 MPa) for a long treatment duration resulted in a low percentage of cells dying from apoptosis. (**C**) Short ultrasound pulses at high pressure amplitudes (e.g. 0.4 MPa and 0.6 MPa) resulted in significantly higher percentages of cell dying from apoptosis. Bars in (**B, C**) denote mean ± SEM for n>3 independent experiments. Scale bars ~20 μm.

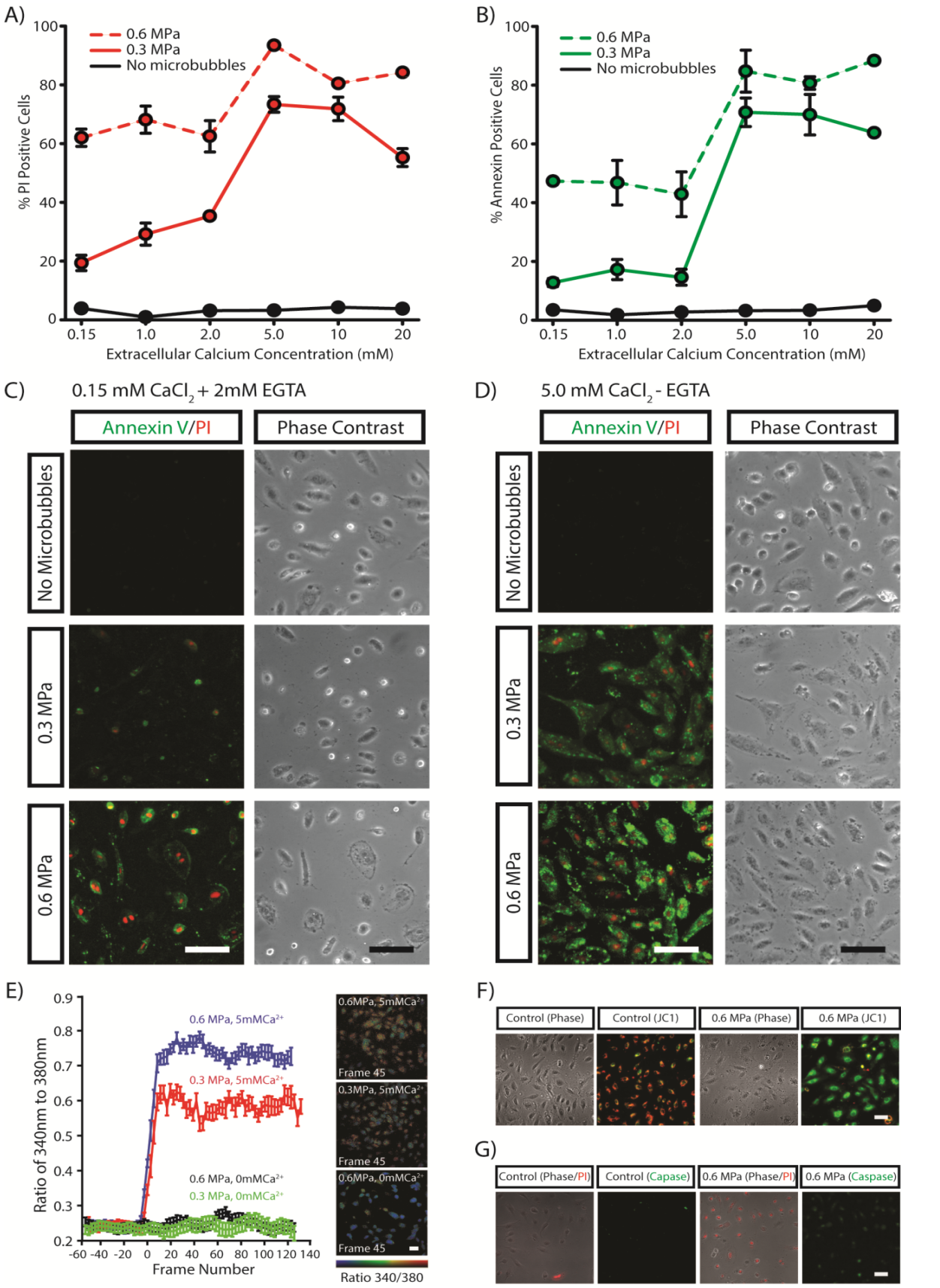
A)
0.6 MPa
0.3 MPa
No microbubbles
% PI Positive Cells
Extracellular Calcium Concentration (mM)
B)
% Annexin Positive Cells
C)
0.15 mM CaCl2 + 2mM EGTA
Annexin V/PI
Phase Contrast
No Microbubbles
0.3 MPa
0.6 MPa
D)
5.0 mM CaCl2 - EGTA
E)
Ratio of 340nm to 380nm
Frame Number
0.6 MPa, 5mMCa2+
0.3 MPa, 5mMCa2+
0.6 MPa, 0mMCa2+
0.3 MPa, 0mMCa2+
Frame 45
Ratio 340/380
F)
Control (Phase)
Control (JC1)
0.6 MPa (Phase)
0.6 MPa (JC1)
G)
Control (Phase/PI)
Control (Capase)
0.6 MPa (Phase/PI)
0.6 MPa (Caspase)

Figure 5.5: Effects of extracellular calcium concentration on apoptosis in microbubble patterned cultures. PI labeling of dead cells (**A**) and annexinV labeling of apoptotic cells (**B**) increased in the presence of high extracellular calcium (≥ 5mM). Solid lines represent 0.3 MPa ultrasound pressure, dashed lines represent 0.6 MPa ultrasound pressure and black lines represent no ultrasound treatment. Bars denote mean ± SEM for n>3 independent experiments. (**C**) Representative images of sonoporated cells in the presence of Cytomix buffer (no free extracellular calcium) for various ultrasound conditions. (**D**) Representative image of sonoporated cells in the presence of 5 mM calcium buffer for various ultrasound conditions. (**E**) Fura-2AM ratiometric calcium imaging of HUVECs treated with either 0 or 5 mM calcium and either 0.3 or 0.6 MPa ultrasound pressure, along with representative images taken at frame 45 of imaging (shortly after the ultrasound pulse). Bars denote mean ± SEM. (**F**) JC1 staining for control (no ultrasound) and ultrasound-treated cells. Red staining indicates normal mitochondrial membrane potential and green staining indicates loss of membrane potential. (**G**) Cell Event caspase staining for control (no ultrasound) and ultrasound-treated cells. Green nuclear staining indicates the activation of caspase in cells. All scale bars ~ 40 μm.

5.5 References

Albertsson, P.-A. *Partition of Cell Particles and Macromolecules,* 3rd edition (Wiley, New York 1986).

Bjerknes, V. *Fields of force; supplementary lectures, applications to meteorology; a course of lectures in mathematical physics delivered December 1 to 23, 1905*, The Columbia University press; New York **1906**.

Czarnota, G. *et al.* Tumor radiation response enhancement by acoustical stimulation of the vasculature. *Proc Natl Acad Sci* **109**, E2033-E2041 (2012).

Douville, N *et al.* Combination of fluid and solid mechanical stresses contribute to cell death and detachment in a microfluidic alveolar model**.** *Lab Chip* **11**, 609-619 (2011).

Fan, Z. *et al.* Spatiotemporally controlled single cell sonoporation. *Proc Natl Acad Sci* **109**, 16486-16491 (2012).

Fang, Y. *et al.* Rapid generation of multiplexed cell cocultures using acoustic droplet ejection followed by aqueous two-phase exclusion patterning. *Tissue Eng Part C Methods* **9**, 647-657 (2012).

Ferrara. *et al.* Lipid-shelled vehicles: engineering for ultrasound molecular imaging and drug delivery. *Accounts of chemical research* **42**, 881-892 (2009).

Fink S. and B. Cookson. Apoptosis, pyroptosis, and necrosis: mechanistic description of dead and dying eukaryotic cells. *Infect Immun* **73**, 1907-1916 (2005).

Hassan, M *et al.* Role of intracellular calcium ions and reactive oxygen species in apoptosis induced by ultrasound. *Drug Discov Today* **15**, 892-906 (2010).

Honda, H. *et al.* Role of intracellular calcium ions and reactive oxygen species in apoptosis induced by ultrasound. *Ultrasound Med Biol* **30**, 683-692 (2004).

Hook, A. L. *et al.* Surface manipulation of biomolecules for cell microarray applications. *Trends in biotechnology* **24**, 471-477 (2006).

Jain, T. and J. Muthuswamy. Microsystem for transfection of exogenous molecules with spatio-temporal control into adherent cells. *Biosens Bioelectron* **22**, 863-870 (2007).

Keese C *et al*. Electrical wound-healing assay for cells in vitro. *Proc Natl Acad Sci* **101**, 1554-1559 (2004).

Kennedy, J. High-intensity focused ultrasound in the treatment of solid tumors. *Nat Rev Cancer* **5**, 321-327 (2005).

Klibanov, A. Preparation of targeted microbubbles: ultrasound contrast agents for molecular imaging. *Med Biol Eng Comput* **8**, 875-882 (2009).

Kudo, N. *et al.* Sonoporation by single-shot pulsed ultrasound with microbubbles adjacent to cells. *Biophys J* **96**, 4866-4876 (2009).

Liang, C *et al*. In vitro scratch assay: a convenient and inexpensive method for analysis of cell migration in vitro. *Nat Prot* **2**, 329-333 (2007).

Linder, J. Microbubbles in medical imaging: current applications and future directions. *Nat Rev Drug Discov* **3**, 527-532 (2004).

Marmottant, S. and J. Hilgenfeldt. Controlled vesicle deformation and lysis by single oscillating bubbles. *Nature* **423**, 153-156 (2003).

Meijering, B. *et al.* Ultrasound and microbubble-targeted delivery of macromolecules is regulated by induction of endocytosis and pore formation. *Circ Res* 104, 679-687 (2009).

Miller, D. *et al.* Sonoporation: mechanical DNA delivery by ultrasonic cavitation. *Somatic cell and molecular genetics* **27**, 115 (2002).

Ohl, C. *et al.* Sonoporation from jetting cavitation bubbles. *Biophys J* **91**, 4285-4295 (2006).

Orrenius, S. *et al.* Regulation of cell death: the calcium-apoptosis link. *Nat Rev Mol Cell Biol* **4**, 552-565 (2003).

Postema, M. and A. van Wamel. Ultrasound-induced encapsulated microbubble phenomena. *Ultrasound Med Bio.* **30**, 827-840 (2004).

Prentice, P. *et al.* Manipulation and filtration of low index particles with holographic Laguerre-Gaussian optical trap arrays. *Opt Express* **12**, 593-600 (2004).

Ringeisen, B. *et al.* Jet-based methods to print living cells. *Biotechnol J* **1**, 930-948 (2006).

Takayama, S. *et al.* Subcellular positioning of small molecules. *Nature* **411**, 1016 (2003).

Takayama, S. *et al.* Selective chemical treatment of cellular microdomains using multiple laminar streams. *Chem Biol* **10**, 123-130 (2003).

Tavana, H. *et al.* Nanolitre liquid patterning in aqueous environments for spatially defined reagent delivery to mammalian cells. *Nat. Mater* **9**, 736-741 (2009).

Tavana, H. *et al.* Polymeric aqueous biphasic systems for non-contact cell printing on cells:

engineering heterocellular embryonic stem cell niches. *Adv. Mater* **24**, 2628-2631 (2010).

Valley, J. *et al.* Parallel single-cell light-induced electroporation and dielectrophoretic manipulation. *Lab Chip* **9**, 1714-1720 (2009).

van Wamel, A. *et al.* Vibrating microbubbles poking individual cells: drug transfer into cells via sonoporation. *J Control Release* **15**, 149-155 (2006).

Villemejane, J. and L. Mir. Physical methods of nucleic acid transfer: general concepts and applications. *Br J Pharmacol* **157**, 207-219 (2009).

Warram, J. *et al.* Systemic delivery of a breast cancer-detection adenovirus using targeted microbubbles. *Cancer Gene Ther* **19**, 545-552 (2012).

Wells, D. Electroporation and ultrasound enhanced non-viral gene delivery in vitro and in vivo. *Cell Biol Toxicol* **26**, 21-28 (2010).

Wickman, G. *et al*. How apoptotic cells aid in the removal of their own cold dead bodies. *Cell Death Differ* **19**, 735-742 (2012).

Wright, D. *et al.* Generation of static and dynamic patterned co-cultures using microfabricated parylene-C stencils. *Lab Chip* **7**, 1272-1279 (2007).

Yaguchi, T. *et al.* Subcellular positioning of small molecules. *Biomacromolecules* **9**, 2655-2661 (2012).

Zhong, W. *et al.* Sonoporation induces apoptosis and cell cycle arrest in human promyelocytic leukemia cells. *Ultrasound Med Biol* 37, 2149-2159 (2011).

Zhou, Y. *et al.* Effects of extracellular calcium on cell membrane resealing in sonoporation. *J Control Release* **126**, 34-43 (2008).

Ziegler, U. and P. Groscurth. Morphological features of cell death. *News Physiol Sci* **19**, 124-128 (2004).

Chapter Six

High-throughput Aqueous Two-Phase Printing of Contractile Collagen Gels

This chapter describes a simple, micropatterning approach to generate a high throughput contractile contraction assay. Briefly, cell-containing collagen microdroplets are spatially patterned and confined within droplets of immiscible aqueous polymer solutions. The fully aqueous conditions enable convenient formation of sub-microliter 'microgels' that are much smaller than is otherwise possible to make while maintaining high cell viability. The produced microgels contract over several days, mimicking the behavior of macroscale contraction assays that have been valued as an important biological readout for over three decades. Utility of the technology is demonstrated by analyzing the effects of TGF-β1 on gel contraction, and we demonstrate that brief 'burst' stimulation profiles in microgels prompts contraction of the matrix, a feature not observed in the conventional macroscale assay. The fully aqueous process also enables the integration of contractile collagen microgels within existing cell culture systems, and we demonstrate proof-of-principle experiments in which a contractile collagen droplet mechanically damages an epithelial monolayer. The simplicity, versatility and ability to robustly produce collagen microgels should allow effective translation of this microengineering technology into a variety of research environments.

6.1 Introduction

The ability for a cell to remodel the surrounding extracellular matrix (ECM) is a critical feature in development, homeostasis and disease progression. In particular, cell-mediated contraction of collagen matrices occurs in a variety of situations including embryo development, wound healing, and the formation of fibrotic scars and lesions (Lee *et al.* 2012; Rolfe *et al.* 2012; de Vlaming *et al.* 2012; Shannon *et al,* 2006; Grinnel 2003; Carlson and Longaker 2012; Ehlrich and Hunt 2012; Wong *et al.* 2012). *In vitro* collagen contraction assays have provided important insights into biological processes, by enabling the production of tissue-like structures that may serve as engineered replacements or as model systems to investigate disease pathologies (Bell and Merrill 1976, Feng *et al.* 2003; Bell *et al.* 1981; Cen *et al.* 2008; Bowles *et al.* 2010; West *et al.* 2012; Yip *et al.* 2009; Eldred *et al.* 2011; Tse *et al.* 2004). Since the collagen contraction assay is simple to perform, captures relevant physiological details, and is broadly applicable in a variety of processes, it has remained an important research tool for over three decades. However, the complex mechanism driving the matrix contraction process, is combinatorially influenced by multiple environmental factors, including the structure of the collagen matrix, the presence of soluble cytokines, and the type and density of cells driving the process (Tse *et al.* 2004; Smith *et al.*, 2006; Zhu *et al.* 2001; Tingstrom *et al.* 1992; Riikonen *et al.* 1995; Montesano and Orci 1988; Wong *et al.* 2000, Gabbiani 2003; Li *et al.* 2007). Given the number of potential combinations of biological variations that influence contraction, there exists a need for high-throughput versions of this assay, particularly for applications in drug screening and personalized medicine.

Several limitations prevent the translation of this assay to a high-throughput format. Each assay requires a substantial volume of collagen material (from 100 µl in a 96 well plate up to 2.5

ml in a 35 mm dish) to enable facile handling (Gulberg *et al.* 1990; Timpson *et al.* 2011). This volume of material requires a correspondingly large number of cells to maintain a sufficient density to contract the collagen matrix, limiting the use of this assay to relatively low-throughput systems for which a sufficiently large supply of cells is easily available (Redden *et al.* 2003). This makes it challenging to use this assay for applications involving primary cell culture, or for personalized medicine, in which large scale expansion of isolated cells may cause significant phenotypic drift (Yao *et al.* 2006). Furthermore, the relatively large volume of collagen gels limit diffusive transport, particularly of high molecular weight growth factors, known to play a significant role in influencing collagen matrix contraction (Wong *et al.* 2000; Raghavan *et al.* 2010). Hence, despite the established role of timing in the application of signaling molecules to cells in the body the large sample volume prevents uniform activation of cells within the matrix by the application of burst or pulsed biochemical stimuli (Jovic *et al.* 2009).

Reducing the initial size of the collagen gels may address these concerns, but fabricating 'microgels' can pose significant technical challenges. While gel microdroplets are achievable in a variety of materials, most processes depend on rapid polymerization of the droplets (Elbert 2011; Wann 2012). Collagen hydrogels are conventionally not amenable to such schemes, as the polymerization mechanism is pH-sensitive, thermally driven and relatively slow (Forgacs *et al.* 2003). Once neutralized, collagen solutions require time at elevated temperatures to undergo complete gelation, with different protocols recommending gelation times from 30 minutes to 12 hours (Fischer *et al.* 2012). While this timeframe presents few concerns in polymerizing large volumes, small droplets are susceptible to a significantly greater degree of evaporation, which can impact cell viability and functionality. Careful control over processing conditions is therefore required to address these issues (Moon *et al.* 2009). While evaporation may be

mediated by polymerizing the collagen in an oil-water system, the thorough wash steps required add time, complexity and uncertainty to the assay (Vernon *et al.* 2002; Solorio *et al.* 2010). Alternatively, small volumes of collagen have been patterned using microfluidic flow systems, or via a microfabricated template to produce small gels within confined boundaries (Raghavan *et al.* 2010; Legant *et al.* 2009; Zhao *et al.* 2013). Each of these techniques requires a substantial investment in microfabrication-related tools, peripherals and expertise, and is therefore challenging to translate into conventional wet-labs.

To simplify the formation of collagen microgels, we demonstrate an approach to maintain collagen in a distinct droplet during the polymerization process, within an aqueous environment. We utilize an aqueous two-phase system (ATPS), in which soluble polymers thermodynamically drive aqueous systems to form two distinct phases. Our research group and others have demonstrated that biomolecules can selectively partition to one of the phases, and we have previously used this phenomena to position and maintain biomolecules on living cells (Tavana *et al.* 2009; Albertsoon 1987). In the present work, we demonstrate that collagen matrix components selectively partition to the interface of a poly(ethylene) glycol / dextran aqueous two-phase system (**Fig. 6.1C**); and exploit this finding to successfully polymerize sub-microliter volumes of cell-laden collagen microdroplets, within an aqueous environment (**Fig. 6.1A-B**). We demonstrate this technology as a simple, versatile and easily managed approach to simplify, increase throughput and extend the capabilities of the widely used collagen matrix contraction assay. While this system is also compatible with more advanced technologies such as high-throughput bioprinters, automated liquid handlers, and microfluidic systems, a simple manual pipette is sufficient for most applications (Moon *et al.* 2009; Tavana *et al.* 2011; Shibata *et al.*

2010). Hence, we envision this aqueous two-phase approach to collagen printing as being broadly applicable in a variety of contexts.

6.2 Materials and Methods

Unless otherwise stated, all chemicals and reagents for cell culture were purchased from Sigma-Aldrich, fluorescent dyes from Invitrogen and all other equipment and materials from Fisher Scientific.

6.2.1 Cell culture

Four cell types were used in these experiments: HEK 293 embryonic kidney cells; NIH 3T3 murine fibroblasts; MC3T3 murine osteoblast precursors cell line; and MCF10A epithelial cells. HEK 293 and NIH 3T3 cells were cultured in fully supplemented Dulbecco's Modified Eagle Medium (DMEM, with 10% heat-inactivated Fetal Bovine Serum (FBS), 1% antibiotics-antimycotics). MC3T3 cells were cultured in fully supplemented Alpha Minimum Essential Media (αMEM with 15% FBS, 1% antibiotics-antimycotics) in an incubator (37 °C, 5% CO2). MCF10A cells were cultured in Mammary Epithelial Growth Medium (MEGM; Lonza). Cells were not allowed to reach confluence, and sub-cultured in 1:10 ratios by trypsinization. When at desired confluence, cells were washed with phosphate buffered saline (PBS) and 0.25% trypsin solution was added to the flask. Cells were incubated for 5 minutes, and then harvested and centrifuged (1000 RPM, 5 minutes) in a conical tube. The supernatant was aspirated and the cell pellet was re-suspended in fully supplemented culture medium. For ATPS-collagen formulations, cells were re-suspended at 13.6x the final desired concentration.

6.2.2 Preparation of aqueous two-phase system reagents

Stock solutions of DEX (20% w/w dextran T500, Pharmacosmos) were prepared in PBS on a rocker overnight, and centrifuged at 3000 RPM for 15 minutes to remove any undissolved particulates. A stock solution of PEG (20 wt%, MW: 35 kDa, Fluka) was prepared in fully supplemented culture media, and centrifuged. Both stock supernatants were removed and passed through a 0.22 μm sterilizing syringe filter. PEG stock solutions were then diluted to working concentrations in fully supplemented culture medium, and balanced to 300 mOsm/kg by the addition of sterile deionized water, as measured with an osmometer (Vapro 5520 Vapor Pressure Osmometer; Wescor). PEG working solutions were stored for up to 2 weeks at 4 °C. Collagen-DEX solutions were prepared by diluting Type I bovine collagen (BD Biosciences) to 2 mg/ml in a sterile solution of 10% v/v 10x DMEM, 1% v/v 3M NaOH, 15% v/v DEX stock solution (to a final concentration of 3% dextran) and 7.3% v/v additional buffer. Depending on the experiment performed, the buffer solution was either DMEM or a suspension of cells in fully supplemented DMEM. Neutralized collagen-DEX solutions were stored on ice for a maximum of 30 minutes before use.

6.2.3 Production of ATPS-collagen droplets

Working solutions of PEG were warmed to 37 °C and pipetted into a 48-, 96- or 384-well plate depending on the assay being performed. For manual production of droplets, collagen-DEX solutions were maintained on ice and pipetted directly into the PEG-enriched media. We experimentally found that rapid expulsion of the droplet from the pipette tip led to more uniform collagen droplets. Automated production of droplets was performed using a CyBiWell automated liquid handler system (CyBi-Well, CyBio). A 96-well plate was chilled

and loaded with collagen-DEX solution, and kept cold during the dispensing process using an ice-pack. The tip magazine was loaded with 96 sterile pipette tips (25 µl, CyBio), programmed to aspirate and dispense a desired volume into the target plate from a height of 1 mm above the plate surface. Following dispensation of the collagen-DEX solution, the plates were placed in an ambient air incubator at 37 °C for 30 minutes to allow the collagen to crosslink fully. The PEG-enriched medium was then carefully aspirated, and the droplets were carefully washed with PBS and maintained under fully-supplemented culture medium with or without additional soluble factors. When applicable, medium was supplemented with varied concentrations of Transforming growth factor (TGF)-β1 (R&D Systems). As a final step, the solutions were pipetted rapidly to dislodge the collagen droplet from the underlying surface, before culture for up to 15 days.

6.2.4 Fluorescent labeling, imaging and analysis

Collagen microgels were imaged at selected timepoints using a standard inverted microscope (TE300, Nikon) and a 4x objective. Measurement of collagen droplet area was performed by analysis of binary threshold images, using a semi-automated script in ImageJ (NIH). For viability assays, cells were encapsulated in collagen droplets, and at the appropriate time point, the surrounding media was replaced with 4 µM Calcein-AM and 2 µM Ethidium Homodimer (EtHD) in PBS for 30 minutes. The media was washed away and droplets were fluorescently imaged to assess viability. Percent viability was calculated as the number of cells labeled with Calcein AM, divided by the total number of cells identified with Calcein AM and EtHD. To distinguish between cell populations, CellTracker dyes were used to label cells as per the manufacturer's protocol. To label and fix cells within microgels, the collagen droplets were

fixed in 4% paraformaldehyde for 20 minutes at room temperature, permeabilized with 0.1% triton-X for 10 minutes, and fluorescently stained for actin structures using FITC-phalloidin. Fluorescently labeled cells were imaged with a confocal microscope to confirm even distribution through the hemispherical gel.

6.2.5 Statistical analysis

All statistics are reported as means ± standard deviation. ANOVA tests were performed using a commercially-available software package (SigmaStat 3.5; Systat Software Inc., San Jose, CA), using the Tukey test for post-hoc pairwise comparisons.

6.2.6 Scanning electron microscopy

Droplets of collagen were prepared in ATPS as described, and allowed to polymerize for 30 minutes on a glass coverslip. The droplets were gently washed in PBS three times, and then rinsed and stored in DI water. Samples were snap-frozen in liquid nitrogen, lyophilized, and coated with 10 nm of gold using a plasma-induced sputter deposition system. Samples were loaded into an XL30 FEG scanning electron microscope (Philips), and imaged at 5000x, with a beam voltage of 5 kV, and spot size of 3. Images were analyzed for fiber sizes using ImageJ, and expressed as a mean ± standard deviation (n = 3).

6.2.7 Determining collagen partitioning behavior

Partitioning of collagen within the aqueous two-phase system was determined by a dot blot assay. 500 μg/ml of collagen was prepared in a solution containing the appropriate total

quantities of PEG and dextran. Acidic collagen solution was prepared by mixing 20 μL 10X PBS, 33.3 μl of collagen stock solution, 30 μl of 20 wt% DEX, 116.2 μl 0.02 N acetic acid, and 200 μl 10% PEG in an Eppendorf tube. After centrifuging at 400 rcf for 7 mins, the PEG, interface and DEX phases were separated and 20 μl of each phase was diluted in 20 μl 0.02 N acetic acid. Small strips of polyvinylidene fluoride (PVDF) membranes (Bioexpress) were placed on the surface of methanol for 15 seconds. Then membranes were washed in distilled water for 2 minutes and PBS for 5 minutes. 0.2 μl samples of the diluted PEG, interface and DEX phases were spotted onto the wet PVDF membrane. The membrane was rinsed in distilled water and then transferred to solution containing Coomassie Blue stain for 10 minutes (0.2 % (w/v) Coomassie Blue, 40% (w/v) methanol, 10 %(w/v) acetic acid). The membrane was then de-stained for 3 minutes in 80 % (w/v) methanol/10 %(w/v) acetic acid. Finally, the membrane was placed in a second de-staining solution for 1 hour (45 %(w/v) methanol/10 %(w/v) acetic acid). Brightfield images showing Coomassie-stained collagen were analyzed based on intensity levels and reported as arbitrary units.

6.2.8 Mass transport simulations

A commercially available finite element package (COMSOL v4.3; Burlington, MA) was used to simulate diffusion in ATPS-generated collagen droplets and in the conventional collagen assay, similar to previous work by Raghavan et al. (Raghavan *et al.* 2010). The geometry of a 5 μl droplet was experimentally determined and modeled as an axisymmetric hemisphere with a 1.75 mm diameter. The conventional assay for collagen contraction was modeled as a cylinder with diameter 6.38 mm and depth 3.125 mm. The diffusion coefficient for TGF-β1 in collagen was estimated as 1.36×10^{-10} m^2/s based on values reported in the literature for bovine serum albumin

(MW 65kDa), and the Stokes-Einstein equation for diffusivity of particles. A boundary concentration was applied to the outside of the droplet, and a time-stepped transport of diluted species analysis was conducted to determine concentrations of TGF-β1 in the center or bottom of the collagen droplet or cylinder.

6.3 Results and Discussion

6.3.1 Characterization of collagen microgels

Dot blot tests reveal that collagen selectively partitions to the interface of a 3% dextran T-500 (DEX) / 5% polyethylene glycol 35k (PEG) system, with a partition coefficient of 0.011 +/- 0.005 (n = 3; **Fig. 6.1**). The partition coefficient is defined as the fraction of collagen that remains in the PEG phase, compared to the DEX and interfacial regions. Since the DEX-enriched phase is denser than the PEG phase, it sinks to the bottom of the two-phase system. Although these measurements indicate that collagen selectively partitions to the interface, when the DEX droplet becomes sufficiently small, the accumulated collagen at the interface forms a hemispherical dome. The formation of a complete hemispherical dome was verified by visual inspection, and through cross-sectional views generated by confocal microscopy of fluorescently labeled embedded cells. Scanning electron microscopy (SEM) of the collagen fibers indicate consistently uniform fiber sizes (70 +/- 24 nm; n =3; **Fig. 6.2A**), consistent with collagen fiber diameters produced in conventional collagen gelation schemes. Introducing a low concentration of mouse fibroblast cells into the collagen droplet appears to locally increase pore size and increase collagen fibril diameter around the cells after one day in culture (**Fig. 6.2B**), consistent with the accepted mechanism by which cells compact collagen matrices (Stevenson *et al.* 2010; Ehlrich and Hunt 2012).

ATPS-collagen droplets dispensed into well-plates demonstrate that the resulting collagen microgel dimensions depend on the volume of dispensed DEX/collagen solutions. Droplets were dispensed using either a manual pipette, or an automated liquid handler system (CyBi Well; CyBio Inc.). The lateral microgel dimensions are similar to those expected for ideal hemispheres (**Fig. 6.2C**), with similar results if collagen droplets are formed on bare tissue-culture plastic (TCP) surfaces, or on a monolayer of viable HEK 293 cells. Our previous work indicated that the presence of cells on the substrate alters the interfacial tension between the two phases, prompting differences in droplet spreading; but this appears to be abrogated in the collagen ATPS (Tavana *et al.* 2011). Though differences do exist between droplets plated on TCP and on cells, the difference is minimal, particularly at smaller droplet volumes.

Microgel dimensions are also affected by the concentration of PEG in the media. At concentrations less than 5%, droplets do not form, and droplets appear to take a more hemispherical shape at concentrations greater than 6%. While the possibility of long-chain PEG molecules interfering with cell function is low due to the excellent resistance of PEG to non-specific binding, all further experiments were conducted at the lowest robustly stable concentration to minimize any potential interactions with cells (Jain *et al.* 2012). Microgel dimensions are also influenced by concentration of collagen in the droplet (**Fig. 6.2D**), suggesting that collagen plays a role in thermodynamically driving separation in the ATPS system. This is supported by the fact that the minimum concentrations of DEX and PEG required to form two phases without a collagen component is greater than the concentrations used in the production of collagen microgels (Tavana *et al.* 2009).

6.3.2 Cell viability and contraction assays

NIH 3T3 cells were used as a model cell line to evaluate viability of cells encapsulated in ATPS-collagen microgel production. Two initial potential polymerization schemes were tested and evaluated for cell viability. In the first, the acidic collagen-DEX component was neutralized before the addition of cells. In the second, cells were mixed with the acidic collagen-DEX component and immediately dispensed into the PEG-enriched medium, where the droplet would neutralize because of the greater volume of the surrounding media. While this approach would eliminate the possibility that the collagen-DEX would polymerize before being dispensed, viability stains indicate that cell viability is significantly impacted using the acidic method ($p < 0.001$ after 24 hours, $n = 5$; **Fig. 6.3C**).

To compare the ATPS-mediated approach with conventional collagen gelation protocols in fabricating low-volume gels, viability of cells in 1 μl droplets was tested 8 hours after droplets were made using each method. When 1 μl droplets were placed on the surface of a Petri dish (without an aqueous environment) and polymerized at 37 °C for 30 minutes viability of cells significantly decreased as compared to those droplets allowed to polymerize within an ATPS ($p < 0.001$, $n = 10$; **Fig. 6.3D**). This is likely due to evaporation of water from the droplets and a consequent increase in osmolality during the time necessary for polymerization. While the conventional process may be optimized for time and humidity, this data demonstrates that such considerations are not necessary when preparing collagen droplets in an aqueous two-phase system.

Sufficiently large concentrations of cells within the collagen microgel cause contraction of the matrix over several days when the matrix is released from the surface (**Fig. 6.4A-B**). ATPS-collagen droplets were easily detached from the surface by pipetting a directed flow of

medium at the droplet during the final washing step of the assay. Contraction rates are strongly dependent on cell type, with HEK 293 cells at 1 million cells / ml providing the smallest contraction over 2 days, and MC 3T3 pre-osteoblasts at the same concentration forcing the largest matrix contraction (**Fig. 6.4C**). As MC 3T3 pre-osteoblasts provided the greatest contraction, all further experiments were conducted using this cell type. These differences demonstrate that the ATPS-mediated production of collagen microgels maintains sensitivity of the assay in measuring contraction of the collagen matrix.

Comparisons between the conventional collagen contraction assay performed with 100 μL of cell-laden collagen in a single well of a 96-well plate and various droplet sizes fabricated using the ATPS production method, indicated that contraction of collagen was not significantly affected by the size of the collagen construct ($p = 0.124$; **Fig. 6.5A**), demonstrating that scaling down the assay volume still provides readouts comparable with the conventional technique (Gullberg *et al.* 1990). As expected, cell density plays a key role in mediating collagen contraction (**Fig. 6.5B**). Collagen droplets expanded slightly when cultured without cells, while a low concentration of 50 cells / μl maintained droplet size over 4 days. Greater cell concentrations caused rapid contraction of the droplets, consistent with reports in conventional assays (Redden and Doolin 2003). To characterize the effect of PEG on the contraction system, collagen microgels were maintained in PEG-enriched media of different concentrations over several days. Interestingly, greater PEG concentrations resulted in reduced levels of contraction (**Fig. 6.5C**), suggesting that PEG interferes with the contraction process, either via a cell-mediated mechanism, or by direct mechanical augmentation of the contracting collagen matrix.

Cell-mediated contraction of the collagen matrix is also influenced by the presence of soluble growth factors, including transforming growth factor β1 (TGF-β1). Concentrations as

low as 1 ng/ml were sufficient to prompt a rapid increase in contraction of the collagen microgels. Concentrations greater than 1 ng/ml had no statistically significant effect on contraction rates (**Fig. 6.5D**). Taken together, these data demonstrate that fabricating collagen microgels via an aqueous two-phase production method produces similar responses as compared to the conventional assay.

6.3.3 Exploiting transport properties of microgels

To demonstrate the potential for microscale systems in improving transport of large molecules such as TGF-β1 (MW 25 kDa) into the collagen matrix, finite element simulations were used to compare passive diffusion of large molecules in the conventional assay (100 µl of collagen in a 96-well plate cylindrical form) against the ATPS-mediated production of microgels (5 µlhemispherical droplets; **Fig. 6.6A, B**). Concentration of the diffusing molecule reaches at least 90% of equilibrium throughout the construct within 30 minutes in the ATPS droplet, while the conventional assay reaches 90% equilibrium after 28 hours; demonstrating that while the conventional collagen contraction assay responds to applied soluble cues, this response is not necessarily homogenous throughout the system, nor does the system allow for burst or timed stimulation by soluble cues. Equilibration of smaller droplets occurs much more rapidly. As timed stimulation is emerging as an important feature in mimicking *in vivo* physiological systems, extending the collagen contraction assay to include a time-dependent component may yield interesting insights into the biology of such systems (Jovic *et al.* 2009).

To explore the possibilities in using this system to apply dynamic stimulation profiles of large molecules to cells within the collagen matrix, we applied timed TGF-β1 stimulation profiles to ATPS-mediated microgels and to the conventional 100 µl assay (**Fig. 6.5C**). After

polymerization and rinsing of the microgels, they were exposed to 1 ng/mL of TGF-β1 for short bursts of time, before washing the gels thoroughly with PBS and allowing them to contract for 1 day. At equilibrium conditions, 1 ng/ml of TGF-β1 was sufficient to induce increased contraction of the collagen matrix within this time frame (**Fig. 6.5D**); and even extremely rapid 1 minute exposures to this concentration of TGF-β1 was sufficient to induce increased levels of contraction in ATPS-mediated gels. In contrast, even 5 minutes of exposure was not sufficient to prompt a similar effect in the conventional assay. This data indicates that penetration of collagen into the large gels is minimal, while penetration into the microgels is completed in a fraction of the time. Hence, utilizing collagen microgels in the contraction assay enables rapid stimulation of cell culture constructs for timed stimulation studies.

Though this effect will be less noticeable with smaller molecules, the ability to remove molecules from the assay will also be of importance in timed stimulation assays. To demonstrate such an application, contracting microgels were exposed to Latrunculin-A, known to disrupt the actin filaments of the cytoskeleton, and hence abrogate contraction of the tissue construct. 24 hours of exposure to Latrunclin A (or Nocodazole, a microtubule disruptor; data not shown) prevented collagen contraction, but limiting exposure to 60 minutes enabled the microgels to recover their contractile ability, showing no significant differences from the control ($p = 0.513$; **Fig. 6.6D**).

6.3.4 Utility of the system within existing tissue-engineered models

In addition to exploiting transport properties resulting from the ability to produce low volume gels, aqueous two-phase mediated patterning of contractile collagen gels also enables the fabrication of collagen microgels within existing cell-culture models. This approach may be

used to rapidly and easily produce complex engineered tissues, in which cell-laden collagen gels are patterned over an existing cell monolayer (**Fig. 6.7A**). Hypothetically, this approach can be extended to build several layers of droplets containing multiple cell types in well-defined patterns. This approach may also be used to introduce a contractile collagen microgel into an existing cell culture model system, to provide a cell-based functional readout for signaling factors produced in that system. As our approach uses fully aqueous environments, this technique should be broadly applicable to all cell culture systems. To demonstrate proof-of-principle of this technique, we patterned contractile collagen microgels containing MC 3T3 pre-osteoblasts over a confluent monolayer of MCF10A breast epithelial cells (**Fig. 6.7B-C**). The epithelial cell sheet is a simple cell culture system, characterized by tight junctions between cells. After four hours in culture the collagen microgel contracted sufficiently to damage the underlying epithelium (**Fig. 6.7C-D**). Damage occurs close to the contractile droplet, while areas further away remain intact, strongly suggesting that the mechanical insult provided by the contractile droplet rips the epithelial monolayer from the substrate. This simple co-culture system enables the study of mechanical interactions between different tissue types, and may be used to simulate certain physiological processes, such as in development or wound healing in the airways. Furthermore, this approach may also be used to measure the influence of soluble cues generated by relevant cell culture model systems on contraction of an *in situ* collagen microgel.

6.4 Conclusion

Aqueous two-phase systems have been used for a variety of biotechnology applications, and here we demonstrate the use of this approach to produce sub-microliter volumes of collagen microgels. Collagen matrix components partition within a polyethylene glycol / dextran aqueous

system, and undergo gelation in an aqueous environment, such that hemispherical microgels can be produced on a variety of substrates, including on live cell monolayers. The aqueous environment prevents evaporation within the small droplet volume, allowing encapsulated cells to remain viable. In contrast, similarly sized gels polymerized using the conventional approach in air suffered significant losses in cell viability. When a sufficiently large number of contractile cells are encapsulated in the droplet, the matrix undergoes remodeling and contraction, at a rate dependent on cell type, cell density, and the presence of soluble factors; mimicking results in conventional macroscale collagen contraction assays. The ability to use collagen microgels for contraction assays not only reduces the volume of reagents and number of cells necessary, but also significantly improves transport of molecules into the bulk of the hydrogel droplet. Hence, collagen microgels may be used to conduct time-dependent and pulsed stimulation, which would not be possible with conventional approaches. Finally, the aqueous two-phase processing system also enables production of collagen microgels within existing cell culture environments, and may be used as either a tool to print complex three-dimensional engineered tissues, or to conduct collagen contraction assays in situ. We demonstrate that the system is scalable to high-throughput screening applications by using an automated liquid handler system, and believe that this approach is simple, versatile and robust to enable translation into a variety of research environments.

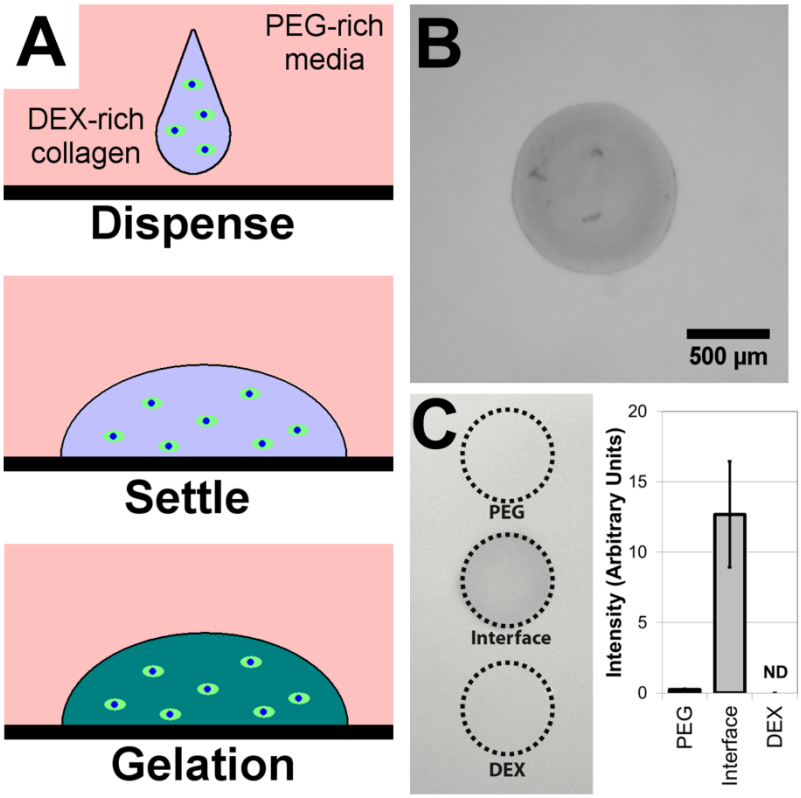

Figure 6.1: Aqueous two-phase patterning of collagen droplets. (**A**) Process schematic in which a droplet of DEX-rich collagen is dispensed into a PEG-rich media, allowed to settle, and undergo thermal gelation. (**B**) A 1 µl collagen droplet after gelation in an ATPS, scale bar = 500 µm. (**C**) Dot blot experiments indicate that collagen strongly partitions to the interface of a 5%PEG-3%DEX aqueous two phase system (K_{part} = 0.011 +/- 0.005; n=3).

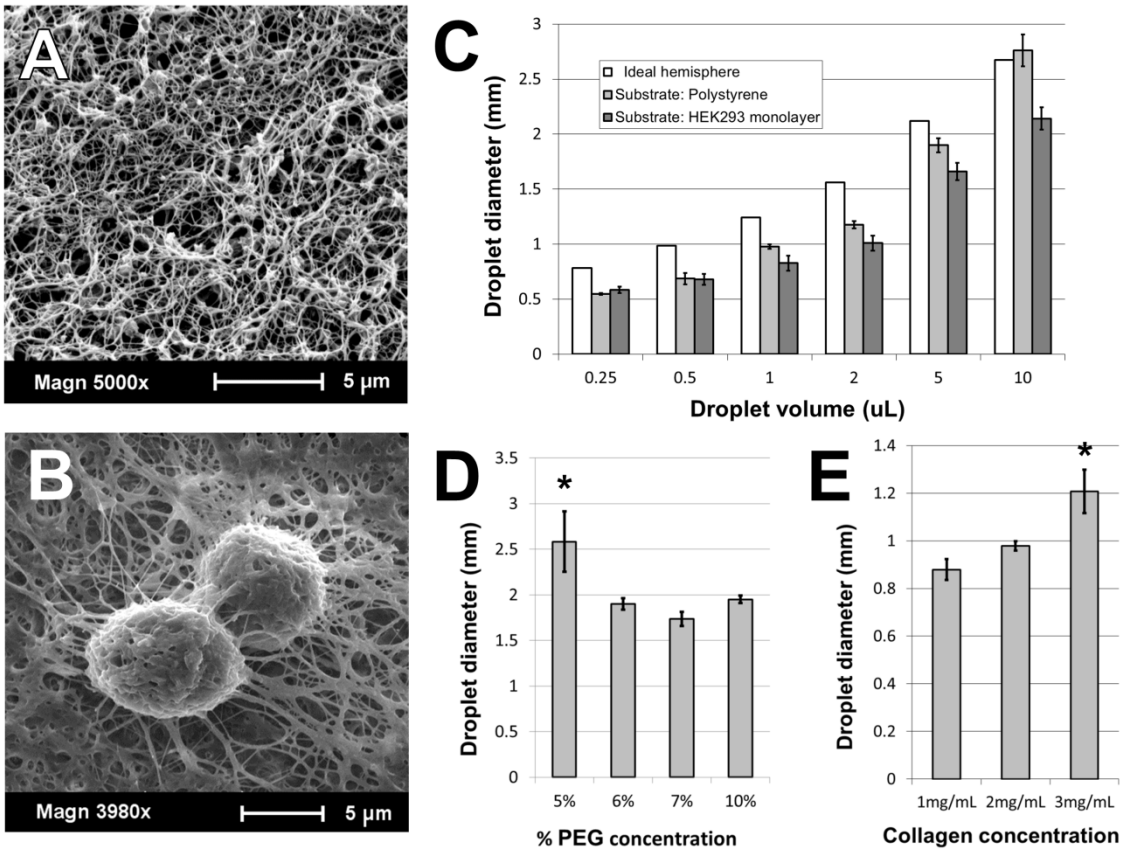

Figure 6.2: Characterization of aqueously-processed DEX-rich collagen. (**A**) Scanning electron micrograph reveals that ATPS-collagen has a fiber size of 70 ± 24 nm, consistent with standard collagen fiber sizes. (**B**) MC3T3 cells actively remodel the collagen matrix. (**C**) Droplet diameter scales with droplet volume producing near-hemispherical domes on either tissue culture polystyrene or a monolayer of HEK 293 cells as a substrate (produced in 6% PEG solution). Droplet diameter is also influenced by (**D**) concentration of PEG in the surrounding media (5 µl droplets), and (**E**) concentration of collagen in the microdroplet (1 µL droplets). All values reported as means ± standard deviation (n = 5; * $p < 0.001$ compared to all other droplets of the same volume).

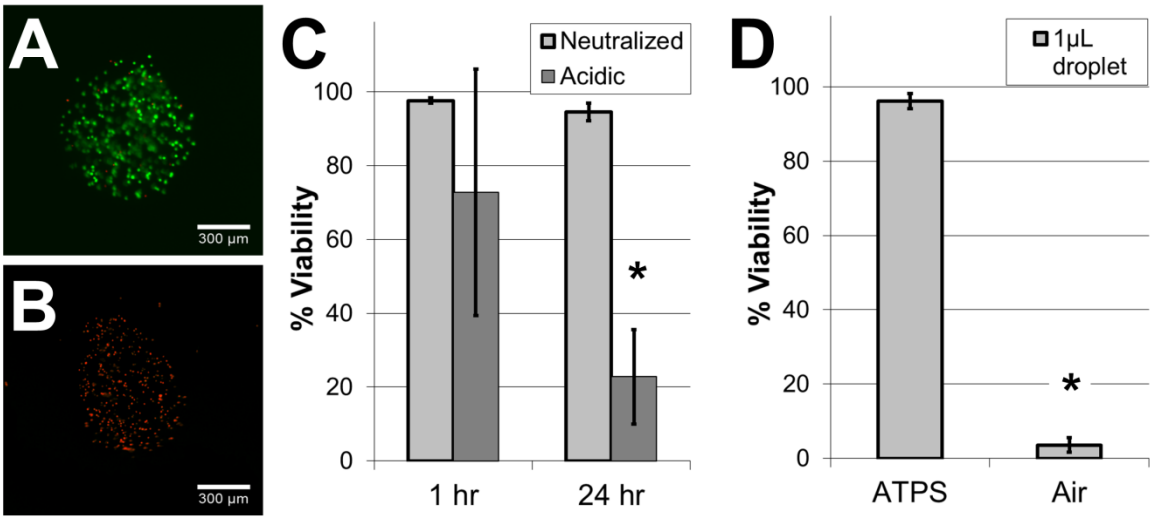

Figure 6.3: Viability of cells within ATPS-collagen microdroplets, as measured by (**A, B**) Live/dead viability assays. (**C**) Cell viability under neutralized and acidic conditions after 1 and 24 hours. Viability is maintained when the collagen-DEX droplet has been neutralized (n = 5). (**D**) Viability of cells encapsulated in small droplets formed under aqueous-two phase and air conditions demonstrate that viability is greatly improved under aqueous processing conditions, most likely due to rapid evaporation of liquid in the small droplets during the gelation time period (values reported as means ± standard deviation, n= 10; * $p < 0.001$, compared within the same time point). Scale bars = 300 µm.

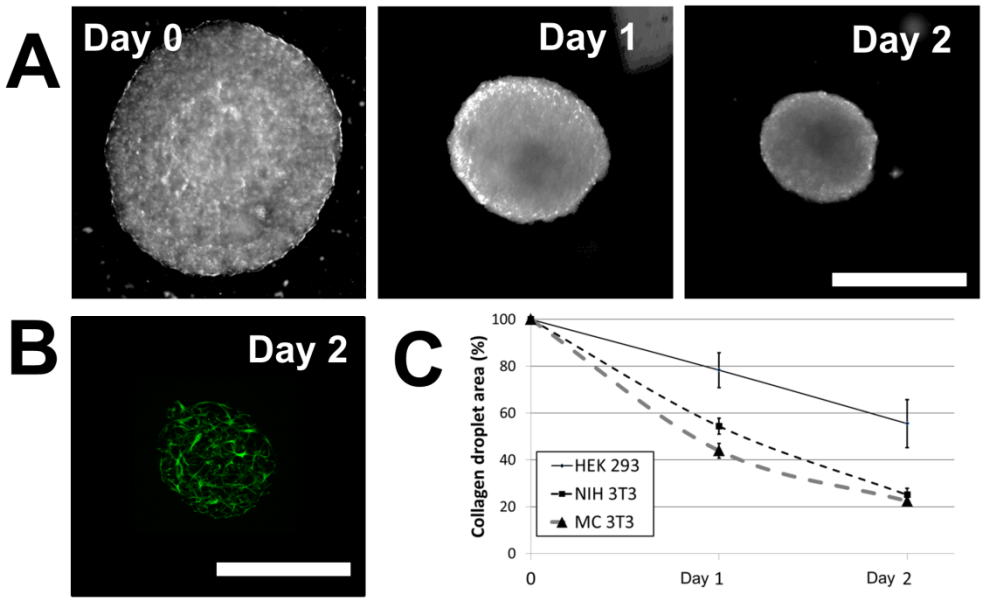

Figure 6.4: Contraction of collagen microdroplets. (**A**) Representative images of MC 3T3 cells contracting the collagen microdroplet over two days in culture. (**B**) Confocal image showing cell spreading within the collagen matrix after 2 days in culture. Scale bar = 1 mm. (**C**) Human embryonic kidney (HEK293), mouse fibroblast (NIH 3T3) and mouse pre-osteoblast (MC 3T3) at densities of $1x10^6$ ml^{-1} reduce the droplet area of collagen at distinctly different rates (n = 3; HEK 293 significantly different ($p < 0.003$) compared with other cell types).

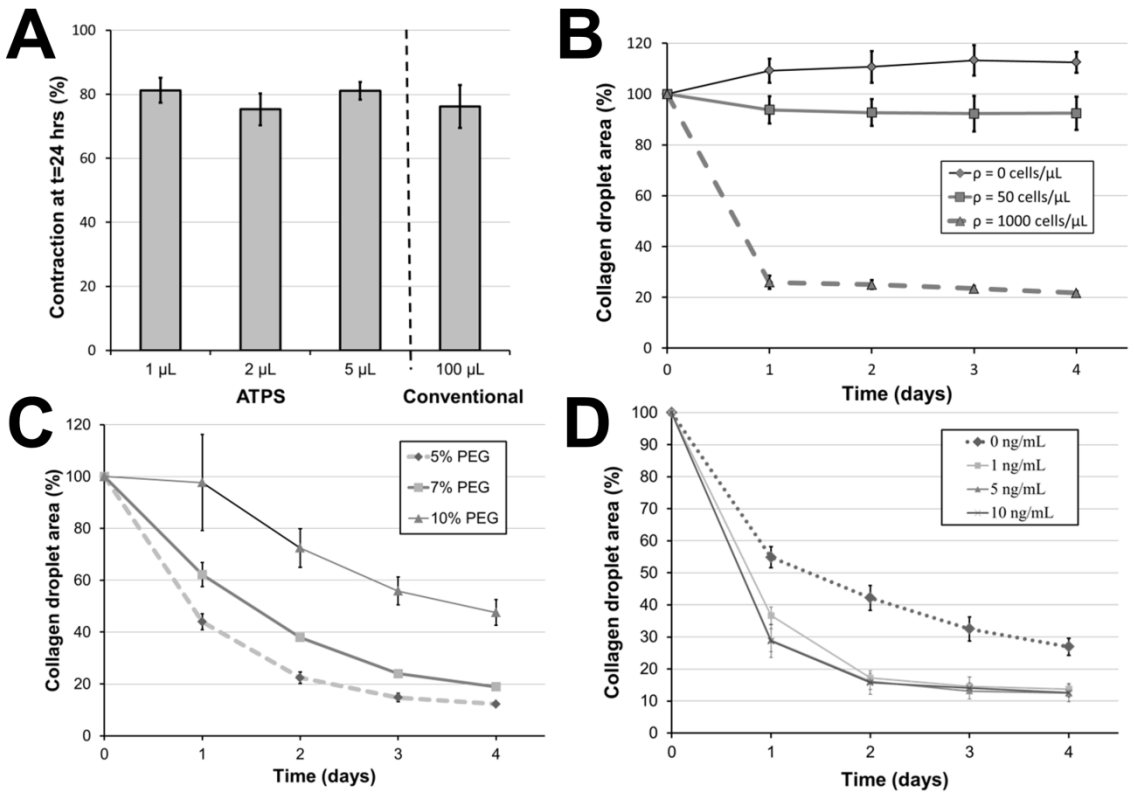

Figure 6.5: Characterization of contraction in collagen microdroplets. (A) Comparison of MC3T3 contraction of ATPS-collagen microdroplets against the conventional collagen contraction assay reveals that baseline percent contraction is independent of droplet or assay volume (n = 7-8 for ATPS; n = 3 for conventional assays). (B) Collagen droplet contraction rates depend on cell density, (C) concentration of PEG in the surrounding media (at cell density of 1000 cells / µl), and (D) presence of soluble factors such as TGF-β1 (at cell density = 500 cells / µl). 1, 5 and 10 ng/ml of TGF-β1 produced similar increases in contraction of the droplets (n = 7-8).

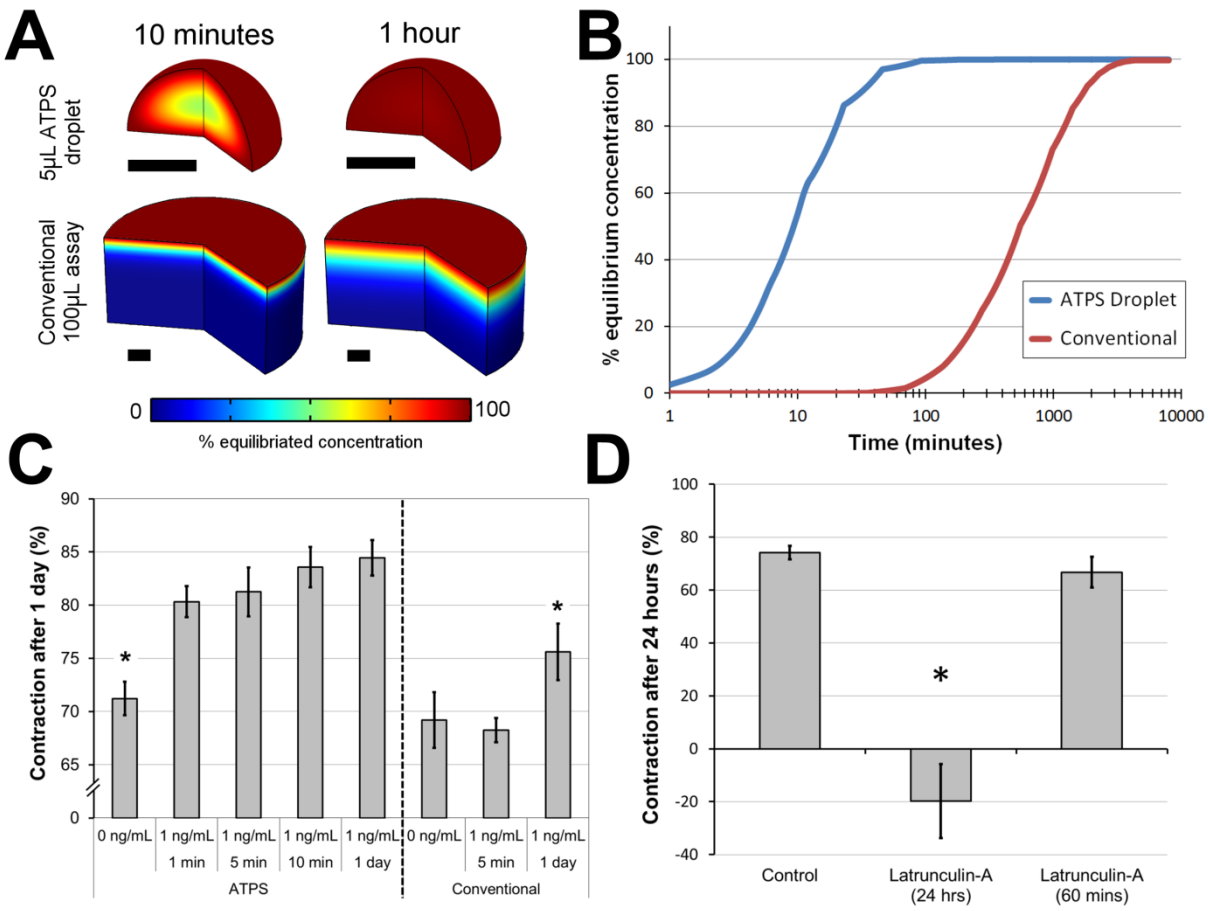

Figure 6.6: Miniaturization of droplets enables rapid diffusive transport through the collagen matrix. (**A**) Simulations indicate that diffusive transport enables equilibration of the TGF-β1 molecule (MW 25 kDa) within 1 hour, as compared to the conventional collagen contraction assay. Scale bar = 1 mm. (**B**) Percent equilibrium concentration at the base of the collagen droplets over time. Conventional assays require ~24 hours to completely equilibrate to added concentrations of TGF- β1. (**C**) Timed stimulation of ATPS-collagen and conventional collagen droplets with TGF-β1. Small volume (5 µl droplets) of ATPS-collagen respond to 1 minute of stimulation with TGF-β1, as compared to conventional assays. (**D**) Small droplet size also enables simple removal of soluble factors for pulsed stimulation experiments. After 24 hours, collagen contraction is strongly inhibited by Latrunculin-A, but contraction is recovered if the surrounding media is changed (n = 7-8 for ATPS assays; n = 3 for conventional assays; * indicates $p < 0.001$ compared to all other conditions in the same assay).

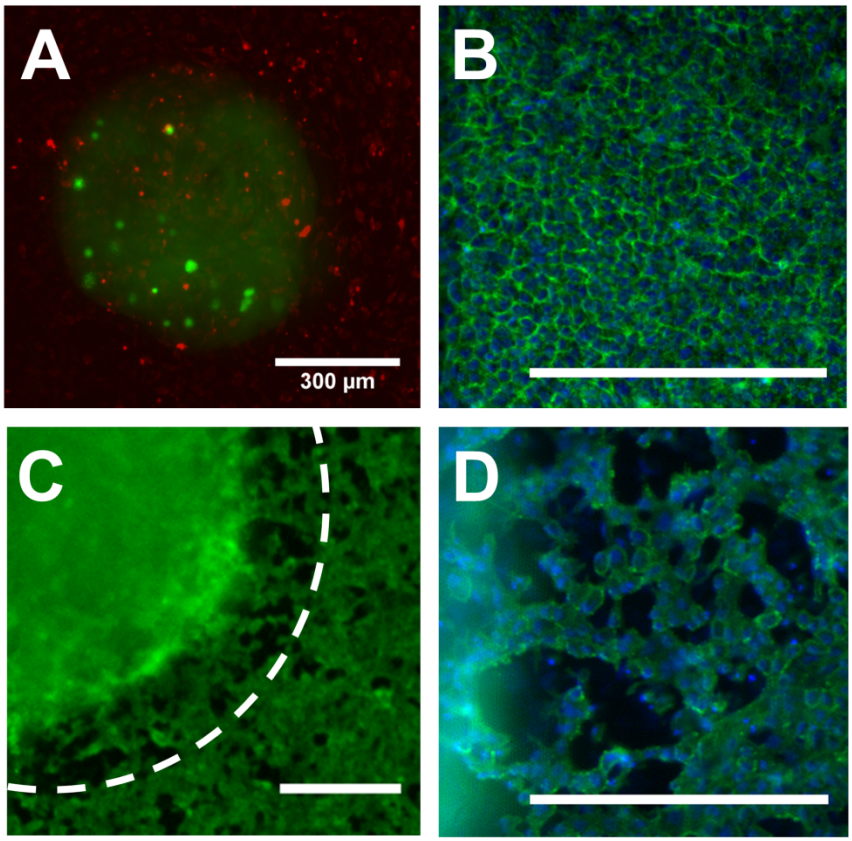

Figure 6.7: Patterning contractile collagen microdroplets within existing live-cell culture environments. (**A**) NIH 3T3 cells (green) are encapsulated within a collagen droplet formed over a layer of HEK 293 cells (red). (**B**) A monolayer of MCF10A cells prior to collagen patterning, stained for actin (green) and nuclei (blue). Actin structures indicate a well-connected epithelial monolayer. (**C,D**) MC3T3 cells encapsulated in collagen (formed via ATPS) on the existing epithelial monolayer. The original boundary of the collagen droplet is marked with a white dashed line. Within four hours, the MC3T3 cells induce contraction of the gel, ripping the cell monolayer beneath it. Scale bars = 300 µm.

6.5 References

Albertsson, P.-Å., Cajarville, A., Brooks, D. E. & Tjerneld, F. Partition of proteins in aqueous polymer two-phase systems and the effect of molecular weight of the polymer. *Biochimica et Biophysica Acta (BBA) - General Subjects* **926**, 87–93 (1987).

Bell, E., Ivarsson, B. & Merrill, C. Production of a tissue-like structure by contraction of collagen lattices by human fibroblasts of different proliferative potential in vitro. *Proceedings of the National Academy of Sciences* **76**, 1274–1278 (1979).

Bell, E., Ehrlich, H., Buttle, D. & Nakatsuji, T. Living tissue formed in vitro and accepted as skin-equivalent tissue of full thickness. *Science* **211**, 1052–1054 (1981).

Carlson, M. A. & Longaker, M. T. The fibroblast-populated collagen matrix as a model of wound healing: a review of the evidence. *Wound Repair and Regeneration* **12**, 134–147 (2004).

Cen, L., Liu, W., Cui, L., Zhang, W. & Cao, Y. Collagen Tissue Engineering: Development of Novel Biomaterials and Applications. *Pediatric Research* **63**, 492–496 (2008).
Bowles, R. D., Williams, R. M., Zipfel, W. R. & Bonassar, L. J. Self-Assembly of Aligned Tissue-Engineered Annulus Fibrosus and Intervertebral Disc Composite Via Collagen Gel Contraction. *Tissue Engineering Part A* **16**, 1339–1348 (2010).

De Vlaming, A. *et al.* Atrioventricular valve development: New perspectives on an old theme. *Differentiation* **84**, 103–116 (2012).

Ehrlich, H. P. & Hunt, T. K. Collagen Organization Critical Role in Wound Contraction. *Advances in Wound Care* **1**, 3–9 (2012).

Elbert, D. L. Liquid-liquid two-phase systems for the production of porous hydrogels and hydrogel microspheres for biomedical applications: A tutorial review. *Acta biomaterialia* **7**, 31–56 (2011).

Eldred, J. A., Dawes, L. J. & Wormstone, I. M. The lens as a model for fibrotic disease. *Phil. Trans. R. Soc. B* **366**, 1301–1319 (2011).

Feng, Z. *et al.* Investigation on the Mechanical Properties of Contracted Collagen Gels as a Scaffold for Tissue Engineering. *Artificial Organs* **27**, 84–91 (2003).

Fischer, R. S., Myers, K. A., Gardel, M. L. & Waterman, C. M. Stiffness-controlled three-dimensional extracellular matrices for high-resolution imaging of cell behavior. *Nature Protocols* **7**, 2056–2066 (2012).

Forgacs, G., Newman, S. A., Hinner, B., Maier, C. W. & Sackmann, E. Assembly of Collagen Matrices as a Phase Transition Revealed by Structural and Rheologic Studies. *Biophysical Journal* **84**, 1272–1280 (2003).

Gabbiani, G. The myofibroblast in wound healing and fibrocontractive diseases. *The Journal of Pathology* **200**, 500–503 (2003).

Grinnell, F. Fibroblast biology in three-dimensional collagen matrices. *Trends in Cell Biology* **13**, 264–269 (2003).

Gullberg, D. *et al.* β1 Integrin-mediated collagen gel contraction is stimulated by PDGF. *Experimental Cell Research* **186**, 264–272 (1990).

Hong, S., Hsu, H.-J., Kaunas, R. & Kameoka, J. Collagen microsphere production on a chip. *Lab on a Chip* **12**, 3277 (2012).

Jain, A., Liu, R., Xiang, Y. K. & Ha, T. Single-molecule pull-down for studying protein interactions. *Nature Protocols* **7**, 445–452 (2012).

Jovic, A., Howell, B. & Takayama, S. Timing is everything: using fluidics to understand the role of temporal dynamics in cellular systems. *Microfluidics and nanofluidics* **6**, 717–729 (2009).

Lee, Y.-S., Wysocki, A., Warburton, D. & Tuan, T.-L. Wound healing in development. *Birth Defects Research Part C: Embryo Today: Reviews* **96**, 213–222 (2012).

Legant, W. R. *et al.* Microfabricated tissue gauges to measure and manipulate forces from 3D microtissues. *Proceedings of the National Academy of Sciences* **106**, 10097 –10102 (2009).

Li, J., Chen, J. & Kirsner, R. Pathophysiology of acute wound healing. *Clinics in Dermatology* **25**, 9–18 (2007).

Montesano, R. & Orci, L. Transforming growth factor beta stimulates collagen-matrix contraction by fibroblasts: implications for wound healing. *Proceedings of the National Academy of Sciences* **85**, 4894–4897 (1988).

Moon, S. J. *et al.* Layer by layer three-dimensional tissue epitaxy by cell-laden hydrogel droplets. *Tissue Engineering Part C: Methods* **16**, 157–166 (2009).

Paralkar, V. M., Vukicevic, S. & Reddi, A. H. Transforming growth factor β type 1 binds to collagen IV of basement membrane matrix: Implications for development. *Developmental Biology* **143**, 303–308 (1991).

Raghavan, S. *et al.* Decoupling Diffusional from Dimensional Control of Signaling in 3D Culture Reveals a Role for Myosin in Tubulogenesis. *J Cell Sci* **123**, 2877–2883 (2010).

Redden, R. A. & Doolin, E. J. Collagen crosslinking and cell density have distinct effects on fibroblast-mediated contraction of collagen gels. *Skin Research and Technology* **9**, 290–293 (2003).

Riikonen, T., Koivisto, L., Vihinen, P. & Heino, J. Transforming Growth Factor- Regulates Collagen Gel Contraction by Increasing 21 Integrin Expression in Osteogenic Cells. *J. Biol. Chem.* **270**, 376–382 (1995).

Rolfe, K. J. & Grobbelaar, A. O. A Review of Fetal Scarless Healing. *ISRN Dermatol* **2012**, (2012).

Shannon, D. B., McKeown, S. T. W., Lundy, F. T. & Irwin, C. R. Phenotypic differences between oral and skin fibroblasts in wound contraction and growth factor expression. *Wound Repair and Regeneration* **14**, 172–178 (2006).

Shibata, H. *et al.* Injectable hydrogel microbeads for fluorescence-based in vivo continuous glucose monitoring. *PNAS* **107**, 17894–17898 (2010).

Smith, K. D., Wells, A. & Lauffenburger, D. A. Multiple signaling pathways mediate compaction of collagen matrices by EGF-stimulated fibroblasts. *Exp. Cell Res.* **312**, 1970–1982 (2006).

Solorio, L., Zwolinski, C., Lund, A. W., Farrell, M. J. & Stegemann, J. P. Gelatin microspheres crosslinked with genipin for local delivery of growth factors. *Journal of Tissue Engineering and Regenerative Medicine* **4**, 514–523 (2010).

Stevenson, M. D. *et al.* Pericellular Conditions Regulate Extent of Cell-Mediated Compaction of Collagen Gels. *Biophysical Journal* **99**, 19–28 (2010).

Tavana, H. *et al.* Nanolitre liquid patterning in aqueous environments for spatially defined reagent delivery to mammalian cells. *Nat Mater* **8**, 736–741 (2009).

Tavana, H., Mosadegh, B., Zamankhan, P., Grotberg, J. B. & Takayama, S. Microprinted feeder cells guide embryonic stem cell fate. *Biotechnology and Bioengineering* **108**, 2509–2516 (2011).

Timpson, P. *et al.* Organotypic Collagen I Assay: A Malleable Platform to Assess Cell Behaviour in a 3-Dimensional Context. *Journal of Visualized Experiments* (2011).

Tingstrom, A., Heldin, C. H. & Rubin, K. Regulation of fibroblast-mediated collagen gel contraction by platelet-derived growth factor, interleukin-1 alpha and transforming growth factor-beta 1. *Journal of cell science* **102**, 315–322 (1992).

Tse, R., Howard, J., Wu, Y. & Gan, B. S. Enhanced Dupuytren's disease fibroblast populated collagen lattice contraction is independent of endogenous active TGF-β2. *BMC musculoskeletal disorders* **5**, 41 (2004).

Vernon, R. & Gooden, M. An improved method for the collagen gel contraction assay. *In Vitro Cellular & Developmental Biology - Animal* **38**, 97–101 (2002).

Wan, J. Microfluidic-Based Synthesis of Hydrogel Particles for Cell Microencapsulation and Cell-Based Drug Delivery. *Polymers* **4**, 1084–1108 (2012).

West, A. R. *et al.* Development and characterization of a 3D multicell microtissue culture model of airway smooth muscle. *AJP: Lung Cellular and Molecular Physiology* **304**, L4–L16 (2012).

Wong, V. W., Longaker, M. T. & Gurtner, G. C. Soft tissue mechanotransduction in wound healing and fibrosis. *Seminars in Cell & Developmental Biology* **23**, 981–986 (2012).

Yao, L., Bestwick, C. S., Bestwick, L. A., Maffulli, N. & Aspden, R. M. Phenotypic Drift in Human Tenocyte Culture. *Tissue Engineering* **12**, 1843–1849 (2006)

Yip, C. Y. Y. *et al*. Calcification by Valve Interstitial Cells Is Regulated by the Stiffness of the Extracellular Matrix. *Arterioscler Thromb Vasc Biol* **29**, 936–942 (2009).

Zhao, R., Boudou, T., Wang, W.-G., Chen, C. S. & Reich, D. H. Decoupling Cell and Matrix Mechanics in Engineered Microtissues Using Magnetically Actuated Microcantilevers. *Advanced Materials* (2013).

Zhu, Y. K. *et al.* Contraction of fibroblast-containing collagen gels: Initial collagen concentration regulates the degree of contraction and cell survival. *In Vitro Cell.Dev.Biol.-Animal* **37**, 10–16 (2001).